National Library of Canada
Bibliothèque nationale du Canada

Canadian Theses Service
Service des thèses canadiennes

Ottawa, Canada
K1A 0N4

NOTICE

The quality of this microform is heavily dependent upon the quality of the original thesis submitted for microfilming. Every effort has been made to ensure the highest quality of reproduction possible.

If pages are missing, contact the university which granted the degree.

Some pages may have indistinct print especially if the original pages were typed with a poor typewriter ribbon or if the university sent us an inferior photocopy.

Reproduction in full or in part of this microform is governed by the Canadian Copyright Act, R.S.C. 1970, c. C-30, and subsequent amendments.

AVIS

La qualité de cette microforme dépend grandement de la qualité de la thèse soumise au microfilmage. Nous avons tout fait pour assurer une qualité supérieure de reproduction.

S'il manque des pages, veuillez communiquer avec l'université qui a conféré le grade.

La qualité d'impression de certaines pages peut laisser à désirer, surtout si les pages originales ont été dactylographiées à l'aide d'un ruban usé ou si l'université nous a fait parvenir une photocopie de qualité inférieure.

La reproduction, même partielle, de cette microforme est soumise à la Loi canadienne sur le droit d'auteur, SRC 1970, c. C-30, et ses amendements subséquents.

NL-339 (r. 88/04) c

Canada

UNIVERSITY OF ALBERTA

THEORY, DESIGN, AND CHARACTERIZATION OF ERBIUM-DOPED FIBER AMPLIFIERS

BY

JAMES EDWARD FREEMAN

A thesis submitted to the Faculty of Graduate Studies and Research in partial fulfillment of the requirements for the degree of **Master of Science.**

DEPARTMENT OF ELECTRICAL ENGINEERING

Edmonton, Alberta

Fall, 1991

National Library of Canada
Bibliothèque nationale du Canada

Canadian Theses Service
Service des thèses canadiennes

Ottawa, Canada
K1A 0N4

The author has granted an irrevocable non-exclusive licence allowing the National Library of Canada to reproduce, loan, distribute or sell copies of his/her thesis by any means and in any form or format, making this thesis available to interested persons.

L'auteur a accordé une licence irrévocable et non exclusive permettant à la Bibliothèque nationale du Canada de reproduire, prêter, distribuer ou vendre des copies de sa thèse de quelque manière et sous quelque forme que ce soit pour mettre des exemplaires de cette thèse à la disposition des personnes intéressées.

The author retains ownership of the copyright in his/her thesis. Neither the thesis nor substantial extracts from it may be printed or otherwise reproduced without his/her permission.

L'auteur conserve la propriété du droit d'auteur qui protège sa thèse. Ni la thèse ni des extraits substantiels de celle-ci ne doivent être imprimés ou autrement reproduits sans son autorisation.

ISBN 0-315-69953-1

Canada

UNIVERSITY OF ALBERTA

RELEASE FORM

NAME OF AUTHOR: **James Edward Freeman**

TITLE OF THESIS: **Theory, Design, and Characterization of Erbium-Doped Fiber Amplifiers**

DEGREE: **Master of Science**

YEAR THIS DEGREE GRANTED: **Fall, 1991**

Permission is hereby granted to the University of Alberta Library to reproduce single copies of this thesis and to lend or sell such copies for private, scholarly or scientific research purposes only.

The author reserves all other publication and other rights in association with the copyright in the thesis, and except as hereinbefore provided neither the thesis nor any substantial portion thereof may be printed or otherwise reproduced in any material form without the author's prior written permission.

James Edward Freeman

#203 4612 106A Street

Edmonton, Alberta, Canada

T6H - 5J3

DATE: October 8, 1991

UNIVERSITY OF ALBERTA

FACULTY OF GRADUATE STUDIES AND RESEARCH

The undersigned certify that they have read, and recommend to the Faculty of Graduate Studies for acceptance, a thesis entitled **THEORY, DESIGN, AND CHARACTERIZATION OF ERBIUM-DOPED FIBER AMPLIFIERS** submitted by **JAMES EDWARD FREEMAN** in partial fulfillment of the requirements for the degree of **MASTER OF SCIENCE** in Electrical Engineering.

Dr. J. Conradi, Co-Supervisor

Dr. J. McMullin, Co-Supervisor

Dr. R.I. MacDonald, Internal

Dr. F. Weichman, External

Dedication

To my parents, Jim and Gail,

who provided an excellent home and a chance

for scholarly growth;

To my family and many friends,

who have encouraged me to achieve my best.

In Memory of My Grandfather

Archibald Armour Petrie

April 2, 1914 - Sept. 16, 1991

His kindness and good humor will never be forgotten

Abstract

A comprehensive theoretical model of the behavior of Erbium-doped fiber amplifiers (EDFAs) is developed. The model minimizes the number of assumptions made and accounts for properties of the fiber guiding medium, such as core diameter and fiber numerical aperture, Erbium dopant characteristics, such as dopant concentration and confinement, and signal properties, such as wavelength and power level. As well, the model considers large signal operation of the amplifier and accounts for the deleterious effects of amplified spontaneous emission (ASE). The model also accounts for the modal characteristics of both the pump laser at 980 nm, and the signal and ASE from 1.47 to 1.60 μm.

The model lends itself well to useful computer simulation and studies were conducted on the effects of various design parameters on amplifier performance. Input parameters such as pump power and modal power distribution, dopant concentration and confinement of Erbium, and fluorescence lifetime are found to have marked effects on the figures of merit such as Gain and Noise Figure for the amplifier.

The experiences of the simulation study are summarized in a comprehensive guide to design of an EDFA. Included also are an actual fiber design submitted for fabrication and ideas for a frequency division multiplexed (FDM) transmitter based on spectral slicing of the broad-band output spectrum of an EDFA. Complete theory and analysis is supplied for a narrow-line filter design to accomplish the spectral slicing, and future implementation of such a scheme in fiber is explored.

A systematic laboratory testing capability using computer control of selected instruments is reported on and results of tests on the design fiber are included.

Acknowledgements

I would like to first express my gratitude to my supervisor, Dr. J. Conradi, whose wisdom and expertise have established a tremendous research environment at TR Labs in the field of Erbium-doped Fiber Amplifiers. His technical support and constructive feedback have helped shape my concept of what research should be.

In addition, I would like to acknowledge the support over the years of Dr. J. McMullin, who first got me strongly interested in research at TR Labs and who has offered many hours of interesting conversation. I would also like to salute Dr. R. I. MacDonald's efforts as the Director for Photonics Research at TR Labs, and for his constant input to all research programs in Photonics.

I would like to acknowledge the close collaboration of Mr. Jay Haugen from AGT Ltd., from whom I have learned much about the industrial side of research as well as the practical aspects of lab work. As well, I would like to thank Mr. Albert Chau for the excellent job done in coding my theory for simulation, and Mr. David Moore for assistance in the lab during the experimental phase of my work. I would also like to acknowledge Mr. Lee Bonnell from the National Optics Institute for many interesting discussions on the practical aspects of fiber design. Finally, I would like to cite Mr. David Clegg's contributions to the engineering and implementation aspects of my project. I highly value his technical advice and look forward to working with him in the future.

I would like to also acknowledge those graduate students who embarked on their studies with me in the fall of 1989. In particular, I would like to recognize Mr. Darren Blair for his many useful conversations and for his on-going friendship and support.

Finally, I would like to acknowledge the financial support and opportunities offered by the Alberta Telecommunication Research Center (now TR Labs), the National Science and Engineering Research Council, the Government of Alberta, and the University of Alberta. Without their generous support, this work would not have been possible.

Table of Contents

1.0 Introduction 1

2.0 Theory of Erbium-doped Fiber Amplifiers 6

2.1 Development of Erbium-Amplifier Equations 8

2.1.1 Stimulated Transition Cross-sections 8

2.2 Laser Rate Equations 10

2.2.1 Application of Analysis to Fiber 12

2.3 Equations for Signal and Pump Propagation 16

2.3.1 Pump Propagation Equation 16

2.3.2 Signal Propagation Equation 20

2.4 Analysis Including Amplified Spontaneous Emission 22

2.5 Interpretation of Results 26

2.5.1 Examination of Pump Equations 26

2.5.1.1 Small-Signal, Large Single-mode Pump 26

2.5.1.2 Small-Signal, Small Single-mode Pump 28

2.5.2 Examination of the Signal Equations 29

2.5.2.1 Small-Signal, Large Single-mode Pump 30

2.5.2.2 Small-Signal, Small Single-mode Pump 31

2.5.2.3 Large Signal Analysis 32

2.5.3 Pump Transparency Powers and Optimal Lengths 32

3.0 Adapting the Theory for Computer Simulation 37

3.1 Structure of Program and Scope of Results 39

3.1.1 Support Calculations 40

3.1.2 Numerical Methods 43

3.2 Simulation Capabilities 44

4.0 Simulation Study of EDFAs 46
4.1 Base Simulation Results 47
4.1.1 Signal Gain 48
4.1.2 Noise Figure 49
4.1.3 ASE Levels 51
4.1.4 Pump, Signal, and ASE Evolution vs. EDFA Length 53
4.1.5 Optimal Lengths 56
4.2 Variations From Base Design 57
4.2.1 Variation of Pump Absorption Cross-Section 57
4.2.2 Variation of Fluorescence Lifetime 59
4.2.3 Variation of Pump Modal Power Distribution (MPD) 59
4.2.4 Variation of Erbium Dopant Confinement 61
4.2.5 Variation of Signal Wavelength 64
4.3 Different Operating Conditions 66
4.3.1 Bi-directional Signaling 66
4.3.2 Bi-directional Pumping 69
4.4 Summary of Observations 73

5.0 Design of Erbium-doped Fiber Amplifiers 74
5.1 Design Variables 74
5.1.1 Fiber Core/Cladding Radius and Numerical Aperture 75
5.1.2 Erbium Dopant Profile and Concentration 80
5.1.3 Core Co-dopants 83
5.2 Design Submitted to NOI 86

6.0 Experimental Characterization of EDFAs 87
6.1 Computer Control of Experiments 87

6.2 Characteristics of EDFA Components 89
6.2.1 Pump Laser Characteristics 89
6.2.2 Signal Laser Characteristics 92
6.2.3 Optical Filters 93
6.2.4 Other Passive Optical Devices Used 94
6.3 Experimental Configurations 95
6.3.1 Measurement of Amplifier Gain (DC) 96
6.3.2 Measure of ASE Power Levels and Spectra 101
6.3.3 Measurement of EDFA Gain-modulation Frequency Response 106
6.3.4 Measurement of Residual Pump 110
6.3.5 Noise Figure 113
6.3.6 Other Measurements 115

7.0 An Application of EDFAs to FDM Transmission 116
7.1 Spectral Slicing 116
7.2 Theory for Multi-cavity Filters 117
7.2.1 Rouard's Treatment 118
7.2.2 S and T Matrix Method 121
7.3 Analysis of Transmission Result 124
7.3.1 Uncoupling of the Cavities 125
7.3.2 Resonant Behavior of a Three-cavity Filter 127
7.3.3 Linewidth of the Main Lobe 133
7.3.4 Suppression of Cavity One and Three Resonances 134
7.3.5 Highest Achievable Suppression 136
7.3.6 Non-Ideal Lengths 136
7.3.6.1 Changes in L1 or L3 137
7.3.6.2 Changes in L2 138

7.4 Conclusions About Design of Multi-cavity Filters 139

8.0 Conclusions 143

8.1 Future Directions 144

References 146

Appendix A: Comments on ASE Distributed Source Term 152

Appendix B: Splice Loss Calculations 155

Appendix C: Erbium Dopant Concentrations 158

Appendix D: Comments about Noise Figures 159

Appendix E: Sample LabVIEW™ Programs 164

Appendix F: Comments About S and T Matrices 175

List of Tables

Table 4.1 : Summary of Base Simulation Parameters 46

Table 4.2 : Comparison of Performance of Base Design with Increased Pump Absorption Cross-section Design 58

Table 4.3 : Comparison of Performance of Base Design with Designs with Modified Fluorescence Lifetimes 59

Table 4.4 : Comparison of Performance of Base Design with Designs with Modified Pump MPDs 61

Table 4.5 : Comparison of Performance of Base Design with Designs with Modified Erbium-dopant Confinements 63

Table 4.6 : Comparison of Performance of Base Design at 1.53 μm and 1.55 μm 65

Table 4.7 : Simulation Results for Forward/Backward-travelling Signals for the Base EDFA Design 67

Table 4.8 : Simulation Results from Base Design with -30 and -10 dBm Signal Inputs 67

Table 4.9 : Comparison of Performance of a Co-directionally Pumped Base Design with a Bi-directionally Pumped Base Design 70

Table 4.10 : Comparison of One Bi-directionally Pumped Amplifier with Two Configurations for a Co-directionally Pumped Amplifier Cascade 71

Table 5.1 : EDFA Design Parameters Submitted to NOI 85

Table 6.1 : Summary of Other Optical Devices Used 95

Table 6.2 : 3-dB Frequencies of Gain Modulation Response 109

Table 7.1 : Transmission Peaks Due to Cavity One and Three Resonances, and FWHM Linewidth of Main Resonance 132

Table 7.2 : Transmission Peaks and Main-lobe Linewidth for a 10 GHz Filter Design.....135

Table B.1 : Parameters Used in Splice Loss Calculations.....155

List of Figures

Figure 1.1 : Typical Configuration of a Fiber Optic Amplifier 2

Figure 2.1 : Conceptual picture illustrating the idea of atomic cross-sections 9

Figure 2.2 : General Three-Level Lasing Scheme 10

Figure 2.3 : Absorption and Emission Cross-sections for a Typical Al-silicate Erbium-doped Fiber 23

Figure 3.1 : Conceptual Flow Diagram of Simulation 39

Figure 3.2 : Conceptual Flow Diagram Illustrating the Technique Used to Calculate Fiber Modal Propagation Constants 42

Figure 4.1 : Conceptual View of Simulation Strategy 47

Figure 4.2 : Gain vs. Signal I/P Power for Various Pump I/P Power Levels 49

Figure 4.3 : Noise Figure vs. Signal I/P Power for Various Pump Power Levels 50

Figure 4.4(a) : Broadband ASE Power vs. Signal I/P Power for Various Pump Power Levels 52

Figure 4.4(b) : In-band ASE Power vs. Signal I/P Power for Various Pump Power Levels 52

Figure 4.5 : ASE Power Spectral Density Between 1.5 and 1.6 μm at L =14.7 m for a Pump of 25 mW and a Signal I/P of -40 dBm 45

Figure 4.6 : Signal and In-Band Forward- and Backward-travelling ASE Power (0.5 nm Bandwidth) vs. Amplifier Length (Total Length = 14.7 m, Pump = 25 mW) 54

Figure 4.7 : Residual Pump Power vs. Amplifier Length for Various Signal I/P Powers 55

Figure 4.8 : Residual Pump Power vs. Amplifier Length for Various Pump I/P Powers 56

Figure 4.9 : Optimal Amplifier Length vs. Signal I/P Power for Various Pump Power Levels 57

Figure 4.10 : Conceptual View of Constant-Concentration Confinement of Erbium Dopant 61

Figure 4.11 : Signal and Pump Evolution for Non-saturating Bi-directional Simulation -30/-30 68

Figure 4.12 : Signal and Pump Evolution for Saturating Bi-directional Simulation -10/-10 69

Figure 4.13 : Residual Pump Power vs. Amplifier Length for the Bi-directionally Pumped Base Design 70

Figure 4.14 : Signal and In-band (1 nm) ASE Evolution vs. Amplifier Length for the Bi-directionally Pumped Base Design 71

Figure 4.15 : Qualitative Summary of Parameter Variation Effects on Simulated Performance of Base EDFA Design 73

Figure 5.1 : Numerical Aperture Required for a Given Signal Mode-field Diameter as a Function of Core Radius from 2.0 to 5.0 μm 77

Figure 5.2 : Numerical Aperture Required for a Given Signal Mode-field Diameter as a Function of Core Radius from 1.0 to 2.0 μm 78

Figure 5.3 : Conceptual View of the Placement of Core Co-dopants 86

Figure 6.1 : Optical Pump Power vs. Drive Current for 980 nm Pump Device Oz #2 91

Figure 6.2 : Spectrum of DFB#1. Resolution = 0.20 nm, Power = -7.39 dBm, Modulated at 622 Mbits/s 92
Figure 6.3 : Experimental Configuration for DC Gain Measurement 99
Figure 6.4 : DC Gain vs. Signal I/P Power for Various Pump Drive Currents. EDFA = NOI3a, Laser = OZ#2 100
Figure 6.5 : Effectiveness of ASE Compensation Technique for DC Gain Measurements 100
Figure 6.6 : Experimental Configuration to Measure Backward-travelling ASE 101
Figure 6.7 : Total Forward- and Backward-travelling ASE and In-band Forward-travelling ASE (BW = 0.8 nm centered at 1550 nm) vs. Pump Drive Current. EDFA = NOI3a, Pump Laser = OZ#1 102
Figure 6.8 : Experimental Configuration to Measure Forward-travelling ASE Spectrum 103
Figure 6.9 : Forward and Backward-travelling ASE Spectra vs. Wavelength for EDFA NOI3a. Measurement Bandwidth = 0.9 nm 104
Figure 6.10 : Normalized Frequency Response of EDFA NOI3a for Given Signal I/P Powers 107
Figure 6.11 : Experimental Configuration for Measurement of EDFA Frequency Response 107
Figure 6.12 : Normalized Frequency Response (dB) for Various Small Signal I/P Powers 108
Figure 6.13 : Experimental Configuration to Measure Residual Pump Power 110
Figure 6.14 : Pump Power at the Input and Output of EDFA NOI3a; Pump Laser = Oz #2 111
Figure 6.15 : Estimated Average Pump Absorption in dB/m When No Signal and a Saturating Signal is Present; EDFA = NOI3a, Pump Laser = Oz#2 112

Figure 6.16 : Pump Laser Oz#2 Spectrum at the I/P to and O/P from EDFA NOI3a. Current = 160 mA, DFB Signal of -4.75 dBm Present 112

Figure 6.17 : Calculated Noise Figure for a Bi-directional Amplifier with Varying Reverse Signal Power Levels 114

Figure 7.1 : Conceptual View of the Operation of a Fabry-Perot Etalon 118

Figure 7.2 : Multi-layer Dielectric Stack with an Incident Field E_o and a Transmitted Field E_t 119

Figure 7.3 : Multi-stage Cascade of Two-port Networks 122

Figure 7.4 : T matrix Schematic of a Three-cavity, Four-mirror Fabry-Perot Filter 123

Figure 7.5 : Conceptual View of a "Triplet Structure" in the Vicinity of a Main Resonance 129

Figure 7.6 : Output Spectrum Corresponding to Cavity FSRs of 20, 100, and 25 GHz Respectively 131

Figure 7.8 : Transmission Characteristic of a Three-cavity Filter Designed for a 10 GHz FSR 141

Figure 7.9 : Detail of the Passband Region of the 10 GHz Filter 142

Figure B.1 : Splice Loss Between Flexcor and SMF-28 Fibers vs. Transverse Angular Offset (degrees) 156

Figure B.2 : Splice Loss Between Flexcor and SMF-28 Fibers vs. Fiber End Separation (μm) 156

Figure B.3 : Splice Loss Between Flexcor and SMF-28 Fibers vs. Transverse Core Separation (μm) 157

Figure F.1 : Schematic Representation of a Two-port Network 175

List of Abbreviations

AC	Alternating Current
AM	Amplitude Modulation
AR	Anti-Reflection
ASE	Amplified Spontaneous Emission
DC	Direct Current
DFB	Distributed Feedback
EDFA	Erbium-doped Fiber Amplifier
FDM	Frequency Division Multiplex(ing)
FM	Frequency Modulation
FOA	Fiber Optic Amplifier
FSR	Free Spectral Range
FTTH	Fiber-To-The-Home
FWHM	Full Width, Half Maximum
GPIB	General Purpose Interface Bus
I/O	Input/Output
LED	Light Emitting Diode
MPD	Modal Power Distribution
MTBF	Mean Time Before Failure
NA	Numerical Aperture
PIN	P-Intrinsic-N
PSD	Power Spectral Density
PTP	Pump Transparency Power
SFL	Super Fluorescent Laser
SNR	Signal-to-Noise-Ratio
SSQW	Strained, Single Quantum Well
VI	Virtual Instrument
VOA	Variable Optical Attenuator
VSB	Vestigial Side-band
WDM	Wavelength Division Multiplex(ing)

1.0 Introduction

The last ten to fifteen years have seen significant growth in both the understanding of optical fiber and its application to communications systems. A number of evolutionary steps in research focus have occurred, transforming the early 820 nm, multi-mode fiber designs to the current 1.3 μm low-dispersion and 1.5 μm low-attenuation single-mode fiber systems of today. Accompanying the improvements in physical design of optical fibers have been improvements in related technologies, such as optics and electronics, for lightwave transmitters and receivers. In addition, changes in conventional wisdom on the design of network architectures have also occurred and resulted in much engineering effort as the economics of fiber-to-the-home (FTTH) becomes more feasible.

A new revolution is occurring in lightwave-systems design. The use of optical amplifiers, both semiconductor and fiber-based, have further broadened the scope of possibilities for communications systems. Research in this area has exploded in the last two years, a strong testament to the potential of this field. Erbium-doped Fiber Amplifiers (EDFAs) in particular have commanded the overwhelming attention of both the research and business communities as practical, amplifier-based network possibilities evolve.

The fact that Erbium possesses optical transitions in the 1.55 μm window when in a silica-glass host has been known since 1965 [1]. However, this knowledge was not fully exploited until new techniques for the fabrication of low-loss, Rare-Earth-doped silica fibers were developed in 1985 and 1986 at the University of Southampton [2]. This coinicided with increased interest in the 1.55 μm window for low-loss fiber transmission, and was thus a significant development. Since that time, research has

shown that the new rare earth-doped fiber amplifier technology possesses a number of attractive features:

1. *High Gain* - Optical gains in the 40 dB range are typical.

2. *Low Noise* - Noise figures of 3 dB, the quantum limit for optical amplifiers, are achieved for 980 nm pumping schemes.

3. *Fiber Compatible* - A fiber-optic amplifier (FOA) works in the optical domain (therefore requiring no opto-electronic conversion), is simple, consisting of only a pump semiconductor laser, a wavelength division multiplexing element, to combine signals and the pump, and the length of amplifying fiber, and has low insertion loss.

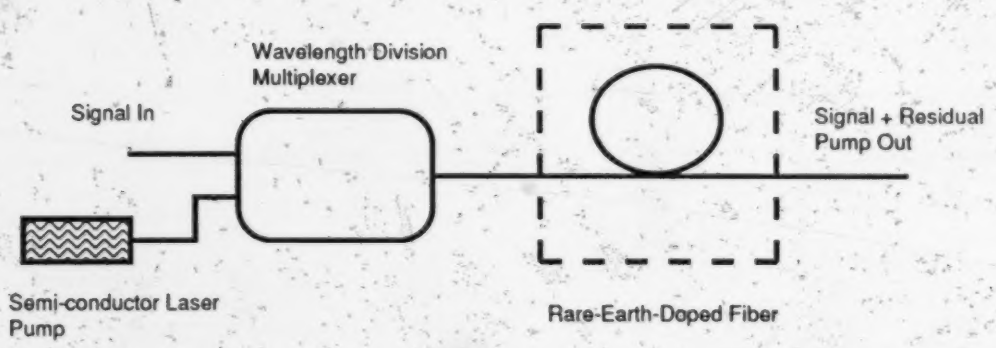

Figure 1.1 : Typical Configuration of a Fiber Optic Amplifier

4. *Wide Bandwidth* - The useable optical bandwidth over which gain can be achieved can be as high as 33 nm, making densely packed WDM (wavelength-division multiplexed) or even FDM (frequency-division multiplexed) networks possible [3].

5. *Polarization, Bit-Rate Insensitive* - So far, indications are that EDFAs are insensitive to polarization of optical signals, and multi-gigabit transmission rates are possible with no band-limiting effects.

6. *High Saturated Output Powers* - EDFAs are capable of high saturated output powers (defined as that output power that occurs when an amplified input signal results in a 3 dB reduction in gain from the small-signal value). Values of +19 dBm have been reported[4].

7. *Low Cross Talk* - EDFAs exhibit low signal cross-talk characteristics in WDM systems, even under saturated operating conditions, due largely to the long fluorescence and stimulated lifetimes of the upper lasing level.

8. *Low Pump Thresholds* - Fiber optical amplifiers in general require low pump powers to achieve appreciable gains, due largely to the confinement of pump and signal by the fiber guiding structure.

9. *Versatility of Application* - An EDFA can be used as a transmitter post-amplifier, as an in-line amplifier, or as a receiver pre-amplifier. In addition, distributed fiber amplifiers can be made, utilizing low

concentrations of dopant over long lengths of fiber for soliton applications.

Given these characteristics, it is not surprising that many field trials have been conducted using EDFAs; EDFAs will get their biggest test in the 2.4 Gbit/s TPC-5 submarine optical cable that will run from the United States to Japan in 1996. This cable will be constructed as a joint venture between AT&T and K.D.D. of Japan and will run 10,000 km. A typical EDFA repeater will cost an estimated $70,000, and the total repeater costs are estimated to be $6 million (U.S.). When this is compared to the TAT-8 cable constructed in 1988, where a six-fiber electronic repeater cost $800,000 and the entire system repeater cost for the 6,500 km cable totalled $100 million, the economic potential of EDFAs becomes dramatically apparent, as does the impetus for the fast transfer of laboratory research to the marketplace [5]. As well, it can be expected that EDFAs will appear in the future TAT-11 cable from the United States to the United Kingdom, as well as in fiber communications network installations and upgrades of archaic systems in Eastern Europe and the Soviet Union.

The work contained in this Thesis is part of the NSERC/BNR/TRLabs chair program directed by Dr. Jan Conradi at TR Labs (formerly, the Alberta Telecommunications Research Center) to explore high-speed optical networks. As part of this overall thrust, it was recognized that an understanding of the operation of EDFAs was essential as EDFAs form an integral part of many projects currently under way at TR Labs under the auspices of the Chair Program.

The Thesis is thus organised to largely reflect the historical progress made in the early development of a research program in the EDFA field. Chapter 2 discusses a fairly comprehensive model of an EDFA that attempts to maximize usefulness as both a tool to understand the dynamics of signal and pump propagation within an amplifier

and as an integral part of a design technique for EDFAs. Chapter 3 discusses how the theory was implemented in the form of a computer-based simulation, and chapter 4 explores some general results of simulation studies performed on EDFAs, with emphasis on the general characteristics of a particular EDFA that was designed as part of this work and subsequently produced at the National Optics Institute in Quebec City. Chapter 5 then proceeds from the conclusions of chapter 4 to explore some of the variables and trade-offs involved with the actual fiber design of EDFAs. Chapter 6 then discusses at length the laboratory infrastructure established at TR Labs for characterising EDFAs, and reports on the results of testing of a designed fiber. Chapter 7 then explores one proposed application under the Chair program of an EDFA in a FDM transmitter topology, and a complete theoretical analysis of a multi-cavity filter is conducted. Chapter 8 then concludes this document with some summary remarks and possible directions for future research, and is followed with a variety of supplemental Appendices.

2.0 Theory of Erbium-doped Fiber Amplifiers

A large number of theoretical studies of EDFAs have appeared in the last few years, motivated by the desire to pursue the limits of capability of such devices. At different times, studies focussed on different topics, such as small signal gains [6], evolution of amplified spontaneous emission (ASE) [7], noise figures, or pump effects, and assumptions appropriate to the particular subject of interest were made [8]. By early 1990, when the theory to be presented here was first developed, no completely satisfying model existed which encompassed a number of design parameters simultaneously while minimizing the number of assumptions being made. Since that time, a number of models similar in scope to the one about to be presented have been developed [9], [10], [11].[1]

The purpose of this theoretical study was to try to remove some of the simplifications made by other early models of EDFAs, allowing maximum flexibility for analysis of various parameters which affect EDFA performance. As well, the focus of the model developed was to enhance understanding of the *physical operation* of EDFAs, once the theory developed was converted into a simulation (See Chapter 3 and 4 for further comments). Some assumptions, also made by all other studies referenced, are listed below.

1) The pump is assumed to possess a *single longitudinal mode* around 980 nm. This means that the effect of multi-longitudinal moded pumps cannot be explored. Modifications could be made to include these effects, but since commercial pump sources available today are single-moded, complicating changes to the theory are not warranted.

1. Some models that have been developed, and were referenced extensively when the theory to be presented was developed, are by Armitage [6] and Desurvire [7] and [8]. Since that time, other models have appeared and are referenced in [9], [10], and [11].

2) *Homogeneous broadening* of the Erbium transitions is assumed. While some inhomogeneous broadening mechanisms do exist, amplifiers can be designed where homogeneous broadening dominates [12].[2] This assumption makes mathematical treatment of saturated regime operation simpler.

3) *Weakly-guiding fibers* are assumed. Typically, the fiber from which the amplifiers are made is single-mode at 1.55 μm, and has a core index which differs little from that of the cladding; therefore, use of the LP_{mn} notation developed by Gloge is possible [13].

4) *Excited state absorption* (ESA), where differences in energy equal to the pump photon energy (E3 - E1, as shown in Figure 2.2) exist between the upper lasing level, E2, and a higher level E4 (not shown), is assumed to be absent. This is a valid assumption when the popular pump wavelengths of 980 nm and 1480 nm are used.

5) The evolution is assumed to be *time-independent*. Only one group has attempted to model transient gain effects in EDFAs, and it was found that gain modulation was negligible for sinusoidal signal modulations above 5 kHz [14]. This was attributed to the slow response of the fiber amplifier's population inversion to high frequency changes in signal power level. Due to this slow response, it is felt that

2. A number of sources discuss broadening mechanisms. The consensus currently appears to be that inhomogeneous broadening effects accompany inclusion of Ge in the core, whereas predominantly Al co-doped cores appear to result in homogeneously broadened behavior in the EDFA. See, for example, reference [12].

steady-state modelling is sufficient to model higher bit-rate performance with negligible error. No further comments will be made, but examination of transient effects could form the basis for future work.

6) A simplified view of the *pump modal power distribution* (MPD) is assumed. Only reference [10] discusses the possibility that the pump may possess multiple fiber modes. It is assumed that the pump propagates in two fiber modes, and that the MPD *remains constant* for the entire transit through the fiber.[3] Ordinarily, mode coupling would be expected and power would shift amongst the modes present. This would then complicate the theory by requiring one propagation equation for each fiber pump mode, and would require modelling of power coupling coefficients between the constituent modes [15]. This will not be explored.

2.1 Development of Erbium-Amplifier Equations

2.1.1 Stimulated Transition Cross-sections

To start the analysis of EDFAs it is useful to begin with a preliminary discussion on stimulated transition cross-sections [16]. Consider a thin slab of material of cross section area A , thickness dz, and density N atoms/unit volume, as shown in Figure 2.1. Each atom within this slab can be thought of as having a "capture area", termed the *absorption cross-section* of σ_{12} cm^2, and a "radiating area", termed the *emission cross-section* of σ_{21} cm^2.

3. Standard telecommunication fiber has a *fiber V number* of about 3.33, which would suggest that two LP fiber modes could be present (See Chapter 3). Some designs of EDFAs will possess comparable V numbers, and thus provision for two LP fiber modes should be made.

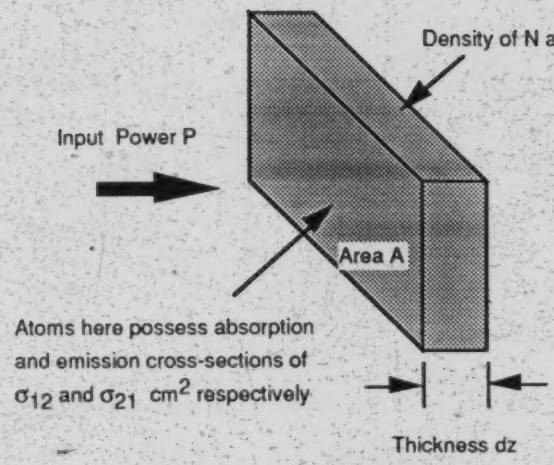

Figure 2.1 : Conceptual picture illustrating the idea of atomic cross-sections

When an incident beam of intensity I W/cm^2 impinges upon this slab, it is absorbed as follows:

$$dI = -\sigma_{12}N_1Idz \tag{2.1}$$

If emission occurs as well, then:

$$dI = \{\sigma_{21}N_2-\sigma_{12}N_1\}Idz \tag{2.2}$$

where

N_1 = the *ground level population* (corresponding to state E1 in Figure 2.2)

N_2 = the *upper lasing level population* (corresponding to state E2 in Figure 2.2)

and

$$N_1 + N_2 = N \tag{2.3}$$

It is assumed in eqn. 2.3 that Erbium behaves as a three - level laser, with the population of the third level, N_3, taken to be negligible. This is valid for the widely used 980 and 1480 nm pump bands.[4]

4. This assumption is used widely. See, for example, reference [8].

2.2 Laser Rate Equations

It can be seen from this preliminary analysis that expressions for N_1 and N_2 will be required to describe the propagation of both pump and signal fields in an EDFA. To determine these expressions, consider a general three-level lasing scheme, as illustrated in Figure 2.2 below:

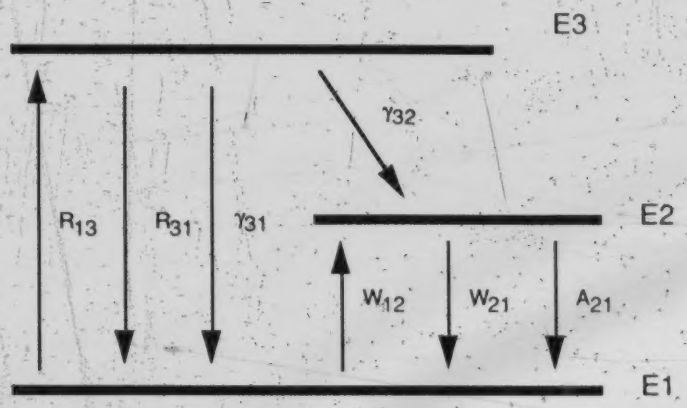

Figure 2.2 : General Three - Level Lasing Scheme

From Figure 2.2, the following terms are defined (all with units 1/s):

R_{13} = *pump absorption rate* between levels 1 and 3

R_{31} = *pump stimulated emission rate* between levels 1 and 3

γ_{31} = *spontaneous relaxation rate* from level 3 to level 1

γ_{32} = *spontaneous relaxation rate* from level 3 to level 2

W_{12}= *absorption rate* between level 1 and level 2

W_{21}= *stimulated emission rate* between level 2 and level 1

A_{21} = *spontaneous emission rate* between level 2 and level 1 (τ, used extensively later and termed the *fluorescence lifetime*, = $1/A_{21}$)

The generalized rate equations can now be written:

$$\frac{\partial N_1}{\partial t} = -(R_{13}+ W_{12})N_1 + (W_{21}+A_{21})N_2 + (\gamma_{31}+R_{31})N_3 \qquad (2.4)$$

$$\frac{\partial N_2}{\partial t} = W_{12}N_1 - (W_{21}+A_{21})N_2 + \gamma_{32}N_3 \qquad (2.5)$$

$$\frac{\partial N_3}{\partial t} = R_{13}N_1 - (\gamma_{32}+\gamma_{31}+R_{31})N_3 \qquad (2.6)$$

Knowing that N_3 is small, and using the fact that γ_{32} is large (a quick non-radiative relaxation from the pump level to the upper lasing level is desirable) and R_{31} is very small [8], expressions for N_1 and N_2 in *steady state* are now sought (Recall the brief introductory discussion about time-dependence). Setting all time derivatives to zero in eqns 2.4 to 2.6, the following expressions can be written:

$$N_1 = N\left[\frac{W_{21}\tau + 1}{(W_{21} + W_{12})\tau + R_{13}\tau + 1)}\right] \qquad (2.7)$$

$$N_2 = N\left(\frac{(W_{12}+R_{13})\tau}{(W_{21} + W_{12})\tau + R_{13}\tau + 1)}\right) \qquad (2.8)$$

$$= N - N_1$$

2.2.1 Application of Analysis to Fiber

Equations for R_{13}, W_{12}, and W_{21} in terms of the pump and signal modal characteristics in a fiber must now be determined. Using cylindrieal coordinates to describe the fiber, the expressions are [8], [17]:[5]

$$W_{21} = \frac{I_{sig}(r,\theta,z,\nu_s)}{I_{21}^{sat}(\nu_s)\tau} = \frac{\sigma_{21}(\nu_s)}{h\nu_s} I_{sig}(r,\theta,z,\nu_s) \tag{2.9}$$

$$W_{12} = \frac{I_{sig}(r,\theta,z,\nu_s)}{I_{12}^{sat}(\nu_s)\tau} = \frac{\sigma_{12}(\nu_s)}{h\nu_s} I_{sig}(r,\theta,z,\nu_s) \tag{2.10}$$

$$R_{13} = \frac{I_p(r,\theta,z,\nu_p)}{I_{pth}(\nu_p)\tau} = \frac{\sigma_{13}(\nu_p)}{h\nu_p} I_p(r,\theta,z,\nu_p) \tag{2.11}$$

where

$I_p(r,\theta,z,\nu_p)$ = the *propagating pump intensity* at frequency ν_p (corresponding to 980 nm as an example); note that the pump could possess multiple *longitudinal* modes, but as mentioned earlier, will be assumed to be single-moded.

$I_{sig}(r,\theta,z,\nu_s)$ = the *propagating signal intensity* at frequency ν_s (corresponds to signals in the 1.55 μm range, for instance). This term will also be modified in Section 2.4 to model amplified spontaneous emission (ASE)

$I_{pth}(\nu_p)$ = the *pump threshold intensity*, and is given by [7]:

$$I_{pth}(\nu_p) = \frac{h\nu_p}{\sigma_{13}(\nu_p)\tau} \tag{2.12}$$

---

5. The first relation in eqns. 2.9 - 2.11 is nomenclature used consistently by Desurvire and appears, for example, in reference [8]. The second relation is a more classical expression, and is seen in reference [17].

$I_{12}^{sat}(\nu_s)$ represents the *signal absorption saturation intensity* [8]:

$$I_{12}^{sat}(\nu_s) = \frac{h\nu_s}{\sigma_{12}(\nu_s)\tau} \tag{2.13}$$

and, $I_{21}^{sat}(\nu_s)$ represents the *signal emission saturation intensity*: [8]:

$$I_{21}^{sat}(\nu_s) = \frac{h\nu_s}{\sigma_{21}(\nu_s)\tau} \tag{2.14}$$

For propagation of pump and signal modes in a fiber, it is assumed that a weakly-guiding, step - index structure exists, i.e. the index difference between the core and the cladding $n_{core} - n_{clad}$ is assumed small. Doing this allows description of the propagating modes using LP_{mn} notation, as mentioned in Section 2.0, and $I_p(r,\theta,z,\nu_p)$ and $I_{sig}(r,\theta,z,\nu_s)$ can be written as:

$$\begin{aligned} I_p(r,\theta,z,\nu_p) &= [\{(1-\eta)t_{p\,01}\Psi_{01}^2(r,\nu_p)\}+\{\eta t_{p\,11}\Psi_{11}^2(r,\nu_p)\}\cos^2(\theta)]P_p(z) \\ &= F(r,\theta,\nu_p)P_p(z) \end{aligned} \tag{2.15}$$

$$\begin{aligned} I_{sig}(r,\theta,z,\nu_s) &= \{t_{s\,01}\Psi_{01}^2(r,\nu_s)\}P_{sig}(z) \\ &= G(r,\nu_s)P_{sig}(z) \end{aligned} \tag{2.16}$$

where, for $r < a$:

$$\Psi_{01}^2(r,\nu_i) = J_0^2\left(\frac{u_{01i}r}{a}\right) \tag{2.17a}$$

$$\Psi_{11}^2(r,\nu_i) = J_1^2\left(\frac{u_{11i}r}{a}\right), \tag{2.17b}$$

and, for $r > a$:

$$\Psi_{01}^2(r,\nu_i) = [\frac{J_0^2(u_{01i})}{K_0^2(\gamma_{01i})}]K_0^2(\frac{\gamma_{01i}r}{a}) \qquad (2.18a)$$

$$\Psi_{11}^2(r,\nu_i) = [\frac{J_1^2(u_{11i})}{K_1^2(\gamma_{11i})}]K_1^2(\frac{\gamma_{11i}r}{a}) \qquad (2.18b)$$

and where

$P_{sig}(z)$ and $P_p(z)$ are the *signal and pump powers* at a given point z within the amplifier, ($P_{sig}(z)$ will later be interpreted as a power spectral density when ASE analysis is included),

u_{01i}, γ_{01i}, u_{11i}, γ_{11i} are the *transverse propagation constants* for the LP_{01} and LP_{11} fiber modes (see reference [15], p. 34),

$J_0(x)$, $J_1(x)$ are *Bessel functions of the first kind of order 0 and 1*, respectively,

$K_0(x)$, $K_1(x)$ are *Bessel functions of the second kind of order 0 and 1*, respectively,

a is the *fiber core radius*,

η models the pump *modal power distribution* (recall that two pump fiber modes are assumed), and

$t_{s\,01}$ and $t_{p\,mn}$ are *fiber modal normalization constants*, given by:

$$t_{s\,01} = \frac{1}{2\pi\int_0^\infty \Psi_{01}^2(r,\nu_s)\, r\,dr} \qquad (2.19a)$$

$$t_{p\,mn} = \frac{1}{\int_0^\infty\int_0^{2\pi} \Psi_{mn}^2(r,\nu_p)\cos^2(m\theta)\, d\theta\, r\,dr} \qquad (2.19b)$$

ν_s and ν_p are the pump and signal frequencies, and "mn" in eqn 2.19b will correspond to "01" for the LP_{01} pump fiber mode, and "11" for the LP_{11} pump fiber mode (if present). Note also in eqns. 2.19a-b that an elemental area is given by $rdrd\theta$, consistent with the choice of cylindrical coordinates for modelling this problem. From eqns. 2.15, 2.16, and 2.19, it can be seen that :

$$\int_0^{\infty}\int_0^{2\pi} I_p(r,\theta,z,\nu_p)d\theta rdr = P_p(z) \tag{2.20a}$$

$$\int_0^{\infty}\int_0^{2\pi} I_{sig}(r,\theta,z,\nu_s)d\theta rdr = P_{sig}(z) \tag{2.20b}$$

A few comments are in order. First of all, the term η is normally determined by the launch conditions from the pump into the fiber and models the amount of power in each of the two LP modes. Noting that the LP_{01} mode actually represents two modes of orthogonal polarization, and that the LP_{11} mode represents four modes (two modes with two orthogonal polarizations), $\eta = 4/6$ or $2/3$ corresponds to equal excitation of all modes, and represents the most multi-moded pump. As discussed in Section 2.0, the modal power distribution is assumed to be constant. In addition, only one equation will be used to model the total pump power as a function of z, where no coupling of fiber modes is assumed [10]. Finally, the frequency dependence of the fiber modal profiles described in eqns. 2.17 and 2.18 arises from the dependence of the transverse fiber modal propagation constants on wavelength; thus, the propagation constants must be evaluated separately at the signal and pump wavelengths.[6]

---

6. See Figure 3.2 in section 3.1.1 for more information on calculation of these propagation constants.

2.3 Equations for Signal and Pump Propagation

In the previous section, use of $P_{sig}(z)$ and $P_p(z)$ was introduced. This was done because these terms depend only on z and lend themselves better to the study of pump or signal propagation than intensities would. Therefore, proceeding from eqns. 2.1, 2.2, and 2.20, the following equations may be written:

$$\frac{\partial P_p}{\partial z} = -\int_0^{\infty}\int_0^{2\pi} \sigma_{13}(\nu_p)N_1(r,\theta,z,\nu)I_p(r,\theta,z,\nu_p)d\theta r dr \tag{2.21}$$

and

$$\frac{\partial P_{sig}}{\partial z} = \int_0^{\infty}\int_0^{2\pi} \{\sigma_{21}(\nu_s)N_2(r,\theta,z,\nu) - \sigma_{12}(\nu_s)N_1(r,\theta,z,\nu)\}I_{sig}(r,\theta,z,\nu_s)d\theta r dr \tag{2.22}$$

Eqns. 2.21 and 2.22 will now be explored in detail.

2.3.1 Pump Propagation Equation

The differential equation describing pump propagation in eqn. 2.21 can be rewritten as follows:

$$\frac{\partial P_p}{\partial z} = -\gamma_p(z, \nu_p)P_p \tag{2.23}$$

where $\gamma_p(z,\nu_p)$ will be interpreted as the *pump absorption coefficient* with units of 1/length. Substituting eqn 2.7 and 2.15 into eqn. 2.21 implies that $\gamma_p(z,\nu_p)$ is given by:

$$\gamma_p(z,\nu_p) = \int_0^{\infty}\int_0^{2\pi} \sigma_{13}(\nu_p)N_t n(r)N_1'(r,\theta,z,\nu)F(r,\theta,\nu_p)d\theta r dr \tag{2.24}$$

where the following expression has been used:

$$N_1(r,\theta,z,\nu) = N_t n(r)N_1'(r,\theta,z,\nu) \tag{2.25}$$

N_t is the *total number of Erbium ions in a given unit volume* (usually taken to be a cubic cm), and n(r) models the *radial dependence* of this concentration. Here, n(r) will be taken to be[7]:

$$\begin{aligned} n(r) &= 1, \text{ for } r < a/w \\ &= 0, \text{ otherwise} \end{aligned} \tag{2.26}$$

The parameter w is used to model the confinement of the Erbium within the core. $N_1'(r,\theta,z,\nu)$ in eqn. 2.25 models the spatial dependence of the population of level one, and may be rewritten using eqns. 2.7, 2.9-2.11, 2.15, and 2.16 to yield:

$$N_1'(r,\theta,z,\nu) = \frac{\left[\frac{P_{sig}(z)}{P_{21}^{sat}(\nu_s)}\Psi_{01}^2(r,\nu_s)+1\right]}{\frac{P_{sig}(z)}{P_{sat}^{*}(\nu_s)}\Psi_{01}^2(r,\nu_s) + P_p(z)\left\{\frac{(1-\eta)}{P_{pth}^{01}(\nu_p)}\Psi_{01}^2(r,\nu_p) + \frac{\eta}{P_{pth}^{11}(\nu_p)}\Psi_{11}^2(r,\nu_p)\cos^2(\theta)\right\} + 1} \tag{2.27}$$

where the following definitions are used:

---

7. This is chosen based on examination of actual Erbium-dopant profiles as determined by the National Optics Institute (NOI) (See Chapter 5), and a flat profile is typically used in the literature. See, for example, references [6] and [7].

$$P_{21}^{sat}(\nu_s) = I_{21}^{sat}(\nu_s)\{\pi\omega_s^{01 2}\} \tag{2.28a}$$

$$P_{12}^{sat}(\nu_s) = I_{12}^{sat}(\nu_s)\{\pi\omega_s^{01 2}\} \tag{2.28b}$$

$$P_{sat}^{*} = \frac{P_{21}^{sat}P_{12}^{sat}}{P_{21}^{sat} + P_{12}^{sat}} \tag{2.28c}$$

$$P_{pth}^{01} = I_{pth}(\nu_p)\{\pi\omega_p^{01 2}\} \tag{2.28d}$$

$$P_{pth}^{11} = I_{pth}(\nu_p)\{\pi\omega_p^{11 2}\} \tag{2.28e}$$

The various ω terms in eqn. 2.28 can be thought of as *effective modal spot sizes*, and are related to the fiber modal normalization constants by:

$$t = \frac{1}{\pi\omega^2} \tag{2.29}$$

Notice that the normalization constant using the Gaussian description of the LP_{01} mode is given by eqn. 2.29 if ω is interpreted as the *field modal spot-size* [18]. It must also be acknowledged that a mode spot-size as such does not really exist for the LP_{11} mode, due to its azimuthal variations.

In addition, it is useful to introduce the expressions in eqn. 2.28 because the values of $P_{sig}(z)$ and $P_p(z)$ in eqn. 2.27 are now "normalized" to terms with units of power. Eqn. 2.27 can, however, still be written in terms of intensities due to the choice of normalization factors made in eqns. 2.19 and 2.29, if this is desired.

As a final comment on eqn. 2.27, note the dependency of N_1' on z is due to the terms $P_{sig}(z)$ and $P_p(z)$. Thus, $\gamma_p(z,\nu_p)$ is taken as a function of z by virtue of the implicit dependence it has on $P_{sig}(z)$ and $P_p(z)$. As well, due to dependencies on ν_s and

ν_p, the subscript on ν in the argument of N_1' has been dropped to reflect a general frequency dependence. This will also be done for γ_p.

Before continuing with the analysis, it is useful to collect terms in the eqn. 2.27 and write them in terms of more compact, defined functions as follows:

$$E_{21}(r,z,\nu_s) = 1 + \frac{P_{sig}(z)}{P_{21}^{sat}(\nu_s)}\Psi_{01}^2(r,\nu_s) \tag{2.30a}$$

$$E_{12}(r,z,\nu_s) = 1 + \frac{P_{sig}(z)}{P_{12}^{sat}(\nu_s)}\Psi_{01}^2(r,\nu_s) \tag{2.30b}$$

$$E(r,z,\nu_s) = 1 + \frac{P_{sig}(z)}{P_{sat}^{*}(\nu_s)}\Psi_{01}^2(r,\nu_s) \tag{2.30c}$$

$$C_0(r,z,\nu_p) = \frac{(1-\eta)P_p(z)}{P_{pth}^{01}(\nu_p)}\Psi_{01}^2(r,\nu_p) \tag{2.30d}$$

$$C_1(r,z,\nu_p) = \frac{\eta P_p(z)}{P_{pth}^{11}(\nu_p)}\Psi_{11}^2(r,\nu_p) \tag{2.30e}$$

The expression for $N_1'(r,\theta,z,\nu)$ in eqn. 2.27 then becomes:

$$N_1'(r,\theta,z,\nu) = \frac{E_{21}(r,z,\nu_s)}{E(r,z,\nu_s)+C_0(r,z,\nu_p)+C_1(r,z,\nu_p)\cos^2(\theta)} \tag{2.31}$$

The next step in simplifying eqn. 2.24 is to evaluate the integral over θ; this can be done with the help of the following expression found in integral tables:

$$\int_0^{\pi} \frac{A + B\cos^2(\theta)}{C + D\cos^2(\theta)}d\theta = 2\pi\left[\frac{B}{D} + \left(A - \frac{BC}{D}\right)\frac{1}{\sqrt{C(C+D)}}\right] \tag{2.32}$$

Applying this result to the integration required in eqn. 2.24 results in the final expression for $\gamma_p(z,\nu_p)$:

$$\gamma_p(z,\nu) = 2\pi\sigma_{13}(\nu_p)N_t\int_0^\infty n(r)\left[\Gamma_{01}(r,z,\nu)t_{p\,01}\Psi_{01}^2(r,\nu_p) + \Gamma_{11}(r,z,\nu)t_{p\,11}\Psi_{11}^2(r,\nu_p)\right]rdr \tag{2.33}$$

Eqn. 2.33 can be interpreted as an *overlap integral* in r between the Erbium dopant profile and the fiber pump modes. Γ_{01} and Γ_{11} are interpreted as *spatial modifiers of the pump fiber modes* and are given by[8]:

$$\Gamma_{01}(r,z,\nu) = \frac{(1-\eta)E_{21}(r,z,\nu_s)}{D(r,z,\nu)} \tag{2.34a}$$

$$\Gamma_{11}(r,z,\nu) = \frac{\eta E_{21}(r,z,\nu_s)}{C_1(r,z,\nu_p)}\left[1 - \frac{E(r,z,\nu_s)+C_0(r,z,\nu_p)}{D(r,z,\nu)}\right] \tag{2.34b}$$

$$D(r,z,\nu) = \sqrt{[E(r,z,\nu_s) + C_0(r,z,\nu_p)][E(r,z,\nu_s)) + C_0(r,z,\nu_p) + C_1(r,z,\nu_p)]} \tag{2.34c}$$

2.3.2 Signal Propagation Equation

The equations for signal propagation will now be considered. Ignoring ASE for the moment, a generalized equation for signal propagation can be written from eqn. 2.22:

$$\frac{\partial P_{sig}}{\partial z} = \{\gamma_e(z, \nu_s) - \gamma_a(z, \nu_s)\}P_{sig} \tag{2.35}$$

8. Note that the product $\Gamma\Psi^2$ could then be interpreted as the *effective fiber-mode shape*.

where $\gamma_e(z,\nu_s)$ and $\gamma_a(z,\nu_s)$ are interpreted as the *signal emission and absorption coefficients*, respectively. Following the development of the previous section, the coefficients here are given by:

$$\gamma_a(r,\nu_s) = \int_0^{\infty}\int_0^{2\pi} \sigma_{12}(\nu_s)N_t n(r)N_1'(r,\theta,z,\nu)G(r,\nu_s)d\theta r dr \tag{2.36}$$

$$\gamma_e(r,\nu_s) = \int_0^{\infty}\int_0^{2\pi} \sigma_{21}(\nu_s)N_t n(r)N_2'(r,\theta,z,\nu)G(r,\nu_s)d\theta r dr \tag{2.37}$$

where, using eqn. 2.8, and eqn. 2.30:

$$N_2'(r,z,\nu) = \frac{C_o(r,z,\nu_p) + C_1(r,z,\nu_p)\cos^2(\theta) + E_{12}(r,z,\nu_s) - 1}{E(r,z,\nu_s) + C_o(r,z,\nu_p) + C_1(r,z,\nu_p)\cos^2(\theta)} \tag{2.38}$$

Continuing in a manner analogous to the development of the previous section yields the following expressions for the signal absorption and emission coefficients:

$$\boxed{\gamma_e(z,\nu) = 2\pi\sigma_{21}(\nu_s)N_t\int_0^{\infty} n(r)\Gamma_e(r,z,\nu)t_0\Psi_{01}^2(r,\nu_s)rdr} \tag{2.39}$$

$$\boxed{\gamma_a(z,\nu) = 2\pi\sigma_{12}(\nu_s)N_t\int_0^{\infty} n(r)\Gamma_a(r,z,\nu)t_0\Psi_{01}^2(r,\nu_s)rdr} \tag{2.40}$$

where eqns. 2.39 and 2.40 are interpreted as *overlap integrals* in r between the Erbium dopant profile and the fiber signal mode. Γ_a and Γ_e are interpreted as *spatial modifiers of the signal fiber mode* and are given by:

$$\Gamma_e(r,z,\nu) = \left[1 + \frac{E_{21}(r,z,\nu_s) - 1}{D(r,z,\nu)} \right] \tag{2.41a}$$

$$\Gamma_a(r,z,\nu) = \frac{E_{21}(r,z,\nu_s)}{D(r,z,\nu)} \tag{2.41b}$$

2.4 Analysis Including Amplified Spontaneous Emission

The equations for the absorption and emission coefficients developed in the previous sections assume only one propagating "signal" component at a frequency ν_s due to stimulated transitions between levels E2 and E1 (See Figure 2.2). The energy levels conceptually represented by E2 and E1 in fact are significantly broadened by effects such as photon broadening and Stark Splitting, and thus a number of transitions at different wavelengths can occur [19]. This gives rise to the concept of a *line-shape*, which in-turn can be related to the absorption and emission cross-sections discussed earlier in this chapter.[9]

If the absorption and emission cross-sections for a given fiber are available as a function of frequency (or, more commonly, wavelength, as shown in Figure 2.3) in the vicinity of the 1.53 μm transition, then an analysis including ASE can be done. In general, spontaneous emission will result in randomly phased, incoherent radiation travelling in any direction. It is only that radiation which is travelling in the "right" direction i.e. roughly paraxially, that will couple effectively into a propagating mode.

9. See also Appendix A for relations between line-shape and the stimulated cross-sections.

Just how this happens, and what a good estimate is for the "coupling efficiency" of spontaneously emitted photons into a guided fiber mode, will be considered in Appendix A [20], [21], [22].[10] However, simple geometric analysis based on ray tracing in spherical coordinates seems to suggest that perhaps 0.1 - 0.5% of the light might be coupled, leaving the vast majority of the spontaneous emission either absorbed in the fiber or exiting through the cladding and jacket.[11]

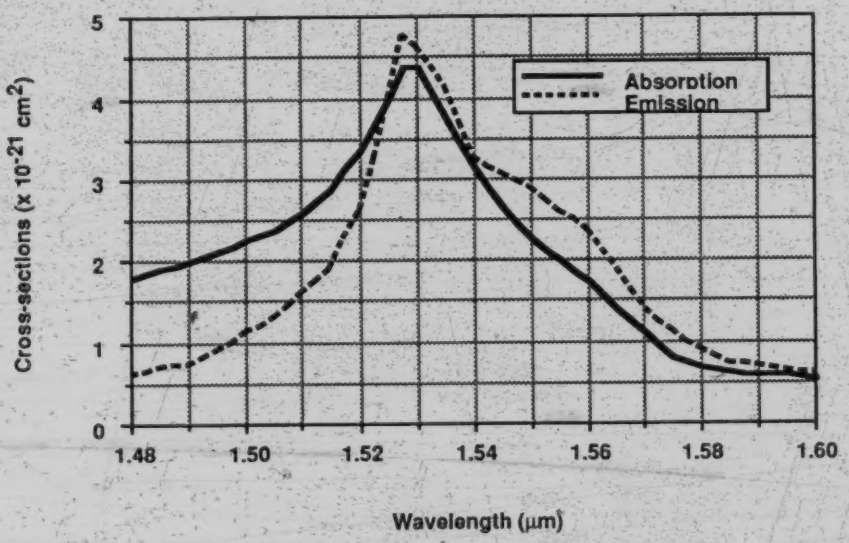

Figure 2.3 : Absorption and Emission Cross-sections for a Typical Al-silicate Erbium-doped Fiber. After reference [10]

The effect of ASE can be included by modifying the signal and pump equations as follows. First, the $P_{sig}(z)$ term must be modified to represent either a *forward- or backward-travelling* component whose *power spectral density* at a frequency $\nu_i \pm \Delta\nu/2$ is given by $P_s^+(z,\nu_i)$ or $P_s^-(z,\nu_i)$, where the frequencies are selected by sampled points

10. Some papers which deal with the subject of coupling incoherent radiation into fibers appear in references [20] and [21]. Of more topical significance is reference [22].
11. With this in mind, perhaps this spontaneously emitted, uncoupled light could be detected by a high sensitivity detection scheme. If, for example, the gain of the EDFA was modulated through modulation of the pump, the resulting AC-modulated spontaneous emission could then be detected via lock-in amplifier detection techniques.

of the cross-section data.[12] Thus the equations of the previous section must be modified so that:

$$P_{sig}(z) \rightarrow \sum_i P_s^{\pm}(z,\nu_i)\Delta\nu \tag{2.42}$$

Clearly, the smaller $\Delta\nu$ is made the more accurate the result, until, in the limit, eqn. 2.42 would become an integral. However, as will be noted in Chapter 3, there is a trade-off between fineness of the grid of cross-sections and computation time required. Also note that the expressions for the various P_{sat} terms are now all frequency dependent, and must be evaluated for each ν_i. Thus:

$$E_{21}(r,z,\nu) = 1 + \sum_i \frac{P_s^{\pm}(z,\nu_i)}{P_{21}^{sat}(\nu_i)}\Delta\nu\Psi_{01}^2(r,\nu_s) \tag{2.43a}$$

$$E_{12}(r,z,\nu) = 1 + \sum_i \frac{P_s^{\pm}(z,\nu_i)}{P_{12}^{sat}(\nu_i)}\Delta\nu\Psi_{01}^2(r,\nu_s) \tag{2.43b}$$

$$E(r,z,\nu) = 1 + \sum_i \frac{P_s^{\pm}(z,\nu_i)}{P_{sat}^{*}(\nu_i)}\Delta\nu\Psi_{01}^2(r,\nu_s) \tag{2.43c}$$

Note that although each component in the summation has a different frequency and thus would have a different modal envelope, (i.e. $\Psi_{01}^2(r,\nu_i)$ should be evaluated for each frequency), the differences in practice are small and will be ignored. Thus, the fiber modal envelope will only be evaluated for one frequency within the transition band, and will then be applied to all components. Also note that the frequency dependence of the

12. The convention used here and throughout this thesis is to denote signals and/or ASE travelling from z = 0 to z = L, i.e. in the positive z direction, as "forward-travelling". All signals and/or ASE travelling from z = L to z = 0, i.e. in the negative z direction, are termed "backward travelling". If a signal is present and the pump propagates in the same direction as the signal, the configuration is said to be "co-directionally pumped"; if the signal and pump travel in opposite directions, then the configuration is said to be "contra-directionally pumped".

various E functions above is generalized to reflect the broadband nature of the emission. Eqn. 2.35, modified to include ASE, is now given by:

$$\frac{\partial P_s^{\pm}(z,\nu_i)}{\partial z} = \pm\left\{[\gamma_e(z,\nu) - \gamma_a(z,\nu)]P_s^{\pm}(z,\nu_i) + \gamma_e(z,\nu)P_o(\nu_i)\right\} \qquad (2.44)$$

where the plus sign applies for forward-travelling ASE (and signal components if present), the minus sign applies for backward-travelling ASE (and signals if present), and $P_o(\nu_i)$ is a distributed source term used as a seed for the generation of the ASE terms. More discussion of this will follow in Chapter 3 and Appendix A. Its value is given by:[13]

$$P_o(\nu_i) = 2h\nu_i \quad \text{W/Hz} \qquad (2.45)$$

The source term represents a spectral density of one photon per unit bandwidth, with the factor of two accounting for both LP_{01} polarizations.[14] As a final comment, if K sample points of the cross-section data were available, then eqn. 2.44 actually represents 2K coupled equations requiring 2K boundary value specifications (one equation and boundary value for each forward- or backward travelling component). If no signals are injected into the amplifier, all boundary values are zero, and only ASE is generated within the amplifier. A signal input is simulated by a non-zero boundary

---

13. Here, ASE generation is attributed to a distributed source term Po where the boundary value P(0) for forward travelling ASE and P(L) for backward travelling ASE are equal to zero (there are no external sources for this noise). This is the most physically appealing description of the problem, since spontaneous emission does occur along the entire length of the optical amplifier. Alternatively, the ASE can be modelled with an equivalent input power that will generate the same amount of output power in an ideal amplifier as the distributed source would. Some good references for both methods are [17], pp. 543, and [23]
14. It is interesting to note eqn. 2.47 also relates to the minimum signal input spectral density required in a shot-noise-limited heterodyne optical receiver in order to achieve a SNR of 1. This is termed the *quantum limit*, and is due to unavoidable shot noise in a photodetector, or can alternatively be attributed to the particle nature of light and the randomness of photon arrival times at the detector, which is assumed to follow a Poisson distribution. See also reference [17], pp. 355

value at a given frequency, but note that ASE will still be generated at that frequency, and the resultant solution to eqn 2.44 at that frequency will consist of both signal *and* ASE.[15]

2.5 Interpretation of Results

Having now amassed the theory describing the propagation of pump and signals in an EDFA, it is now of interest to stand back and make some simplifying assumptions in order to enhance physical understanding of the problem and to make predictions of performance.

2.5.1 Examination of Pump Equations

One of the first observations that can be made by examining eqn. 2.33 is that since the pump absorption coefficient γ_p is not constant, the solution to eqn. 2.23 cannot be an exponential. It is then interesting to explore some limiting cases to see what the functional form of some "partial solutions" to eqn. 2.23 might be.

2.5.1.1 Small-Signal, Large Single-mode Pump

For the first analysis, it will be assumed that operation is in the small-signal regime and that the pump possesses only the LP_{01} fiber mode, either due to fiber geometry or launch conditions, and possesses a high initial power. Therefore:

$$E_{21} = E_{12} = E \approx 1 \quad \text{(small-signal analysis)} \tag{2.46a}$$

$$\eta = 0 \quad \text{(single-mode pump)} \tag{2.46b}$$

$$\frac{P_p(0)}{P_{pth}^{01}(\nu_p)} >> 1 \quad \text{(high initial pump power), such that :}$$

15. Techniques for solving these equations will be discussed in chapter 3.

$$C_0(r,z,\nu_p) + 1 = C_0(r,z,\nu_p) \tag{2.46c}$$

Eqns. 2.34a and 2.34b then become:

$$\boxed{\Gamma_{01}(r,z,\nu) = \frac{1}{P_p(z)/P_{pth}^{01}(\nu_p)}} \tag{2.47a}$$

$$\boxed{\Gamma_{11}(r,z,\nu) = 0} \tag{2.47b}$$

Now, the expression for γ_p becomes:

$$\boxed{\gamma_p(z,\nu_p) = \frac{2\pi\sigma_{13}(\nu_p)N_t t_{p\,01}P_{pth}^{01}(\nu_p)}{P_p(z)}\int_0^\infty n(r)rdr} \tag{2.48}$$

Using eqn. 2.48 in eqn. 2.23 results in:

$$\boxed{\frac{\partial P_p}{\partial z} = \text{-constant}} \tag{2.49}$$

It can thus be said that a nearly single-moded, high-initial-power pump will decay linearly over amplifier length when the net signal and ASE power spectral density are small. This is observed in simulation data and has been reported in other sources [24], [7].

2.5.1.2 Small-Signal, Small Single-mode Pump

It is now natural to explore the case where the pump power is low. In order to validate the assumptions to be made here, the length of the amplifier would have to be much greater than optimum design would dictate, so that the pump power is much less than the *Pump Transparency Power* (PTP) (See Section 2.5.3). Presumably, since the pump is very small, the combined signal and ASE power spectral density will also be relatively small due to absorption. Thus, the approximations of eqn. 2.46 will still apply, with the following exception:

$$\frac{P_p(z >> L)}{P_{pth}^{01}(\nu_p)} << 1 \tag{2.50}$$

From eqns. 2.46 and 2.50, it follows that:

$$\boxed{\Gamma_{01}(r,z,\nu) = 1} \tag{2.51a}$$

$$\boxed{\Gamma_{11}(r,z,\nu) = 0} \tag{2.51b}$$

and the expression for γ_p becomes:

$$\boxed{\gamma_p(\nu_p) = 2\pi\sigma_{13}(\nu_p)N_t\int_0^\infty n(r)t_{p\,01}\Psi_{01}^2(r,\nu_p)rdr} \tag{2.52}$$

The pump propagation equation then becomes:

$$\boxed{\frac{\partial P_p}{\partial z} = -\gamma_p(\nu_p)P_p} \tag{2.53}$$

which implies an exponential decay of the pump.

2.5.2 Examination of the Signal Equations

As was the case with the pump equations, the signal equations 2.35, 2.39, and 2.40 suggest that signal evolution is also not exponential. This is to be expected for an amplifier whose operation is governed by three-level lasing mechanisms. Length of the amplifier, hitherto not considered in depth, becomes a critical element in the solution of the equations and strongly impacts the signal evolution. A pump travelling co-directionally with a signal will eventually be attenuated to the point where the EDFA can no longer supply gain and begins to re-absorb the signal. The point z = L beyond which signal re-absorption would occur determines the *optimal length* for the EDFA.[16] Graphical exploration of these points will appear in Chapter 4.

It is thus expected that for an optimally designed amplifier with either co- or contra-directional pumping, that:[17]

$$\frac{\partial P^{+}_{sig}}{\partial z} \geq 0$$

$$\frac{\partial P^{-}_{sig}}{\partial z} \leq 0 \qquad (2.54)$$

where equality holds only at z = L, the optimum length, for both cases above. Clearly, the above discussion reveals that a strictly exponential growth of signals in the amplifier should not be expected. It will be interesting, however, to examine the two special

16. Amplifier lengths greater than the optimal length result in lower net gain due to re-absorption, while lengths shorter than the optimal length also result in lower net gain due to pump wastage.
17. It is important here to consider how z is defined. For a backward-travelling signal, z decreases but the signal increases. Strictly speaking, then, the derivative is negative when considering the functional behavior for increasing z.

cases previously discussed for the pump, i.e. small-signal, large single-moded pump, and small-signal, small single-moded pump. As well, it will be interesting to try to predict results for large signals.

2.5.2.1 Small-Signal, Large Single-mode Pump

Applying the approximations made in eqn. 2.46, eqn. 2.41a and 2.41b become:

$$\Gamma_e(r,z,\nu) \approx \frac{C_0(r,z,\nu_p)}{1 + C_0(r,z,\nu_p)} \tag{2.55a}$$

$$\Gamma_a(r,z,\nu) = \frac{1}{1 + C_0(r,z,\nu_p)} \tag{2.55b}$$

and so:

$$G(z,\nu) = 2\pi\sigma_{21}(\nu_s)N_t \int_0^{\infty} n(r)t_o\Psi_{01}^2(r,\nu_s)\left[\frac{C_0(r,z,\nu_p) - \sigma_{12}/\sigma_{21}}{C_0(r,z,\nu_p) + 1}\right]rdr \tag{2.56}$$

where

$$G(z,\nu) = \gamma_e(z,\nu) - \gamma_a(z,\nu) \tag{2.57a}$$

and so

$$\frac{\partial P_{sig}}{\partial z} = G(z,\nu)P_{sig} \tag{2.57b}$$

The ratio of σ_{12}/σ_{21} can be seen from Figure 2.3 to be relatively close to unity, and so the bracketed modifier term in eqn. 2.56 is close to one when the approximations in

eqn. 2.46 are fully applied. Under this condition, signal (or ASE) propagation would be exponential for small-signal values. Two other comments can be made about eqn. 2.56. Since the absorption and emission cross-sections are signal wavelength dependent, it can be concluded that different signals will experience different gains. In addition, the right hand side of eqn 2.57b can be made zero if, ignoring fiber modal effects:

$$C_0(\nu_p) = \sigma_{12}(\nu_s)/\sigma_{21}(\nu_s) \tag{2.58}$$

G(z,ν) will equal zero at the optimum length, and the pump power at this length, termed the pump transparency power, is estimated from eqn. 2.58 to be:

$$PTP(\nu) = \frac{\sigma_{12}(\nu_s)}{\sigma_{21}(\nu_s)} P^{01}_{p\ th}(\nu_p) \tag{2.59}$$

Eqn. 2.59 is a first guess at the pump transparency power and the same result appears in [7]. A more detailed result will be considered further in the next section.

2.5.2.2 Small-Signal, Small Single-mode Pump

When the pump and signal/ASE power levels are low as is discussed in Section 2.5.1.2, the approximations of eqns. 2.46 and 2.50 are appropriate. The signal absorption and emission coefficients are found to be:

$$\gamma_e(z,\nu_s) \rightarrow 0$$

$$\gamma_a(\nu_s) = 2\pi\sigma_{12}(\nu_s)N_t \int_0^\infty n(r)t_o\Psi^2_{01}(r,\nu_s)rdr \tag{2.60}$$

Comparing the eqn. 2.60 with eqn. 2.52, it is thus expected that the signal would experience exponential decay.

2.5.2.3 Large Signal Analysis

The signal equations should now be re-examined for the case when large (probably saturating) signals are present and arbitrary pump powers are present. It is possible to have both a fairly large signal and pump present simultaneously if contra-directional pumping, for example, is used. Unfortunately, when considering large signal conditions it is difficult to draw any simple conclusions about the functional dependence of the signals, because terms involving the pump will still be significant compared to terms involving the large signals, and so simplifying approximations to the equations are difficult to make. However, since the gain of such saturated amplifiers is observed to drop, it is expected that the value of γ_e will approach that of γ_a so that $G(z,\nu)$ approaches zero.

2.5.3 Pump Transparency Powers and Optimal Lengths

It would be interesting to derive expressions for the PTP and optimal length which apply over a broad range of signal values. Unfortunately, it is difficult to consider the large-signal regime, due to the presence of pump terms in the signal propagation constant expressions that cannot be neglected. However, for the small-signal regime, some predictions can be made [25].

The analysis begins with a small-signal approximation of the pump propagation constant, which can be derived from eqn. 2.33:

$$\gamma_p(z,\nu_p) = 2\pi\sigma_{13}(\nu_p)N_t\int_0^\infty n(r)\Gamma_{01}(r,z,\nu_p)t_{p\,01}\Psi_{01}^2(r,\nu_p)rdr \tag{2.61}$$

$$\Gamma_{01}(r,z,\nu_p) = \frac{1}{1 + C_0(r,z,\nu_p)} \tag{2.62}$$

Eqn. 2.61 is the equation used in many other EDFA analyses to describe the pump absorption coefficient.[18] It is further assumed here that the pump modal intensity profile is Gaussian, with form:

$$\Psi_{01}^2(r,\nu_p) = \exp\left[-r^2/\omega_p^{01\,2}\right] = x \tag{2.63}$$

Using the definition of n(r) in eqn. 2.26 (where dopant is confined to the central core), then eqn. 2.62 becomes:

$$\gamma_p(z,\nu_p) = \sigma_{13}(\nu_p)N_t\int_0^B \left[\frac{x}{1 + \left(P_p(z)/P_{pth}^{01}(\nu_p)\right)x}\right]dx \tag{2.64}$$

where

$$B = \exp\left[-(a/w)^2/\omega_p^{01\,2}\right]$$

and eqn. 2.29 was used to simplify the expression. The above function can be integrated to yield, after simplification:

18. See, for example, reference [25]

$$\gamma_p(z,\nu_p) = \frac{\sigma_{13}(\nu_p)N_t P^{sat}_{pth}(\nu_p)}{P_p(z)} \ln\left[\frac{1 + \left(P_p(z)/P^{sat}_{pth}(\nu_p)\right)}{1 + \left(P_p(z)/P^{sat}_{pth}(\nu_p)\right)e^{-\Gamma}}\right] \tag{2.65}$$

where

$$\Gamma = (a/w)^2/\omega_p^{sat\,2}$$

Eqn. 2.23 describing pump propagation thus becomes:

$$\frac{\partial P_p}{\partial z} = -\sigma_{13}(\nu_p)N_t P^{sat}_{pth}(\nu_p) \ln\left[\frac{1 + \left(P_p(z)/P^{sat}_{pth}(\nu_p)\right)}{1 + \left(P_p(z)/P^{sat}_{pth}(\nu_p)\right)e^{-\Gamma}}\right] \tag{2.66}$$

Eqn. 2.66 can be separated and integrated, yielding:

$$L_{opt}(\nu) = -\int_{P_p(0)}^{PTP(\nu)} [\gamma_p P_p]^{-1}\, dP_p = \int_{PTP(\nu)}^{P_p(0)} [\gamma_p P_p]^{-1}\, dP_p \tag{2.67}$$

Unfortunately, this is not a closed form expression, and requires a value for PTP(ν) in the lower integral limit. To develop an expression for the PTP(ν), first consider the signal propagation equations, assume small-signal operation, and set the derivative to zero; therefore, it is required that:

$$\frac{\partial P_{sig}}{\partial z} = G(z,\nu)P_{sig} = 0 \tag{2.68}$$

where

$$G(z,\nu) = 2\pi\sigma_{21}(\nu_s)N_t\int_0^{a/w} t_o\Psi_{01}^2(r,\nu_s)\left[\frac{\left(P_p(z)/P_{pth}^{01}(\nu_p)\right)\Psi_{01}^2(r,\nu_p) - \sigma_{12}(\nu_s)/\sigma_{21}(\nu_s)}{1 + \left(P_p(z)/P_{pth}^{01}(\nu_p)\right)\Psi_{01}^2(r,\nu_p)}\right]rdr \tag{2.69}$$

The confined dopant profile for n(r) in eqn. 2.26 was assumed here, but any arbitrary profile can be accommodated in eqn. 2.69. The pump transparency power is that pump power for which G(z,ν) in eqn. 2.69 is equal to zero. Thus:

$$\boxed{\int_0^{a/w} \Psi_{01}^2(r,\nu_s)\left[\frac{\left(PTP(\nu)/P_{pth}^{01}(\nu_p)\right)\Psi_{01}^2(r,\nu_p) - \sigma_{12}(\nu_s)/\sigma_{21}(\nu_s)}{1 + \left(PTP(\nu)/P_{pth}^{01}(\nu_p)\right)\Psi_{01}^2(r,\nu_p)}\right]rdr = 0} \tag{2.70}$$

PTP(ν) can be determined by iteration of the above equation, and then the optimal length can be determined from eqn. 2.67. It is interesting to note that the PTP(ν) is independent of the Erbium dopant concentration N_t and the input pump power to the amplifier, but depends on the fiber geometry via the mode intensity profiles, and, through P_{pth}^{01}, is quite dependent on τ and $\sigma_{13}(\nu_p)$. As expected, the optimal length is inversely proportional to both $\sigma_{13}(\nu_p)$ and N_t, and does not depend on the input pump power.

As a final comment, it is important to note that the results in eqns. 2.67 and 2.70 apply only to the small-signal regime. In the case of a saturating signal, the pump is depleted to the PTP level over shorter lengths and thus the optimal length is shorter. Also note that the effect of ASE on signal and pump propagation has been ignored; this is consistent with the other assumptions made in the derivation, but note that high initial pump values and low input signals can result in high levels of ASE generation which

will affect the accuracy of the results of this section. As well, the eqns. 2.67 and 2.70 assumed a pump which possesses a single fiber mode. A multi-moded pump will result in higher PTPs and longer required lengths; this will be examined in the simulation studies of Chapter 4.

3.0 Adapting the Theory for Computer Simulation

The next logical step in examining the performance of EDFAs is to design a computer program that will take the theory developed in Chapter 2 and produce useful results. The program developed should adequately balance run-time considerations with accuracy of results, should allow easy input of parameters, and should maximize analysis capability once runs have been performed.

Eqns. 2.23 and 2.44, which describe signal/ASE and pump propagation, are coupled via the absorption and emission coefficients by virtue of the signal saturation functions described in eqn. 2.43 and by the pump functions, described in eqn. 2.30d-e. In addition, as mentioned in Section 2.4, the total number of coupled, differential equations is determined by the number of frequency intervals used to sample the emission and absorption cross-sections. One differential equation must be written for each frequency interval for both forward- and backward-travelling components, where the boundary conditions at $z = 0$ and $z = L$ determine whether a signal or ASE alone exists in that frequency slot. As well, one equation must be written for the pump (two if a second pump is added). Therefore, $2K + 1$ equations are required, where K is the number of frequency intervals. For simulations performed here, the cross-sections were sampled between 1.47 μm and 1.6 μm at 2.5 nm intervals, resulting in $K = 53$ intervals; therefore, a total of 107 coupled equations were required. As well, 107 boundary values were required, and are assigned as follows:

$$P_p(0) = P_{in}$$
$$P_s^+(0,\nu_i) = 0$$
$$P_s^-(L,\nu_i) = 0 \qquad (3.1)$$

for all frequency intervals where no signal is present, and where a forward-travelling pumping scheme is used. For those intervals where a signal is present, the boundary value is set to the appropriate input spectral density. In addition:

$$P_s^{\pm}(z,\nu_i) = 0, \text{ for } z \neq 0, L \tag{3.2}$$

for all variables. Therefore, two two-dimensional matrices of initial values exist, one for all forward-travelling components, the other for all backward-travelling components. These initial values are required so that the first iteration over the entire frequency range can be conducted.

Illustrated in Figure 3.1 is a conceptual view of how the simulation proceeds. Since there are 107 simultaneous equations, and a fourth-order Runge-Kutta technique taken over 50 steps in z is used,[1] it is easier to solve each equation for each signal/ASE component and the pump with estimates of all the other signal/ASE power spectral densities and iterate to a solution. These estimates are taken to be the results of the previous iteration, or zero as discussed above for the first iteration. Within a given iteration, steps in frequency must be taken, first in the forward direction, and then in the reverse direction, where the most recent values are always used for any given variable. Once all signal and the pump values are calculated, the results are compared to those of the previous run, and if a certain error criterion is met, the simultaneous solution of all equations is achieved. Typically, it takes about 5 to 6 iterations to reach convergence, and this technique has subsequently been used by others.[2]

---

1. Note that solving the backward-travelling signal/ASE equations requires slight modification to the Runge-Kutta expression, since steps are now taken in the negative z direction
2. Subsequent to the simulation being written, reference [11] was published and in words describes very closely the steps taken to solve the problem here.

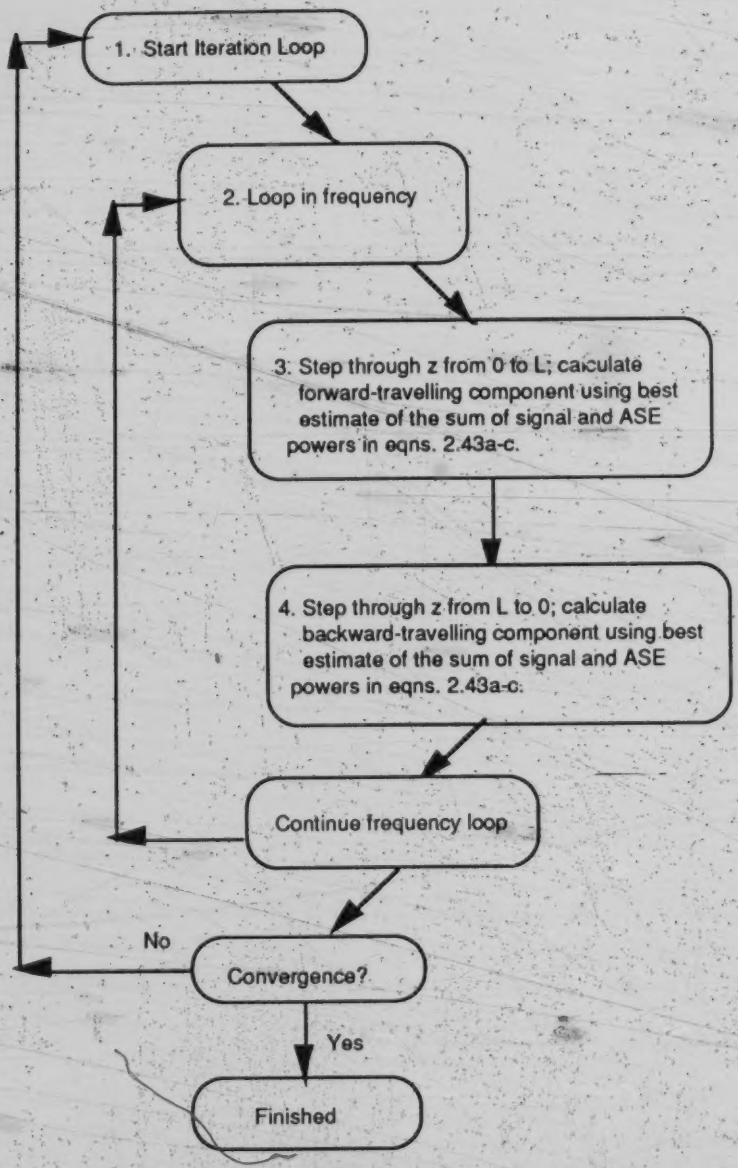
1. Start Iteration Loop
2. Loop in frequency
3. Step through z from 0 to L; calculate forward-travelling component using best estimate of the sum of signal and ASE powers in eqns. 2.43a-c.
4. Step through z from L to 0; calculate backward-travelling component using best estimate of the sum of signal and ASE powers in eqns. 2.43a-c.
Continue frequency loop
No
Convergence?
Yes
Finished

Figure 3.1 : Conceptual Flow Diagram of Simulation

3.1 Structure of Program and Scope of Results

The main program implementing the theory was written in the computer language C for use on the DEC 3100 workstations resident at TR Labs. Mr. Albert Chau, a Co-op student who worked on the program from October to December, 1990, coded the program following the structure outlined in Figure 3.1. The program

implemented was highly modular, had an extensive input parameter file where 39 or more parameters could easily be modified, and had an excellent user interface including feedback on the status of the simulation. As a final comment, one simulation requires 190 CPU minutes to complete. This can be reduced by running the simulation on a SPARC 2 RISC machine now available at TR Labs, and possibly by re-examining the use of Simpson's Rule to evaluate the overlap integrals in eqns. 2.33, 2.39, and 2.40.

3.1.1 Support Calculations

A number of calculations preliminary to the actual EDFA calculations were required. These include calculation of the modal propagation constants for use in the mode-field expressions and calculation of other fiber parameters.

Calculation of the transverse fiber modal propagation constants u_{01i}, γ_{01i}, u_{11i}, γ_{11i} proceeded as follows. First, the *normalized frequency* V has to be determined for both the pump and signal wavelengths, based on input values for the core radius and NA supplied by the user, where V is given by:[3]

$$V = \frac{2\pi a NA}{\lambda} \tag{3.1}$$

where

a = the fiber core radius,

NA = the fiber Numerical Aperture, and

λ = the pump or signal wavelength

Next, an iterative process takes place (See Figure 3.2 on the following page), and involves guessing the *normalized fiber propagation constant* b, calculating the *axial*

3. Note that the signal will always possess only one fiber mode, and the pump *may* also only possess one fiber mode, if Vp < 2.405; otherwise, it could possess two fiber modes.

propagation constant β and the transverse propagation constants u and γ. Finally, the constants are inserted into the eigenvalue equation for the mode in question to check for convergence to within a certain error criterion. If the equation is not satisfied, a new value of b is determined, followed by another round of iteration. Determining the value of b is useful because the final solution for the propagation constants can be checked against existing data.[4] A simpler alternative method exists if the fiber mode in question is close to cut-off,[5] as is outlined in eqns. 3.2:

$$\gamma = 1.122e^{-\left[J_0(V)/VJ_1(V)\right]} \tag{3.2a}$$

$$u^2 = V^2 - \gamma^2 \tag{3.2b}$$

$$\beta^2 = (\gamma/a)^2 + (k_o n_{clad})^2 \tag{3.2c}$$

where the usual definitions to the various terms above apply.

4. A useful graph of b vs V appears in reference [13].
5. This method assumes that u = V, i.e. that the mode is near cut-off, where $\gamma = 0$. The approximation used applies only for the LP_{01} mode, and is accurate to within 10% for V ranging from 0 to 2.5; this includes all single-mode fiber V numbers. For further reference, see [15], pp. 37

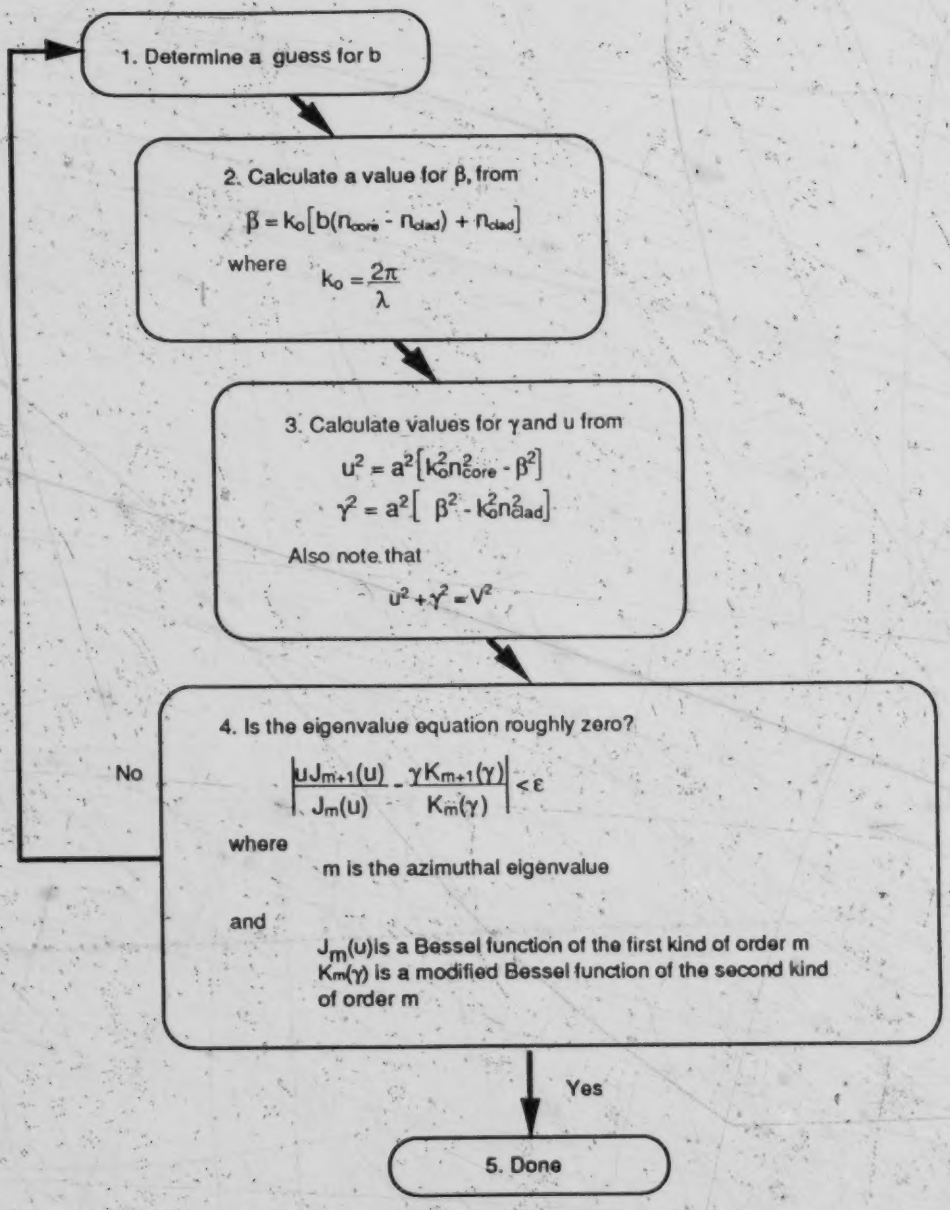
1. Determine a guess for b
2. Calculate a value for β, from
$\beta = k_o[b(n_{core} - n_{clad}) + n_{clad}]$
where $k_o = \frac{2\pi}{\lambda}$
3. Calculate values for γ and u from
$u^2 = a^2[k_o^2 n_{core}^2 - \beta^2]$
$\gamma^2 = a^2[\beta^2 - k_o^2 n_{clad}^2]$
Also note that
$u^2 + \gamma^2 = V^2$
4. Is the eigenvalue equation roughly zero?
No
$\left|\frac{uJ_{m+1}(u)}{J_m(u)} - \frac{\gamma K_{m+1}(\gamma)}{K_m(\gamma)}\right| < \varepsilon$
where
m is the azimuthal eigenvalue
and
$J_m(u)$ is a Bessel function of the first kind of order m
$K_m(\gamma)$ is a modified Bessel function of the second kind of order m
Yes
5. Done

Figure 3.2 : Conceptual Flow Diagram Illustrating the Technique Used to Calculate Fiber modal Propagation Constants

3.1.2 Numerical Methods

Both a fourth-order Runge-Kutta technique and Simpson's Rule were used in the program. The Runga-Kutta technique was used to solve the coupled differential equations as alluded to earlier, and Simpson's Rule was used for numeric integration over the radius r in the expressions for the propagation constants. The Runga-Kutta technique had 50 steps in z over which it would calculate solutions to the differential equations, and Simpson's Rule calculated the integrals with 32 divisions.[6] Both the number of steps in z and the number of integration divisions appear in the input parameter file and thus can easily be altered.

3.2 Simulation Capabilities

The theory and program have been designed to be as flexible as possible. The following parameters may be altered in the parameter files for simulation purposes:

a) Fiber Parameters (radius a, core and cladding indices, modal power distribution parameter η, amplifier length L)

b) Doped fiber characteristics (concentration N_t, pump absorption cross-section, confinement factor w, fluorescence lifetime τ, signal absorption and emission cross sections)

c) Inputs to the fiber (input pump power, input signal power spectral density and bandwidth of signal, wavelength of signal)

In addition, the program has the following additional capabilities:

---

6. Note that integration to $r = \infty$ was really done to $r = 5a$. In restrospect, this choice of upper limit could have been reduced dramatically, and should in fact be set to $r = a/w$ if n(r) is defined by eqn. 2.26

a) ability to add multiple signals, with possibly different signal bandwidths and power levels, separated by at least $\Delta\nu$, the spacing between sample points of the cross-section (here, 2.5 nm), both in the forward and/or the reverse direction. Thus, multi-channel, bi-directional WDM performance of the amplifier can be simulated.

b) ability to add a backward-travelling pump; thus, co-, contra-, or bi-directional pumping or the addition of a mirror to reflect pump can be simulated.

The following output analysis capabilities exist:

a) ability to examine pump, signal and/or ASE evolution along the amplifier at a given wavelength, for both forward- and backward-travelling signals

b) ability to examine the signal and ASE spectrum vs. wavelength at any length along the amplifier, for either forward- or backward-travelling signals

c) ability to compute the total broadband power at a given amplifier length for either forward- or backward- travelling signals, or power within specific bandwidths (multiples of 2.5 nm)

d) ability to produce 3D plots of ASE and/or signal power spectral density vs. wavelength and amplifier length

e) ability to calculate gain and noise figure in both forward and backward directions based on signal/ASE evolution results.

f) ability to determine optimal length and PTP, again based on analysis of signal evolution.

As well, certain capabilities can be shut off to allow faster computation of any one particular desired result. As a final comment, the raw data files are saved to disk, so that any processing for a given desired result can occur at any time, while a lasting record of the simulation remains.

4.0 Simulation Study of EDFAs

Having considered the theory governing the operation of EDFAs, it is now time to study the results of a series of simulations performed on a design whose parameters are listed in Table 4.1. The rationale behind these parameter choices will be discussed in Chapter 5, but here they will serve as a useful basis for comparison when variables are selectively varied and their effects are observed.

Parameter	Value
Core radius a	4.15 μm
Core index of refraction	1.471
Cladding index of refraction	1.4657
Erbium dopant concentration N_t	9.9×10^{18} cm^{-3}
Pump absorption cross-section	1.75×10^{-21} cm^2
Dopant confinement factor w	2.0
Modal Power Distribution parameter η	0.5
Fluorescence lifetime τ	12 ms
Length of Amplifier	varies from 5.9 to 15.0 m
Input Pump Power	varies from 10 to 25 mW
Signal wavelength	1.55 μm
Signal Power Spectral Density	varies from 1.6026×10^{-15} mW/Hz
Signal Bandwidth	62.4 GHz (0.5 nm)

Table 4.1 : Summary of Base Simulation Parameters

In addition, the absorption and emission cross-sections shown in Figure 2.3 were sampled as discussed in Chapter 3 and used to model ASE generation. The values chosen for the pump absorption cross-section, $\sigma_{13}(\nu_p)$ and the fluorescence lifetime τ

were taken from [26], and choice of signal bandwidth was based on measurements taken in the lab (see Figure 6.2).

The approach to the simulation study which follows is summarized in Figure 4.1. The items shown within the dotted box form the base simulation, in which only pump input power and signal input power are varied. From this initial study, an analysis of gain, noise figure, total broadband ASE, in-band ASE, pump/signal evolution, signal/ASE spectra, and optimal length can be performed, and follows in Section 4.1. In following Sections, individual changes as suggested by Figure 4.1 will be made to the base design for a fixed pump and signal input , allowing systematic comparison of results.

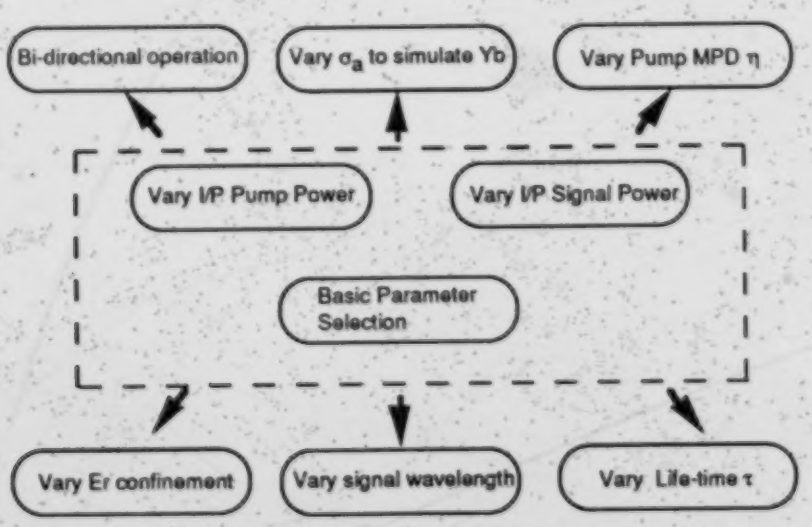

Figure 4.1 : Conceptual View of Simulation Strategy

4.1 Base Simulation Results

This section will show that the parameter choices made for the design being considered lead to very modest results, given what has been reported for many other designs in the literature. This design does result in low splice-losses to standard

telecommunications fiber, and includes many parameters in Table 4.1 whose values are quite conservative.

4.1.1 Signal Gain

One of the most interesting parameters which can be considered is the gain performance of a particular design for different pump levels, as shown in Figure 4.2. It is important to note that when simulating behavior of the EDFA, or in actual measurements made on EDFAs, care must be taken in distinguishing the signal from the ASE. This is because in-band ASE will always contribute to either the value read by the optical power meter, or to the numbers calculated from the model, but this is only a significant contribution when the signal is small. Since the in-band ASE contribution is observed to be constant in the small-signal regime, it can therefore be subtracted from measurements or calculated results to yield a true measure of the signal power for gain calculations. This technique and its usefulness will be discussed further in Chapter 6. The results shown in Figure 4.2 have been corrected for ASE presence, and thus reflect true signal gain.

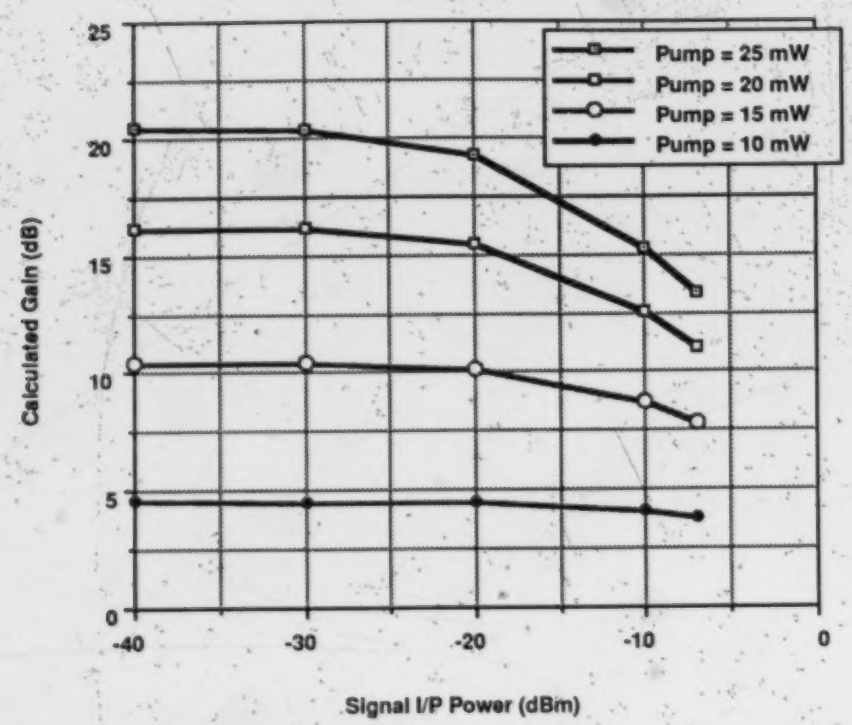

Figure 4.2 : Gain vs. Signal I/P Power for Various Pump I/P Power Levels[1]

From Figure 4.2, the Saturated Output Power has a peak value of +2.5 dBm for the 25 mW pump case, and all gains are calculated for the optimal length for the given pump and signal input powers.

4.1.2 Noise Figure

The *noise figure* for a particular amplifier can be estimated as follows [27]:[2]

$$NF \approx 10 \log\left[\frac{P_{ASE}}{h\nu B_o(G - 1)}\right] \qquad (4.1)$$

where

1. Gain can also be plotted as a function of *Output Signal Power*; this will clearly yield curves of slightly different shapes, but is useful in that it directly shows the *Saturated Output Power*, which is the output signal/ASE power from the amplifier when the gain has fallen by 3 dB
2. See Appendix D for some comments on noise figures for EDFAs

P_{ASE} = the total ASE power in a given optical bandwidth B_o

$h\nu$ = the photon energy, and

G = the amplifier gain

This formula has assumed that the *noise factor* is given by $2n_{sp}$, where n_{sp} is the spontaneous emission factor, and eqn. 4.1 is quite accurate for most calculations. Note that at maximum population inversion, with ideal filtering, $n_{sp} = 1$, and the noise figure can be made to equal the *quantum limit* of 3 dB. This has been achieved in actual experimental configurations when 980 nm pumping is used [28]. For this analysis, recall from Table 4.1 that the signal optical bandwidth is taken to be 0.5 nm, but the ASE filter optical bandwidth used is 1.0 nm, to better reflect currently available filters at TR Labs.

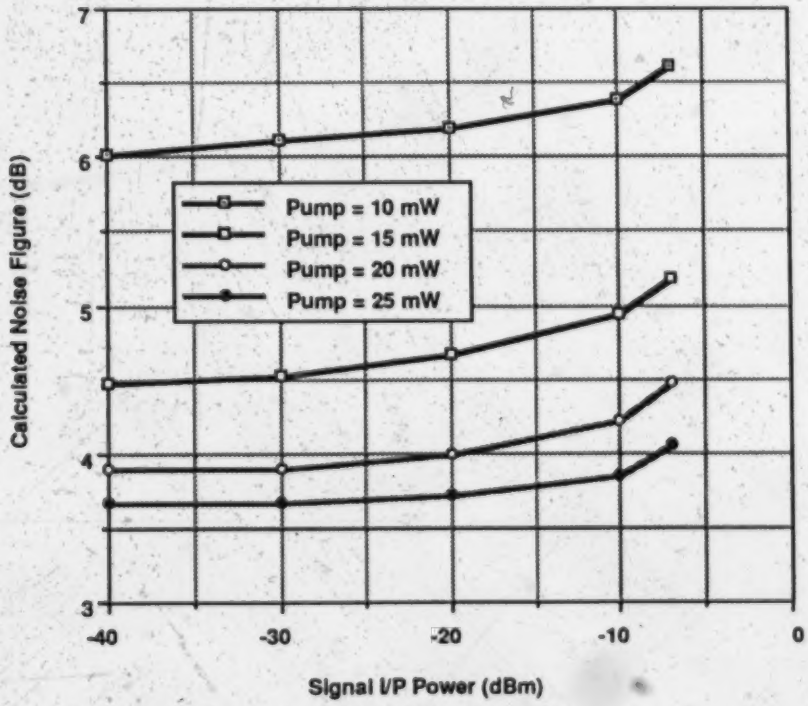

Figure 4.3 : Noise Figure vs. Signal I/P Power for Various Pump Power Levels

Note that the derivation of eqn. 4.1 done in Appendix D assumes signal-spontaneous beat noise dominates all other noise terms, and thus a rise in noise figure for very low signal power levels due to the increasing importance of spontaneous-spontaneous beat noise, goes unnoticed. Note also that the minimum noise figure of 3 dB is not achieved due to incomplete inversion at lower pump levels, incomplete filtering of ASE, and limited accuracy of the model used.

4.1.3 ASE Levels

The amount of broadband and in-band ASE (ASE in a given optical bandwidth around the signal wavelength) has been determined for the base simulation study, and is illustrated in Figures 4.4 (a) and (b). These results are of interest because they are easily obtainable in the lab and the in-band ASE results can be used to determine the noise figure of the amplifier, as done in the previous section. At this time, further comments should be made on how the in-band ASE contribution is calculated. As discussed in Section 2.4, the total optical output spectral density computed at the signal wavelength consists of an ASE component and a signal component, which must somehow be distinguished. As is seen in Figure 4.5, however, the ASE spectrum is fairly flat in the vicinity of the 1.55 μm signal and so ASE spectral densities on either side of the signal interval are averaged to give an estimate of what the in-band ASE contribution might be. This, of course, assumes no hole burning is occurring, and is expected to be a reasonable assumption for small-signal operation at room temperature in homogeneously broadened amplifiers [12].

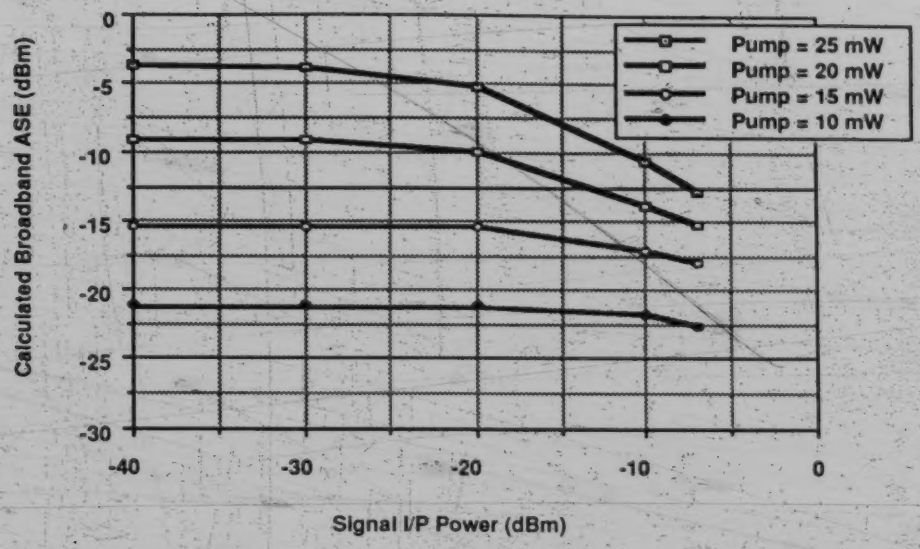

Figure 4.4(a) : Broadband ASE Power vs. Signal I/P Power for Various Pump Power Levels

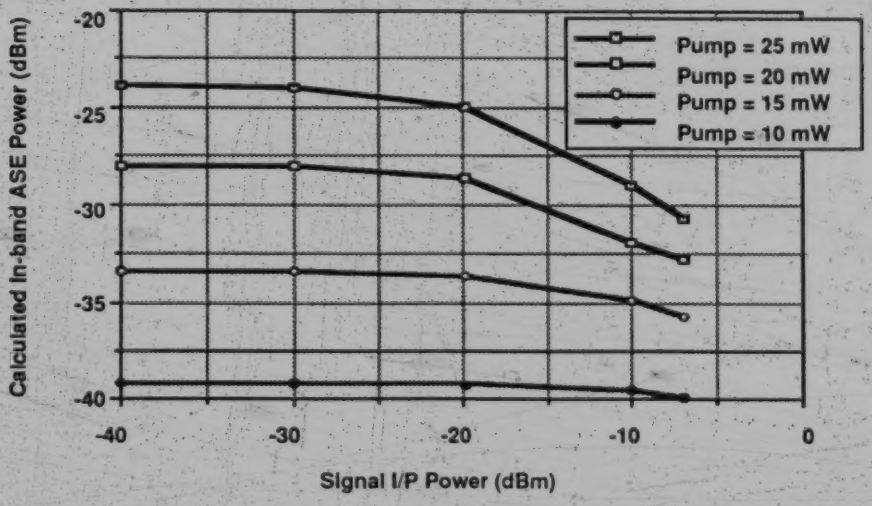

Figure 4.4(b) : In-band ASE Power vs. Signal I/P Power for Various Pump Power Levels

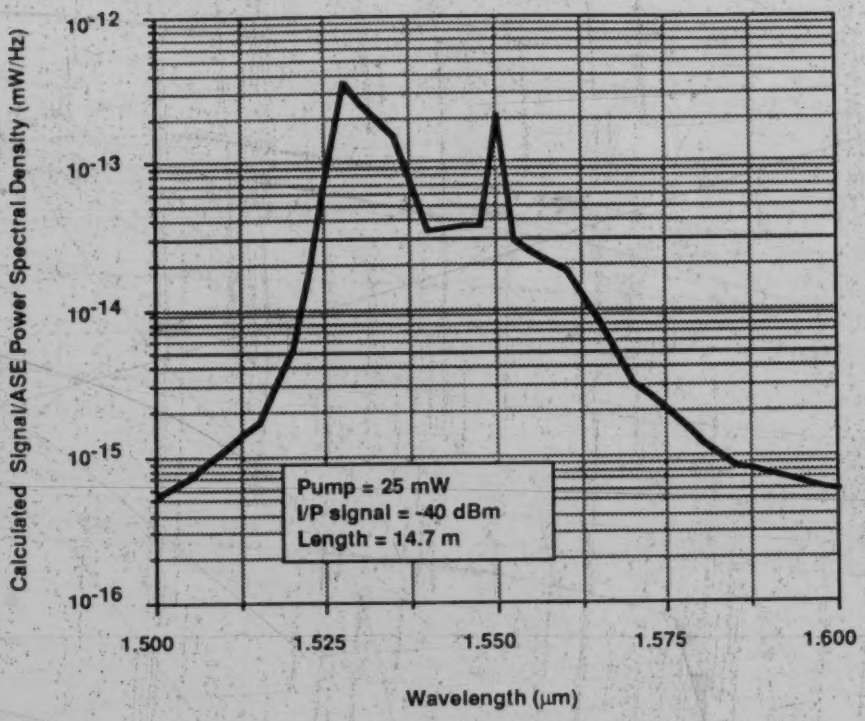

Figure 4.5 : Signal and ASE Power Spectral Density Between 1.5 and 1.6 μm at L =14.7 m for a Pump of 25 mW and a Signal I/P of -40 dBm, located at 1.55 μm

It is interesting to note that the ASE measured in a 1 nm optical bandwidth around 1.55 μm represents only 1.0 to 1.9 % of the total ASE calculated from 1.47 to 1.6 μm. As seen from the ASE spectrum shown in Figure 4.5, the majority of the ASE is seen to be around 1.53 μm due to the Al-codoped fiber absorption and emission cross-sections pictured in Figure 2.3. It would then be expected that the noise figure of amplifiers operating at this wavelength might be higher (see Section 4.3.6), and this is indeed what others have observed [29].

4.1.4 Pump, Signal, and ASE Evolution vs. EDFA Length

Examination of the pump, signal, and ASE evolution as a function of amplifier length is useful in illustrating how an optimal length and a Pump Transparency Power

(PTP) arise in an amplifier whose operation is governed by three-level lasing physics. Shown in Figures 4.6 and 4.7 are such curves.

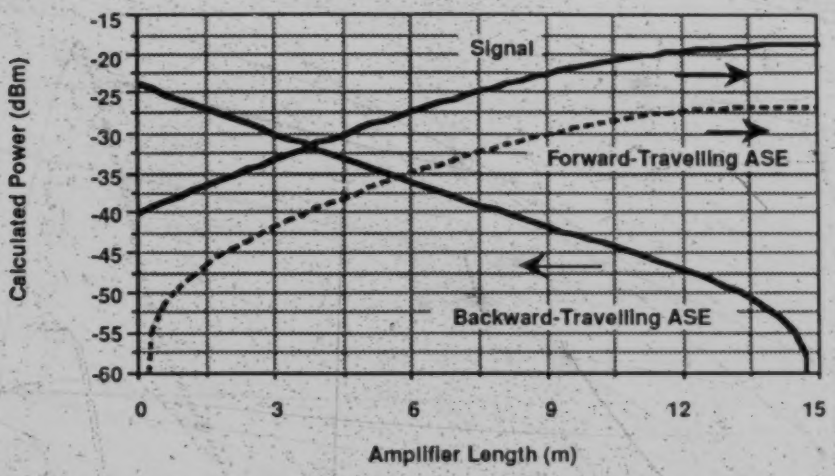

Figure 4.6 : Signal and In-Band Forward- and Backward-travelling ASE Power (0.5 nm Bandwidth) vs. Amplifier Length (Total Length = 14.7 m, Co-directional Pump = 25 mW)

A number of observations can be made from Figure 4.6. First of all, due to the single-ended entry of the pump power, the forward- and backward-travelling ASE evolve differently; the backward-travelling ASE is seen to grow exponentially[3], but the forward-travelling ASE deviates from exponential growth when the optimal length is approached. This sort of signal/ASE evolution was predicted in Section 2.52 when small-signal conditions prevailed, as they do here. Thus, the backward-travelling ASE exits the front-end of the amplifier at a higher power, -24 dBm, versus -26.8 dBm for the forward-travelling ASE.

Pump evolution is shown in Figures 4.7 for various input signal power levels, and in Figure 4.8 for various input pump power levels. As was discussed in Chapter

3. Note that linear growth on the log scale shown implies exponential growth of the signal power over length

2.5.1, the initial pump decay is observed to be linear for high initial pump powers, and becomes more exponential as the input power is reduced. Also note that the absorption rate over length of the pump increases when saturated behavior is occurring, resulting in the pump falling to the PTP for a shorter length of amplifier. The actual PTP for this design was typically 3.6 ± 0.1 mW, with variation due to the presence of large signals, different initial pump powers, and coarseness in the computation grid over z.

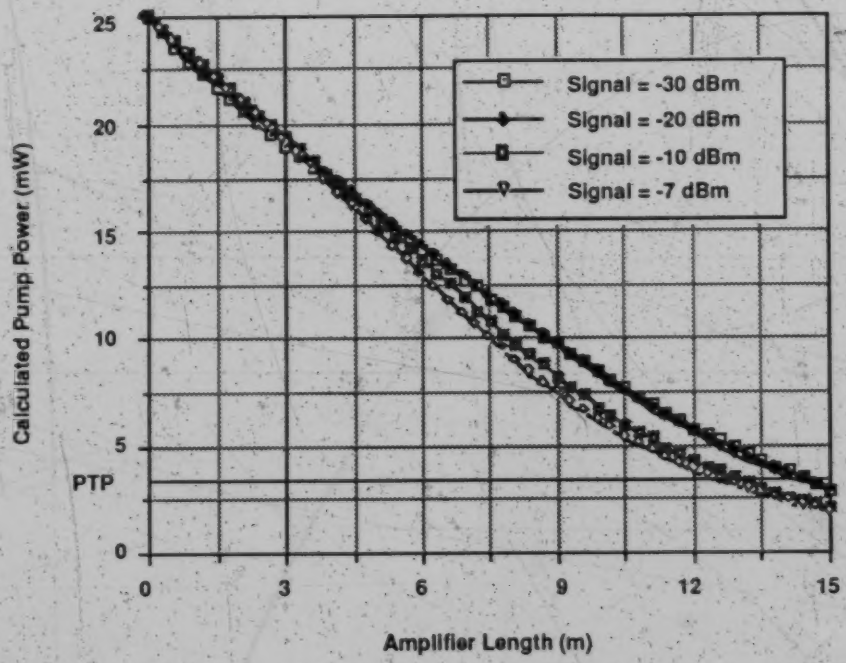

Figure 4.7 : Residual Pump Power vs. Amplifier Length for Various Signal I/P Powers

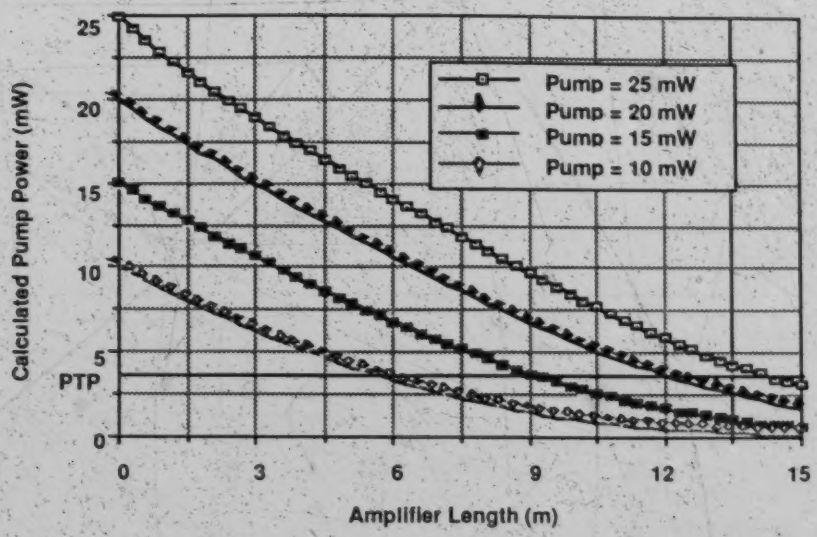

Figure 4.8 : Residual Pump Power vs. Amplifier Length for Various Pump I/P Powers and an I/P Signal of -30 dBm

4.1.5 Optimal Lengths

The optimal lengths for the amplifier designed are shown in Figure 4.9. Note that the optimal length for saturated amplifiers is lower due to faster absorption of the pump as seen in Figure 4.7. As well, recall that the analysis of Section 2.5.3 was for small-signal regimes only, and thus the reduced length could not be predicted from eqn 2.66. The optimal length thus varies for different signal levels, and if an amplifier is to be designed for operation over a broad range of anticipated signal levels, it can only truly be optimized for one particular signal level. However, as seen from Figure 4.6, the maximum in signal over length is quite broad, so that amplifiers designed with slightly offset lengths will still perform with only 1 to 2 dB degradation in gain at most. Also note the strong dependence of optimal length on I/P pump power, with a weaker dependence on signal I/P power also noted.

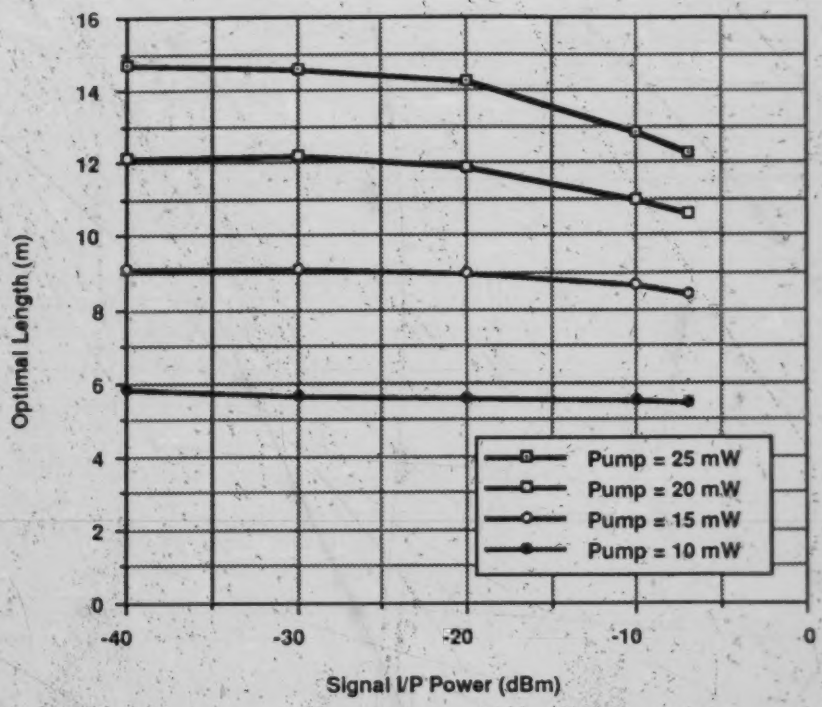

Figure 4.9 : Optimal Amplifier Length vs. Signal I/P Power for Various Pump Power Levels

4.2 Variations From Base Design

Having thoroughly considered the base design, it is now of interest to explore individual variation of certain key design parameters. For the following comparative simulations, the signal input power will remain fixed at -30 dBm (small-signal regime) with the initial pump power set to 25 mW.

4.2.1 Variation of Pump Absorption Cross-Section

Variation of the pump absorption cross-section is of interest because of the effect σ_{13} has on almost every aspect of EDFA operation.[4] As well, addition of Yb as a fiber core co-dopant is expected to increase the pump absorption cross-section under

4. A quick review of the equations in Chapter 2 reveals theoretical dependency on σ_{13} for all parameters that dictate successful operation of the EDFA.

certain conditions which will be discussed in Chapter 5. Therefore, for one simulation, the absorption cross-section was increased by a factor of 10 from its base value, with the following results:

Variable\ Design	Base Design	Modified Design
Gain	20.35 dB	23.9 dB
PTP	3.40 mW	90 μW
Broadband ASE Power	412.4 μW	1.88 mW
In-band ASE Power	4.03 μW	7.66 μW
Calculated NF	3.67 dB	2.89 dB
Optimal Length	14.6 m	9.45 m

Table 4.2 : Comparison of Performance of Base Design with Increased Pump Absorption Cross-section Design. In-band ASE Calculated is for a 1.0 nm Bandwidth Centered at 1555 nm

Clearly, the modified design has better gain due in-part to a lower PTP (more of the pump gets absorbed and converted to signal) and it has a shorter length. The noise figure of 2.89 dB for the modified case cannot be considered valid because the large amount of ASE present is contributing to saturation of the amplifier. As well, the applicability of eqn. 4.1 in this context is in doubt because of other assumptions made in its derivation.[5] It is thus shown here only for qualitative comparison. Other results, such as the increased gain, lower length, and lower PTP are expected.

5. See Appendix D for a discussion of noise figures

4.2.2 Variation of Fluorescence Lifetime

Variable\Design	τ = 11 ms	τ = 12 ms	τ = 13 ms
Gain	19.12 dB	20.35 dB	21.30 dB
PTP	3.80 mW	3.40 mW	2.76 mW
Broadband ASE Power	285.0 μW	412.4 μW	555.7 μW
In-band ASE Power @ 1.55 μm	3.06 μW	4.03 μW	5.1 μW
Calculated NF	3.72 dB	3.67 dB	3.74 dB
Optimal Length	13.75 m	14.6 m	15.7 m

Table 4.3 : Comparison of Performance of Base Design with Designs with Modified Fluorescence Lifetimes

Variations in the fluorescence lifetime τ are expected to affect EDFA performance in a manner similar to the previously discussed pump absorption cross-section, due in part to the number of expressions seen in Chapter 2 where both τ and σ_{13} appear as products. As well, better performance might intuitively be expected from an amplifier whose Erbium atoms possess a longer fluorescence time, since the population inversion is maintained over a longer period. Better performance is observed in two comparative simulations, with one possessing a shorter lifetime (11 ms), and the other possessing a longer lifetime (13 ms).

4.2.3 Variation of Pump Modal Power Distribution (MPD)

Recall from eqn 2.21 that the assumed multi-modedness of the pump for typical fiber designs could be controlled through a parameter η, which for the base simulations

was set to 0.5, favoring slightly the LP_{01} mode. Normally, it is expected that the MPD will be determined by the launch conditions into the fiber, and over relatively short lengths (tens of meters) will probably not reach an equilibrium distribution. Here, however, the distribution is assumed constant. Given that the equations governing the propagation constants in Chapter 2 are essentially overlap integrals, the best physical overlap between the pump, signal, and the Erbium distribution will produce the best performance. Since confinement of Erbium is favored because of good overlap with the LP_{01} mode, it is best to also have a predominantly single-mode pump, which is simulated by setting $\eta = 0$. Recall that $\eta = 2/3$ represented equal excitation of all modes present, and is the most multi-moded case.

The performance simulation results are summarized in Table 4.4. Trends show that the gain is higher and the noise figure and PTP are lower when the LP_{01} mode is favored; all are expected results. Note as well that the optimal length is shorter, reflecting the fact that the pump is indeed being more rapidly depleted due to better overlap with the confined Erbium distribution which is the same in all cases and is confined to half the core ($w = 2$ in eqn. 2.26).

Variable\Design	$\eta = 0.0$	$\eta = 0.5$	$\eta = 2/3$
Gain	21.99 dB	20.35 dB	18.76 dB
PTP	1.90 mW	3.40 mW	4.48 mW
Broadband ASE Power	790.4 μW	412.4 μW	243.0 μW
In-band ASE Power	5.58 μW	4.03 μW	2.91 μW
Calculated NF	3.43 dB	3.67 dB	3.86 dB
Optimal Length	13.30 m	14.6 m	15.0 m

Table 4.4 : Comparison of Performance of Base Design with Designs with Modified Pump MPDs

4.2.4 Variation of Erbium Dopant Confinement

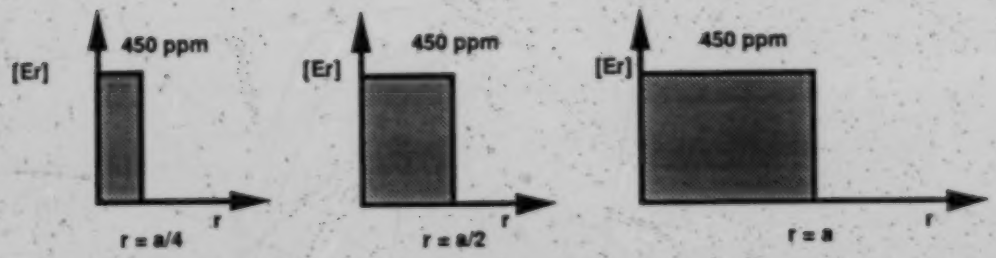

Figure 4.10 : Conceptual View of Constant-Concentration Confinement of Erbium Dopant

Confinement of the Erbium dopant is an interesting design problem which will be dealt with at length in Chapter 5. Here, two simulations of EDFAs with dopant confinements of half and double that of the base design will be considered. Since the overall dopant concentration is kept the same, fewer Erbium ions are intercepted in a

given cross-section of fiber when the confinement is doubled, while more will be intercepted when the confinement is halved, as shown schematically in Figure 4.10.

Some a priori predictions can be made about the effects of this confinement on performance. First, start by assuming that the pump absorption coefficient is simply a radial overlap integral over transverse area (no azimuthal dependence) as shown below (compare with eqn. 2.33):

$$\gamma_p = k\int_0^{\infty} Er(r)Pump(r)rdr \tag{4.2}$$

where, for simplicity:

$$\begin{aligned} Er(r) &= N_o \,, r < a/w \\ &= 0 \,, r > a/w \end{aligned} \tag{4.3}$$

and

$$Pump(r) = \exp\left[-r^2/\omega_p^2\right] \tag{4.4}$$

Evaluation of eqn. 4.2 then leads to:

$$\gamma_p = kN_o\frac{\omega_p^2}{2}\left[1 - e^{-\left(\frac{a}{w\omega_p}\right)^2}\right] \tag{4.5}$$

For typical values of confinement , $w \geq 1$, and ω_p is typically on the order of a. When the argument of the exponential is small, a Taylor series expansion can be used to write:

$$e^{-x} \approx 1 - x \tag{4.6}$$

and so eqn. 4.2 becomes:

$$\gamma_p = k\frac{N_o}{2}\left[\frac{a}{w}\right]^2 \qquad (4.7)$$

Noting the similarities between this analysis and that in Section 2.5.3, where an expression for the optimal length was derived, the amplifier lengths here might be expected to drop by a factor of 4 for halved confinement, and raised by a factor of 4 for doubled confinement, as a first guess. To prevent these length alterations, eqn. 4.7 suggests that the concentration could be altered appropriately in either case by a factor of 4 to yield the same length. This technique has been tried in other simulations and yielded improved performance for a highly confined, increased-concentration design [30]. The simulation results are summarized in Table 4.5.

Variable\Design	w = 1.0	w = 2.0	w = 4.0
Gain	13.87 dB	20.35 dB	21.00 dB
PTP	4.49 mW	3.40 mW	3.45 mW
Broadband ASE Power	68.6 μW	412.4 μW	491.8 μW
In-band ASE Power	0.944 μW	4.03 μW	4.87 μW
Calculated NF	3.99 dB	3.67 dB	3.83 dB
Optimal Length	3.80 m	14.6 m	85.5 m

Table 4.5 : Comparison of Performance of Base Design with Designs with Modified Erbium-dopant Confinements (See Figure 4.10)

A few comments are in order. In the w = 1 run, the length is seen to fall by a factor of 3.84, as predicted, and the gain is noted to fall by 6.48 dB, or a factor of 4.45. The total ASE and in-band ASE also fall, by factors of 6.01 and 4.27, respectively. This is seen to be roughly consistent with what was predicted earlier. However, for the w = 4 case, the predictions are not consistent. For example, while the length does increase, it does so by a factor of 5.86. The gain, broadband ASE, and in-band ASE all increase by factors of 1.16, 1.19, and 1.21, respectively, which, are relatively consistent but which are not the predicted values. Clearly, the usefulness of these predictions is qualitative only. As a final comment, the results of the w = 4 simulation might well be questioned on the basis of the long length of the amplifier; at the pump wavelength of 980 nm, Rayleigh scattering, not considered in the simulation, might become a significant factor and unfavorably alter the results.[6]

4.2.5 Variation of Signal Wavelength

The simulations performed here assumed a signal wavelength of 1.55 μm, due to the availability of sources at that wavelength at TR Labs. However, as inspection of the ASE spectrum in Figure 4.5 suggests, the gain will be higher at a signal wavelength of 1.53 μm. It is thus natural to compare the two wavelengths for performance characteristics, and this is done at a small-signal power input power of -30 dBm and a saturating input power of -10 dBm. The results are summarized in Table 4.6 on the following page.

It is seen that the 1.53 μm wavelength signal does experience more gain but is also accompanied by a much larger amount of in-band ASE, which would in-turn result in a poorer noise figure, consistent with other results [28]. It is interesting to note that

6. While scattering losses might be around 2 dB/km at 980 nm for standard telecommunications fiber, they are higher for fiber fabricated at NOI.

the total broadband ASE is lower when the signal is located at 1.53 μm; this is because the emission and absorption cross-section in the Erbium give rise to a peak in the gain spectrum at 1.53 μm and thus larger signal powers will be generated (compare +6.7 dBm to +5.25 dBm, or -2.11 dBm to -9.65 dBm). To conclude that signals at 1.53 μm cause more ASE suppression than those at 1.55 μm would be inaccurate because the model assumes homogeneous broadening, and because the output saturating signal levels here are different. The assumption of homogeneous broadening implies that the total signal and ASE power within the amplifier at a given point will cause suppression, independent of where within the spectrum the power is concentrated.

	1.53 μm	1.53 μm	1.55 μm	1.55 μm
Variable\Design	-30 dBm signal	-10 dBm signal	-30 dBm signal	-10 dBm signal
Gain	27.89 dB	16.7 dB	20.35 dB	15.25 dB
PTP	4.45 mW	4.35 mW	3.40 mW	3.50 mW
Broadband ASE Power	320.4 μW	58.7 μW	412.4 μW	87.1 μW
In-band ASE Power	40.0 μW	3.1 μW	4.03 μW	1.27 μW
Calculated NF	6.07 dB	6.24 dB*	3.67 dB	3.85 dB*
Optimal Length	13.10 m	11.15 m	14.6 m	12.85 m

*Note : amplifier saturated, so qualitative comparison only

Table 4.6 : Comparison of Performance of Base Design at 1.53 μm and 1.55 μm

As one last comment, the optimal lengths for the different signal wavelengths are seen to be different. This is because of the spectral dependence of the cross-sections, which result in shorter optimal lengths for shorter wavelengths. This is an important consideration in the design of a WDM system, where different wavelengths

are used. For example, if an amplifier was designed to operate at 1.55 μm, it would be too long for 1.53 μm operation, and some signal and ASE re-absorption would occur, lowering the effective gain. Conversely, if the EDFA was designed for 1.53 μm operation, it would be too short for the other wavelength, also resulting in a lower gain due to pump wastage.

4.3 Different Operating Conditions

The previous Section focussed primarily on modifications that could be made to the physical design of EDFAs. Here, different operating conditions have been simulated, and will be discussed. Of interest is the bi-directional operation of amplifiers, which includes both full duplex signal transmission characteristics, and bi-directional pumping for enhanced gain performance.

4.3.1 Bi-directional Signaling

To simulate bi-directional signaling, the base design used in Section 4.3 will have a backward-travelling signal at a wavelength of 1547.5 nm (2.5 nm less than the forward-travelling signal wavelength) added, with signal powers varied between -30 and -10 dBm for the forward-travelling signal, and a like amount for the backward-travelling signal [31].[7]

7. The results here are useful because operation as a bi-directional mid-span repeater or post/preamplifier can be simulated. See reference [31]

Variable\Design	forward/backward -30/-30 dBm	forward/backward -30/-10 dBm	forward/backward -10/-30 dBm	forward/backward -10/-10 dBm
Gain	20.31/19.76 dB	15.48/14.80 dB	15.21/14.64 dB	13.44/12.75 dB
PTP	3.51 mW	3.70 mW	3.70 mW	3.67 mW
Broadband ASE Power	416.7/867.7 μW	108.7/192.5 μW	86.3/205.6 μW	58.4/132.1 μW
In-band ASE Power	4.00/7.76 μW	1.53/2.40 μW	1.26/2.65 μW	0.935/1.75 μW
Calculated NF	3.68/7.11 dB	4.42/7.08* dB	3.85*/7.67 dB	4.40*/7.85* dB
Optimal Length	14.4 m	12.75 m	12.6 m	12.2 m

*Note : amplifier saturated, so qualitative comparison only

Table 4.7 : Simulation Results for Forward/Backward-travelling Signals for the Base EDFA Design.

In order to compare the degradation expected to the base design, the results for the -30 dBm and -10 dBm forward-travelling signal *alone* are included below:

Variable\ Design	Base Design, -30 dBm	Base Design, -10 dBm
Gain	20.35 dB	15.25 dB
PTP	3.40 mW	3.50 mW
Broadband ASE Power	412.4 μW	87.1 μW
In-band ASE Power	4.03 μW	1.27 μW
Calculated NF	3.67 dB	3.85* dB
Optimal Length	14.6 m	12.85 m

*Note : amplifier saturated, so qualitative comparison only

Table 4.8 : Simulation Results from Base Design with -30 and -10 dBm Signal Inputs

Comparing the results of Tables 4.7 and 4.8, it can be seen that the addition of a small, backward-travelling signal (the -30/-30 and -10/-30 cases in Table 4.7) has little deleterious effect on the performance of the EDFA in the forward direction. Note the higher noise figure and lower gain for the EDFA in the reverse direction; this is consistent with other results [29]. The lower gain and higher noise figure in the reverse direction is a result of the optimal length of an EDFA being a function of wavelength, and so the length here, optimized for the forward-travelling signal, is in fact too long for the 1.5475 μm signal, which therefore experiences some absorption over about 1 m near the positive-z exit of the amplifier.

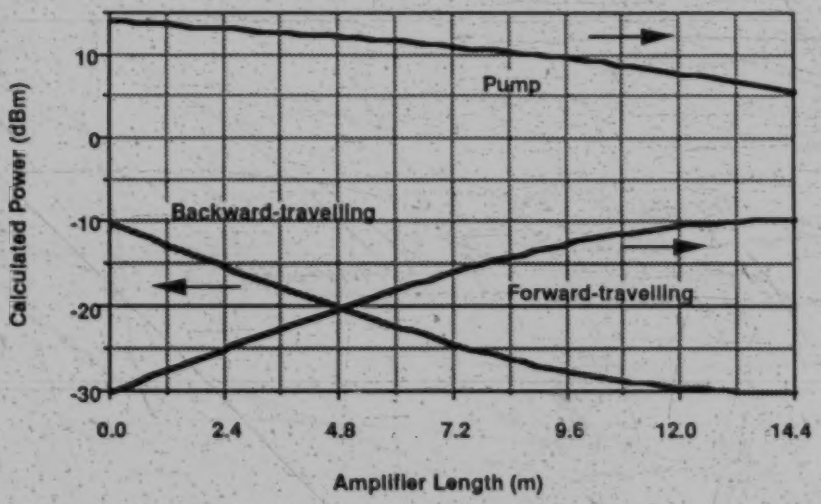

Figure 4.11 : Signal and Pump Evolution for Non-saturating Bi-directional Simulation -30/-30

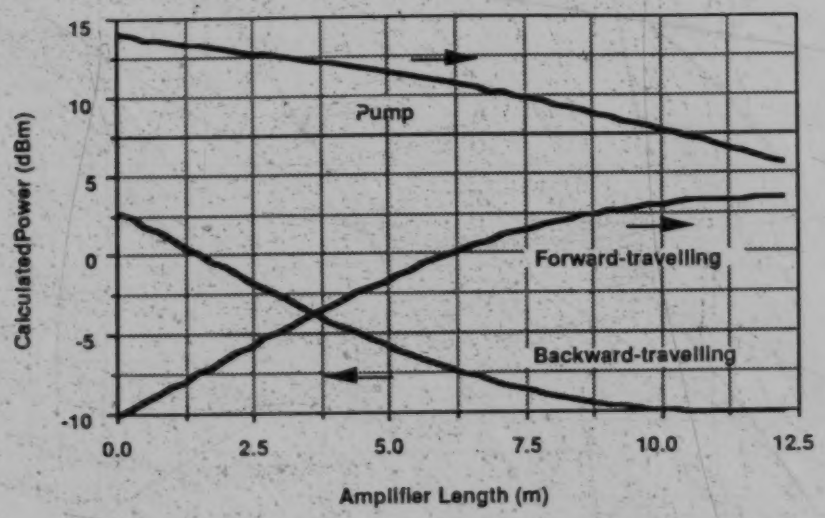

Figure 4.12 : Signal and Pump Evolution for Saturating Bi-directional Simulation -10/-10

4.3.2 Bi-directional Pumping

Having just discussed the simulated performance of an EDFA under full-duplex signaling, it is natural to wonder what effects the addition of a second pump might have on amplifier performance. The characteristics of signal evolution now change; intuitively, it is expected that the signal evolution will be dominated early in its transit through the amplifier by the co-propagating pump, and exhibit characteristics similar to those of the forward travelling signal in Figure 4.11, for example. An optimally designed length for the amplifier would then require that the signal just reach the pump transparency power when the contra-directional pump then becomes the dominant source. Thus, signal evolution would then be expected to proceed similarly to that of the backward-travelling signal in Figure 4.11 for the second part of the amplifier.

Variable\ Design	Base Design	Bi-directional Pump
Gain	20.35 dB	30.26 dB
PTP	3.40 mW	3.40 mW
Broadband ASE Power	412.4 μW	3.13 mW
In-band ASE Power	4.03 μW	43.5 μW
Calculated NF	3.67 dB	4.06 dB
Optimal Length	14.6 m	32.0 m

Table 4.9 : Comparison of Performance of a Co-directionally Pumped Base Design with a Bi-directionally Pumped Base Design

As well, when a small signal is present and equal pump powers are injected at both ends, the ASE evolution in both directions is expected to be *symmetric*. Only a saturating signal can result in enough of an asymmetry to cause the ASE to propagate differently in both directions. Figures 4.13 and 4.14 explore these thoughts graphically.

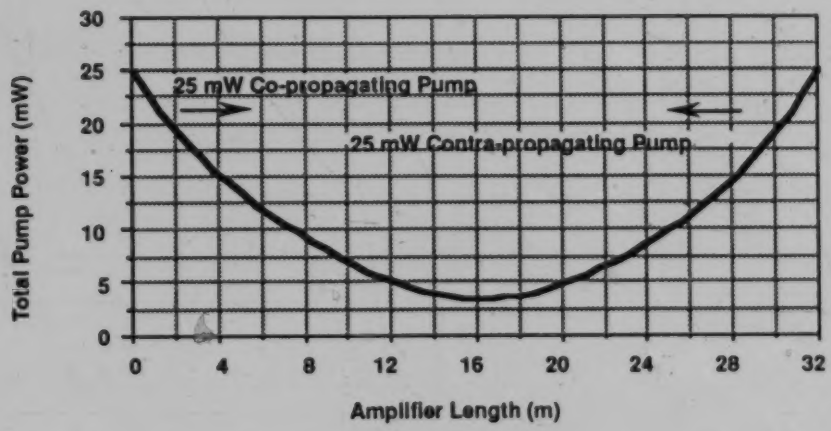

Figure 4.13 : Residual Pump Power vs. Amplifier Length for the Bi-directionally Pumped Base Design

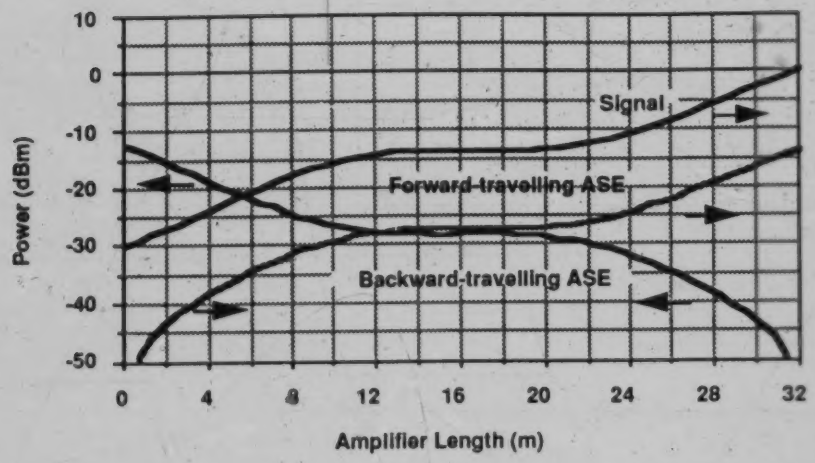

Figure 4.14 : Signal and In-band (1 nm) ASE Evolution vs. Amplifier Length for the Bi-directionally Pumped Base Design

A few comments should be made. First notice from Figures 4.13 and 4.14 that the pump power distribution over amplifier length is symmetric, with the pump power level equal to the PTP for a length of 16 m. Note that the overall length of 32 m is more than double the original amplifier length of 14.6 m because of the combined effect of both pumps near the center of the amplifier. Also note that with the longer overall length of the amplifier, the residual pump exiting either end is now 0.112 mW, substantially lower than the PTP. This would be advantageous in system configurations where residual pump can be a nuisance, such as in pre-amplifiers. In Figure 4.14, the in-band ASE and signal evolutions are shown and reveal the anticipated behavior. Recall that the forward-travelling in-band ASE has to be calculated by interpolation, and so does not exactly mirror the backward-travelling ASE, as would be expected due to the symmetry of the pump. Also note that the input signal power of -30 dBm is seen to have little effect on the suspected symmetry of operation, and, even though the output signal is +0.26 dBm, little saturation is expected because the *Output Saturation Power* for bi-directionally pumped amplifiers would be high.

How useful is this configuration, and what might be the motivation to use it? To address these questions, it is useful to consider how this amplifier might compare to two successive co-directionally pumped amplifiers, supplied with a like amount of pump power; this configuration appears in line 2 of Table 4.10. Alternatively, a configuration supplying a similar amount of gain could be examined, and is shown in line 3 of Table 4.10.

Configuration	Gain (dB)	Residual Pump (mW)	NF (dB)
Bi-directionally pumped EDFA	30.26	0.112	4.06
Two co-pumped 25 mW I/P EDFAs	40.70	3.40	7.34*
One 25 mW and one 15 mW co-pumped EDFA	30.76	3.40	8.20*

*Note: Sum noise figure of two individual stages (See Figure 4.3)

Table 4.10 : Comparison of One bi-directionally Pumped Amplifier with Two Configurations for a Co-directionally Pumped Amplifier Cascade, for Signal I/P of -30 dBm

From Table 4.10, it is easy to see the advantages conferred by the bi-directional case. As well, it is very important to note that an amplifier cascade is not expected to perform as well as the numbers above suggest, because of residual pump and ASE that forms part of the input to the second amplifier in the cascade. If this input is reduced by inclusion of an optical filter, the noise figure of the second amplifier would then be degraded by the insertion loss of such a filter. It is seen, when comparing the cases discussed, that while more gain can be obtained given the available pump power, the surplus is used to reduce the noise figure by better maintaining a population inversion through-out the amplifier. Thus, the bi-directionally pumped configuration is

operationally more attractive and would require the same number of components as long as isolation is not required for the pump sources due to residual pump power.[8]

4.4 Summary of Observations

Before going on to Chapter 5 and Design of EDFAs, it is useful to summarize all the observations made on the qualitative changes that occur to EDFA performance when parameters are selectively varied. This is best done graphically.

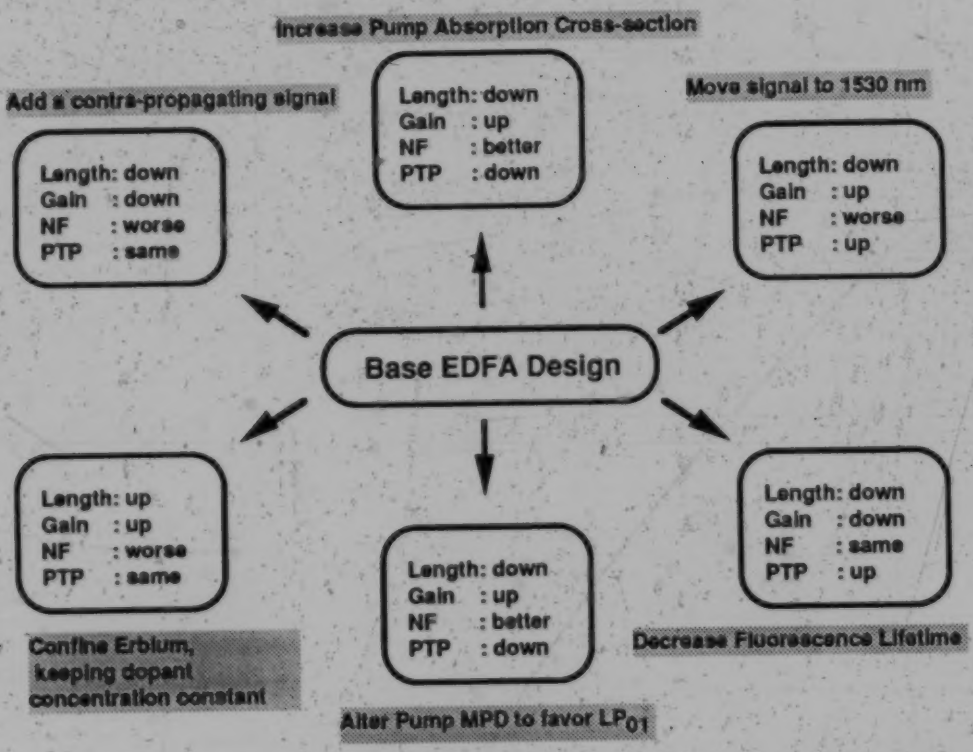

Figure 4.15 : Qualitative Summary of Parameter Variation Effects on Simulated Performance of Base EDFA Design

8. One possibility to avoid the problem of residual pump feed-through is to use two different pump wavelengths, such as 980 nm for one and 1480 nm for the other.

5.0 Design of Erbium-doped Fiber Amplifiers

As seen in Chapter 4, design of an EDFA is a multifaceted challenge. This is due to the large number of design variables which jointly affect performance of the designed amplifier. As well, trade-offs exist when choosing parameters for the designed fiber when high gain, low noise, and low splice loss to standard telecommunications fiber are desired. Due to the scope of the design problem, a good simulation package as discussed in previous chapters is a necessary tool and many iterations on a given design will usually be required before a suitable result is achieved. Currently, fiber designs from TR Labs are submitted to the National Optics Institute in Quebec City for fabrication, and so far TR Labs has acquired three types of Erbium-doped fiber; two were from stock supplies and the third was designed by TR Labs and was used extensively in the experimentation reported in Chapter 6.

5.1 Design Variables

The following fiber parameters are considered in the design:

a) Fiber core and cladding radii
b) Fiber Numerical Aperture (NA)
c) Erbium dopant profile
d) Erbium dopant concentration
e) Core co-dopants

As well, the following must be considered:

a) Availability of pump power
b) Acceptable splice losses
c) Desired gain
d) Desired noise figure
e) Wavelength of signal operation

Each issue will be addressed separately.

5.1.1 Fiber Core/Cladding Radius and Numerical Aperture

The choice of a fiber core radius and numerical aperture will strongly affect splice loss, gain, and length of the designed amplifier. Generally, the cladding diameter will be designed to be 125 μm, in accordance with international standards. If two fibers are to be fusion spliced together, it is particularly important that fiber end-areas be comparable, so that equal power densities in the arc of the fusion splice set exist on both fiber end-faces during the fusion process. The core diameter and NA are designed on a different set of priorities. Consider first splice loss. The splice loss for a joint of two single-mode fibers is given by [32]:

$$\Gamma\,(\mathrm{dB}) = -10\log\left[\frac{16n_{co}^2 n_o^2}{[n_{co}+n_o]^4}\,\frac{\sigma}{q}\,e^{\left[\frac{-pu}{q}\right]}\right] \tag{5.1}$$

where

$$p = \frac{(k_s\omega_T)^2}{2}, \quad q = G^2 + \frac{(\sigma+1)^4}{4}, \quad k_s = \frac{2\pi n_o}{\lambda}, \quad \sigma = \left[\frac{\omega_R}{\omega_T}\right]^2,$$

$$u = (\sigma+1)F^2 + 2\sigma FG\sin(\theta_t)\cos(\gamma) + \sigma\sin^2(\theta_t)\left[G^2 + \frac{(\sigma+1)}{4}\right],$$

$$F = \frac{r_o}{k_s\omega_T^2}, \quad G = \frac{z_o}{k_s\omega_T^2},$$

and where

n_{co} and n_o are the indices of refraction of the fiber cores (assumed the same) and the gap between the fiber ends, respectively

ω_T and ω_R are the mode-field radii of the transmitting and receiving fibers,

λ is the wavelength of the light,

r_o, z_o, θ_t are the transverse, longitudinal, and angular misalignments, and

γ is another angular misalignment relating to the transverse offset.

Fortunately, eqn. 5.1 may be reduced to a simple result if r_o and θ_t are assumed to be zero and n_{co} and n_o are assumed to be equal:

$$\Gamma\,(\mathrm{dB}) = -10\log\left[\frac{\sigma}{q}\right] \tag{5.2}$$

which further reduces to:

$$\Gamma\,(\mathrm{dB}) = -10\log\left[\frac{4\sigma}{(\sigma+1)^2}\right] \tag{5.3}$$

when z_o equals zero. Eqn. 5.3 is useful in that it shows that an unavoidable splice loss will exist between two single-mode fibers that have mismatched mode-field diameters at a given wavelength. The mode-field diameter, in turn, can be calculated from the following expression:[1]

$$\omega = 2a\left[0.65 + \frac{1.619}{V^{1.5}} + \frac{2.879}{V^{6}}\right] \tag{5.4}$$

where a is the fiber core radius and V is the normalized frequency of the light. The core radius is thus seen to impact the mode-field diameter (and recall from eqn. 3.1 that V is directly proportional to core radius as well), and will therefore affect the splice performance of a designed amplifier. In Figures 5.1 and 5.2, the effect of core radius on NA required to give a certain mode-field diameter at 1550 nm is plotted. As well, refer to Appendix B for further exploration of splice losses.

1. This expression is widely used and assumes a Gaussian fiber modal profile, in lieu of the Bessel Functions. It describes the diameter as measured from the $1/e^2$ points of the *intensity* profile. See, for example, reference [18].

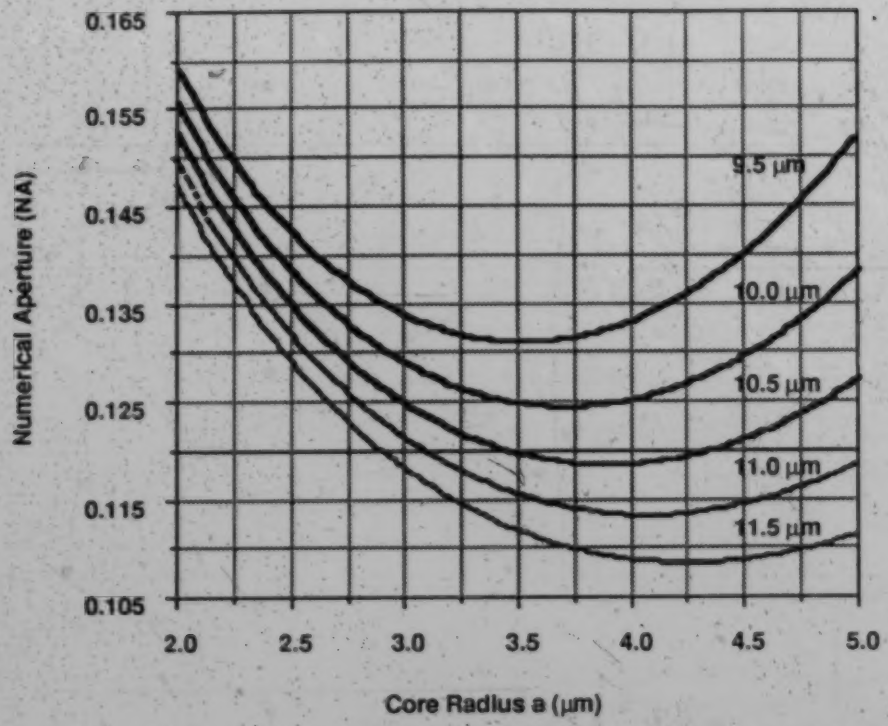

Figure 5.1 : Numerical Aperture Required for a Given Signal mode-field Diameter as a Function of Core Radius from 2.0 to 5.0 µm

A couple of comments should be made about Figure 5.1. First of all, standard telecommunications fiber, which is similar to SMF-28 fiber from Corning, has a nominal mode-field diameter at 1550 nm of 10.5 µm, a core radius of 4.35 µm, and a NA of 0.126. This fiber thus exists as a single point on the above graph. Any fiber designed with the appropriate NA and core radius such that the signal mode-field diameter is 10.5 µm will theoretically splice with zero loss to SMF-28. In addition, it is interesting to notice the minimum in all curves occurs for V = 1.873 at 1.55 µm, independent of the mode-field diameter. So, in principle, low splice-loss amplifiers can be designed and still maintain a degree of flexibility in the joint choice of fiber core and NA.

Now consider amplifier gain. Trends in amplifier design have lately focussed on high gain designs and it is reported that fibers with high NA can produce high gain coefficients [33].[2] However, little comment has been made about such fibers and their connectivity to standard telecommunications fiber [34].[3] Smaller core radii and their corresponding NA can now be examined for a given signal mode-field diameter to explore possible low splice loss, high gain designs.

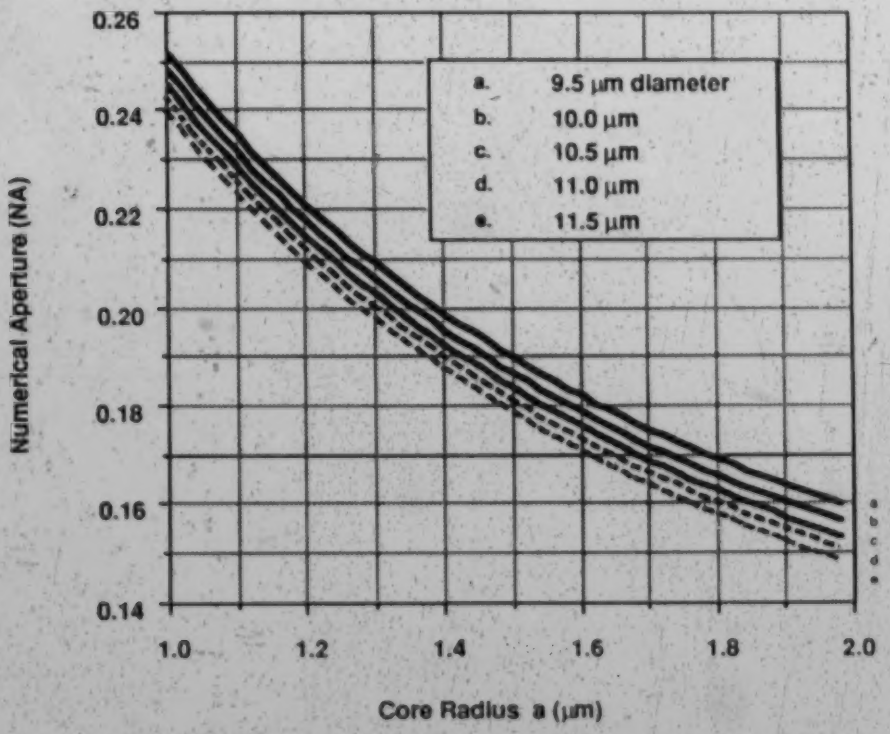

Figure 5.2 : Numerical Aperture Required for a Given Signal mode-field Diameter as a Function of Core Radius from 1.0 to 2.0 μm

2. Gain coefficient is typically measured in dB/mW as the slope of a tangent to the curve of Gain vs. Pump Power where the tangent passes through the origin.
3. Some interesting ideas do exist. For example, see reference [34]. As well, discussions with NOI suggest that tapering the core at the end of the amplifier to act as a mode-field transformer may also be an option.

When comparing Figure 5.2 to 5.1, it is seen that the spacing between the family of curves narrows. This is unfortunate if high NA designs are sought, because the mode-field diameter becomes more sensitive to manufacturing tolerances in NA. To illustrate this point, suppose a 10% tolerance exists on any specified design NA[4]. For small core radii, this equates to roughly a ±3 μm variation in mode-field diameter, which in turn could cause an increase in splice loss of 0.3 to 0.5 dB, as well as significant deviations from desired performance. For larger core radii, where the mode-field curves are further apart and the slope is smaller, a 10% tolerance in NA might result in as little as a ±0.5 μm variation in signal mode-field diameter and very low splice loss. This point is discussed here because NOI, at this stage of development in their Erbium-doped fiber manufacturing capability, seems to have difficulties in achieving designed NAs. This seems largely due to control over index-influencing core co-dopants, such as Aluminum, Germanium, and Phosphorus, and will be discussed further later. To conclude, while high NA designs have been seen in both simulation and experimentation to increase the gain, at this time it appears that more conservative designs will yield more predictable results.

When considering NA and core radius in the design of an amplifier, other design philosophies do exist and are worth mentioning. For example, the 980 nm pump is double-moded in standard telecommunications fiber, and, as already discussed in previous chapters, the LP_{11} mode is not as efficient as the fundamental mode in pumping the Erbium. Thus, design might focus on the cut-off wavelength of the amplifier fiber instead of on splice loss, where it is clearly hoped that improvements in pumping efficiency might out-weigh deleterious effects of splice loss [35], [36].

---

4. This is a generous figure. When a design was submitted to NOI for fabrication requesting a NA of 0.126, the resultant fiber had a NA of 0.16, a 27 % relative increase.

Another consideration in design is ultimate packaging, especially of the pump source and the safety considerations which must be considered. If an amplifier of appreciable length must be coiled to be packaged, a good design might consider the macrobending loss characteristics of the fiber, especially at the pump wavelength. Here, the design of NA and core radius will seek to minimize the minimum tolerable bend radius R_b [37].

5.1.2 Erbium Dopant Profile and Concentration

Of critical importance to the design of an amplifier is the selection of a dopant profile and concentration. This selection is strongly influenced by fiber core radius and NA, and pump modal characteristics, and will strongly influence the optimal length of the amplifier, as discussed in Chapter 2. Each topic will be discussed in turn.

It has been shown in a number of references [11], [35], [38], that confining the Erbium distribution to a radius less than that of the fiber core radius improves the pumping efficiency and thus the gain of the amplifier. This occurs due to better overlap between the Erbium and the LP_{01} mode of the pump. Keeping the Erbium concentration fixed and decreasing the confinement radius w from w = a to w = 0.2a can improve the gain by as much as 10 dB. However, the optimal length required to exploit this improvement will increase by more than a factor of 5 when w = 0.2a.[5] If a certain length must be maintained and confinement is sought, then the concentration must be reduced according to:

$$\frac{N_1}{w_1^2} = \frac{N_2}{w_2^2} \tag{5.5}$$

where

5. Recall the discussion of Section 4.3.4.

w_1, w_2, are the initial and modified confinement radii, and

N_1, N_2, are the initial and required Erbium concentrations.

The Erbium profile itself is generally assumed to have a brickwall characteristic, where:

$$[Er^{3+}] = N_0 \text{ for } r < w, \text{ and } 0 \text{ otherwise} \tag{5.6}$$

However, this is unlikely. Analysis at NOI of their manufactured amplifier fiber suggests that the Erbium dopant profile is strongly correlated to that of the Ge co-dopant concentration profile, which is observed to possess a dip near the center of the core due to "burn-off" [39].[6] For Aluminum co-doped fibers, fairly flat Erbium dopant profiles can be obtained, and so the brickwall approximation is reasonable [26].

Concentration of Erbium dopant is an interesting design problem. On the one hand, if the Erbium concentration approaches zero, no amplification is expected from the fiber. However, a number of undesirable effects occur when the concentration is too high. First of all, clustering effects of the dopant in certain manufacturing processes can occur, leading to poor dispersal of dopant throughout the host. In addition, ions in close proximity can experience cooperative up-conversion, whereby a one atom in an excited state can non-radiatively decay to a lower state and cause an upward transition of equal energy difference in another nearby atom. This reduces the population of the upper lasing level and is thus undesirable. Finally, in a related effect, the fluorescence lifetime, τ, is found to depend on dopant concentration according to [26]:

---

6. Electron Probe Micro-Analysis (EPMA) was performed on the preform. This consists of bombarding the surface of the preform with X-rays and counting and interpreting reflections as various constituents.

$$\tau = \frac{\tau_o}{1 + [\rho/Q]^2} \qquad (5.7)$$

where

ρ = the Erbium concentration in ions/cm^3, and

Q = the Quenching Concentration, and ranges from 3.9 to 6.0 x 10^{20} cm^{-3} for Silicate glasses.

Having described both extreme possibilities for dopant concentration, it is interesting to thus pursue what an optimal concentration might be. Research by others suggests that concentrations on the order of 10 - 200 ppm (molar) are acceptable, and yield EDFAs with higher gain coefficients, lower pump transparency powers, and higher saturated output powers [40], [41], [42]. Recent trends in fiber design have thus used much lower concentrations of Erbium than two or three years ago. A concentration of about 100 to 200 ppm is probably acceptable when pumped with a 980 nm source; if the concentration is too low, the optimal fiber length will be too long and Rayleigh scattering of pump light and other background loss mechanisms become significant.

5.1.3 Core Co-dopants

A number of additions can be made to the chemical composition of a Silicate-glass fiber core which alter the performance of the designed amplifier. Aluminum and Germanium are the most common additions, but Phosphorus, Fluorine, and Ytterbium have also been added to Erbium-doped Silica-based fibers.

Aluminum has a number of important effects when added to the core of the fiber. First of all, it impacts the refractive index of the core and thus provides a

measure of control over the numerical aperture of the designed fiber. This has helped make high-NA designs possible. As well, the addition of Al substantially broadens the fluorescence spectrum of the amplifier, to FWHM values as high as 40 nm from 26.5 nm for Ge co-doping alone. Amplifiers designed with broader gain spectra could thus find application in WDM systems, where various gain-flattening techniques can be used to equalize channel gain [3]. Another important feature of Al co-doped fibers which is useful for broadband operation is better immunity to gain coefficient (dB/mW) variations with signal wavelength [11]. As well, the broader spectrum may be useful in the design of a superfluorescent laser, which finds application in fiber gyroscopes. Aluminum is also found to aid in incorporation of Erbium into the glass when the solution-doping technique for fiber fabrication is employed. Clustering of Erbium, which could give rise to inhomogeneous broadening effects, can be minimized, and it is found that the Erbium dopant profile in the core will mimic that of the Al when the Ge:Al ratio is 10 or less, which typically implies an Al:Er ratio of 50 [26]. This is good because Al does not suffer the central core dip that Ge does. Typically, fibers can be made with two distinct core regions; the outer core region incorporates Ge co-doped fiber, and the inner core region incorporates Al and Er, resulting in a confined Er dopant profile as discussed before.

Ge is added to the core to raise the index of refraction, and high NA fibers typically use Ge in lieu of Al since Al co-doped fibers suffer higher background losses and the Ge doping process is said to be more controllable.[7] As well, adding Ge alters the spectral shape of the fluorescence spectrum, favoring two peaks, one around 1535 nm and the other near 1555 nm. In addition, Ge co-doped fibers seems to exhibit stronger inhomogeneously broadened tendencies than do predominantly Al co-doped

7. NOI claims it is easier to control the incorporation of Ge into the core than Al, even though an uncontrollable dip in concentration appears near the center of the core.

fibers. This would have implications on the saturated operation of the amplifiers when multiple channels are present, as well as operation as a post/preamplifier in a bi-directional transmission system, currently being examined at TR Labs. As a final note, Ge co-doped fibers have pump absorption cross-sections which are more than twice those of strictly Al co-doped fibers [11]. This, of course, impacts amplifier design optimal lengths, gain, and pump transparency powers.

The effects on amplifier characteristics of adding Phosphorous to the core are not as clear. Its addition has been noted to improve incorporation of Al into the silicate glass, allowing high NA fibers to be made without the doping with Ge [11]. In one report [42], the addition of P to a Ge co-doped fiber was seen to improve the efficiency of pump conversion to signal. As a final note, P also appears in the cladding in conjunction with Fluorine, where the combined effect is to lower the index of the glass.

Ytterbium co-doping was originally proposed as a means of improving 820 nm band pump absorption in Erbium-doped fiber lasers. The Yb-Er co-doped fiber was observed to have a huge absorption cross-section over tens of nm, and was found to have minimal effect on the output characteristics of the laser while allowing shorter lengths and more flexibility in pump absorption [43]. More recently [44], Yb was studied for use with a diode-pumped Nd:YAG pump laser at 1064 nm in Erbium-doped fibers. One issue raised was the transfer efficiency of the Yb-to-Er excited state transition. It appears that P must be added in conjunction with the Yb to improve this transfer efficiency. Since the absorption band of the Yb-sensitized Er is so broad, one thought for future work at TR Labs would be to produce an amplifier co-doped with Yb and low concentrations of Er for pumping at 980 nm. This may then allow for shorter amplifier lengths, and discussions on fabrication of such a fiber are currently underway with NOI.

5.2 Design Submitted to NOI

Based on the considerations discussed the following design was submitted to NOI for fabrication, and the fabricated fiber values are shown in comparison.

Parameter	Designed Value	Fabricated Value
Core radius a	4.15 μm	3.05 μm
Core index of refraction	1.471	unknown
Numerical Aperture	0.126	0.16
Erbium dopant concentration	450 ppm	750 ppm
Calculated Signal*mode-field diameter	10.0 μm	7.8 μm
Calculated Pump mode-field diameter	7.6 μm	5.8 μm
Dopant confinement factor w	2.0	4.0

*Note: Signal at 1.55 μm

Table 5.1 : EDFA Design Parameters Submitted to NOI

The desired fiber geometry is recognized to be that of SMF-28; this choice was made in an effort to reduce splice loss, especially at the pump wavelength, of the amplifier to JDS FC/APC connectorized fiber pigtails, which are composed of SMF-28, and were used extensively as the standard inter-connect for optical devices in the lab (see Chapter 6). As well, testing on previous Erbium-doped fiber samples from NOI suggested very poor splice performance was being obtained. Splice loss was thus a strong consideration, especially since a low amount of pump power available. Other aspects of the design, including the relative amounts of Al, Ge, P, and F added to the design were left to the discretion of Mr. Lee Bonnell of NOI; it was understood, however, that Al was to be the dominant core co-dopant, and ASE spectra measured at TR Labs (see next chapter) confirm that this was the case. The core was fabricated in

two stages, with an outer core composed of Ge co-doped glass, and an inner core composed of Al and Er co-doped glass to achieve the specified confinement.

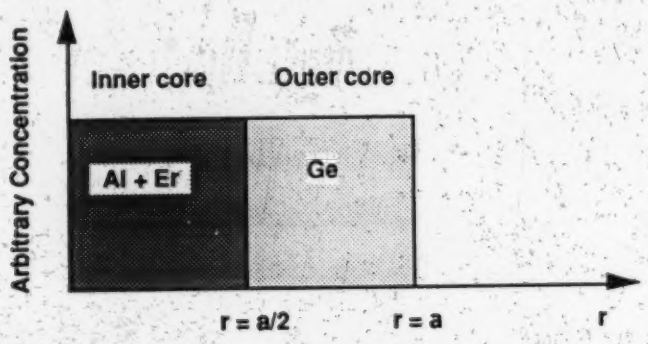

Figure 5.3 : Conceptual View of the Placement of Core Co-dopants

6.0 Experimental Characterization of EDFAs

Once simulations, design, and fabrication of a particular EDFA have been completed, it is important to then test the amplifier and compare the results with those expected. A variety of experimental test configurations involving a vast array of equipment are required to analyze the behavior of the EDFA thoroughly. Since it is desirable to have repeatability in all test configurations, it has been advantageous to bring all experiments under computer control. This has been done using a software package on a Macintosh II si called LabVIEW™ from National Instruments, which controls eligible instruments over a General Purpose Interface Bus (GPIB), otherwise known as an IEEE 488.2 interface. With this facility, a complete set of tests can be performed in about a day.

6.1 Computer Control of Experiments

Section 6.3 outlines the experimental configurations used to characterize the designed EDFA's performance. The key to fast, repeatable experiments was the presence of the following pieces of equipment which possess GPIB capability:

1. JDS Series 7000 Variable Optical Attenuator (VOA)
2. Stanford Research SR 530 Lock-in Amplifier
3. CVI Digikrom 240 Digital Monochromator
4. Newport 835 Optical Power Meters
5. Anritsu ML93B Optical Power Meter
6. HP 8116A Signal Generator
7. HP 3478A Digital Multimeter
8. Keithley 576 D/A Data Aquisition System

Using the Keithley 576, control of any device with an analog input could be accomplished. This made possible remote control of the Light Control Model 502 Laser Driver.

LabVIEW™ is a software package that combines many conventions and structures of traditional programming languages like Pascal and C into a menu-driven, icon-based programming language. The user designs *Virtual Instruments* (VIs) which are application programs specifically designed to control certain devices over the GPIB. Programming is done at two levels. First, a *Front Panel* is designed using a variety of possible graphics to simulate mechanical buttons, sliders, or knobs that might be found on the actual instrument's front panel. In addition, displays and graphs are available to supply the user with results or status information while an experiment is in progress, and all *Front Panel* controls are computer-mouse driven. A LabVIEW™ program also possesses a *Block Diagram*, which describes graphically how a particular device is to be controlled, how data is to be acquired and possibly conditioned, and how results are to be supplied to the *Front Panel* for viewing by the user. This portion of the program resembles a circuit diagram, with *wires* connecting various elements of the *Diagram* together. Since the package is menu-driven, has excellent on-line help, and is quite intuitive, it is possible to become a proficient programmer quickly, and fairly complex programs with extensive I/O operations to both the computer screen and to a disk or Hard-Drive of a computer can be written in about one hour. Some sample programs are included in Appendix E.

6.2 Characteristics of EDFA Components

As discussed in Chapter 2, an EDFA requires a pump laser, a WDM, and a source of signal, and the characteristics of these components, especially the pump, are critical in determining the overall performance of the amplifier. Therefore, these devices have been thoroughly examined.

6.2.1 Pump Laser Characteristics

A number of pump lasers were initially made available by RCA (Now EG & G Canada). These devices were strained, single quantum well (SSQW) devices, with active areas of about 2 μm by 0.2 μm and cavity lengths of 750 μm. Measured perpendicular far-fields were typically 70° measured at the $1/e^2$ points (40° when measured at Full Width, Half Maximum (FWHM)), and stayed fairly constant for wide drive current ranges. The parallel far-fields were typically 30° at the $1/e^2$ points (20° FWHM) for low drive currents, but would broaden substantially for higher drive currents to as much as double the quoted figures above. The devices had multiple longitudinal modes, showed evidence of single transverse-moded operation from spots observed on IR-sensitive screens, and operated at nominal wavelengths ranging from 975 to 990 nm depending on the pump drive current. For higher drive currents, the wavelength shifted towards longer wavelengths due to thermal effects; a figure of 0.3 nm/°C roughly correlates temperature to wavelength shift. The devices were rated to 200 mA, typically had a forward voltage drop of 1.5 to 2.0 V, and had threshold currents ranging from 15 to 20 mA..

Since the devices were mounted in an RCA T-5 co-axial can package, with direct access to one laser facet and no coupling optics, careful design of a system to couple light effectively from the devices to nominally single-mode fiber had to be

considered. This was made more difficult by the high effective NA of the laser due to its divergent far-fields. Eventually, two methods yielded satisfactory coupling of the pump to fiber, where it was nominally double-moded:

a) Use of fiber tapers from BNR. The tapers required very stable and close positioning to the laser O/P facet, but could achieve 30 to 40 % coupling over short periods of time (minutes). As the mechanical positioners drifted, or as the far-fields of the laser changed, the coupling efficiency would drop and retuning would be required. Also, since the fiber was positioned close to the facet, care had to be taken not to contact the facet with the fiber, as this results in the reduction of the laser to an LED due to facet destruction. Fiber tapers are reported to be used in newly available commercial products from Pirelli and EG & G Canada, but the tapers there are of higher quality and are epoxied into position once coupling is optimized.

b) A series of collimating and focussing lenses can also be used to couple light into fibers, and Oz Optics Ltd. were willing to take supplied 980 nm lasers plus fiber desired for a pigtail and package the appropriate coupling optics into a stable, anodized aluminum housing. In consideration of the broad far-field of the lasers the output light is first collimated by a high NA lens; for this, an AR-coated aspheric lens was used by Oz Optics. Next, a focussing lens coupled the collimated beam into the SMF-28 FC/APC-connectorized pigtail, and coupling efficiencies for the devices coupled in this manner (three were ultimately packaged this way) ranged from 35 to 40 % at low current levels down to around 25 to 30% at the higher, more useable current levels. Coiling the pigtail around a mandrel and even straightening or twisting of the fiber affected the power observed at the connector, suggesting the presence of LP_{11} modes. However, the change observed varied in magnitude from device to device, implying different launch conditions, and were least severe in Oz-coupled device #2 (Oz #2),

whose L-I curve is shown in Figure 6.1. Unfortunately, the launch conditions and their repeatability were unknown, so the exact modal power distribution (MPD) could not be determined for simulation purposes. Referring further to Figure 6.1, it is interesting to note that the curve loses linearity for currents greater than 130 mA. This may be due to changes in the far field pattern which would affect coupling efficiency, and due to observed shifts in the output lasing spectrum towards 990 nm and beyond.

As a final comment, two of the three Oz-coupled devices had suffered reduced performance after about 8 to 10 h of intermittent use. Burn-in had not been performed by RCA on the lasers, which were prototypes, and no mean-time-before-failure (MTBF) measurements were available either. Reliability of these devices has been the subject of on-going dialog between TR Labs and EG&G Canada.

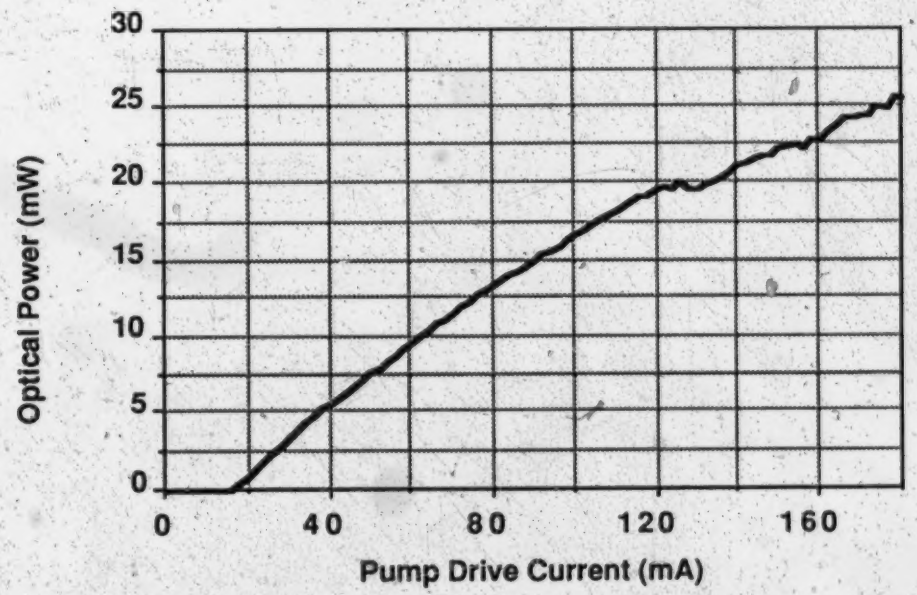

Figure 6.1 : Optical Pump Power vs. Drive Current for 980 nm Pump Device Oz #2

6.2.2 Signal Laser Characteristics

Two NT 1550 DFB lasers were acquired from BNR and incorporated onto circuit boards at TR Labs to include both temperature and optical power output control. The laser thresholds for both devices were about 20 mA, the slope efficiency was 0.011 W/A for one DFB and about half that for the other, and side modes were evident as illustrated in Figure 6.2. In addition, both had an AC-coupled SMA connector receptacle so that direct modulation of the lasers was possible.[1] Both devices nominally lased at a wavelength of 1550 nm, but this was tunable over 2 to 3 nm by altering the temperature of operation. Thus, separation of the two signals for WDM applications could be achieved. Both devices were typically biased at -3.0 dBm when modulated by a 622 Mbit/s data signal, providing an extinction ratio of about 10:1.

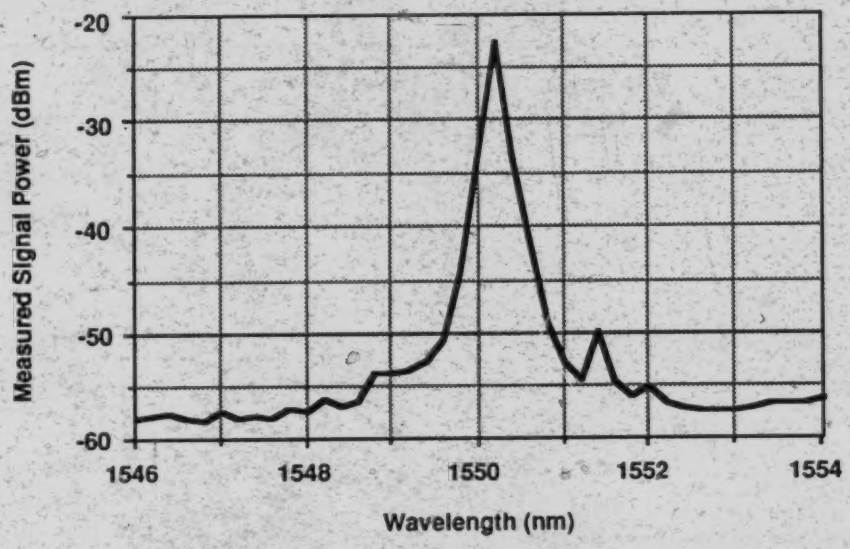

Figure 6.2 : Spectrum of DFB#1. Resolution = 0.20 nm, Power = -7.39 dBm, Modulated at 622 Mbits/s

1. The lower 3 dB cut-off frequency was around 200 Hz, due to capacitive coupling to the gate of the drive FET in the drive current circuit.

6.2.3 Optical Filters

Three means were available to achieve tunable, bandpass optical filtering in the 1550 nm window. First, a tunable device from Queensgate was considered for applications requiring narrow filtering around 1550 nm, but this device was found to suffer from stability problems giving rise to drifts which caused loss of alignment of the etalon forming the filter. In addition, the filter's narrow bandpass (0.5 nm) did not permit sufficient passage of the modulated DFB spectrum and resulted in an insertion loss of 5 - 6 dB, depending on the success of tuning.

If filtering prior to detection was desired, the CVI Digikrom 240 Monochromator could be used as an optical filter, whose bandwidth is given by [45],[46]:

$$B_o = SW\left[\frac{10^6 \cos\left[\sin^{-1}\left[\frac{\lambda}{1.654}\right]\right]}{240 \times 1200}\right] \qquad (6.1)$$

where

SW = slit width in μm
240 = width of Grating in mm
1200 = number of lines/mm
λ = wavelength in μm

At 1550 nm, this gives 0.12 nm as the bandwidth for 100 μm slits. For typical filter applications, it was found that an exit slit width of 600 μm (Bandwidth = 0.72 nm) was sufficient to pass the modulated DFB signal with minimum insertion loss. This is consistent with the measured -20 dB bandwidth of the DFB, which was found to be about 0.75 nm. The minimum insertion loss of the CVI was found to range from 6 to 8 dB, and depends on the quality of the cleave of the input fiber, the degree of success in

the alignment of the optics through the monochromator, and the efficiency of the grating and optics within the device at a particular wavelength.

As a final note, a fiber-coupled, tunable optical bandpass filter, with insertion loss of about 1.0 dB and a 4 nm bandwidth, was purchased from JDS. This device would follow an EDFA and help reduce the amount of broadband ASE present with any signal present. The device was found to be stable and allowed good fiber-to-fiber transmission when tuned to pass the modulated DFB. Note, however, that its wide bandwidth will allow larger amounts of ASE to pass as well.

6.2.4 Other Passive Optical Devices Used

A number of fiber-optic couplers and wavelength division multiplexers (WDMs) were used in the various experimental configurations. There performance is summarized in the Table 6.1.

Devices	Schematic	Insertion losses
Gould 90/10 Splitter		90%: 0.8 dB 10%: 18.0 dB
Gould 50/50 Coupler	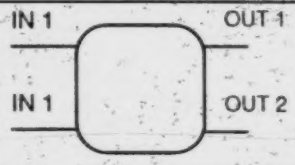	IN 1 to OUT 1: 4.06 dB IN 1 to OUT 2: 5.05 dB IN 2 to OUT 1: 5.08 dB IN 2 to OUT 2: 4.06 dB
JDS WDM Device #1 Device #2	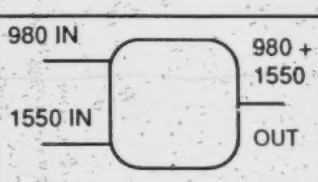	Device #1 980 IN to OUT: 1.2 dB 1550 IN to OUT: 1.0 dB Device #2 980 IN to OUT: 1.0 dB 1550 IN to OUT: 0.7 dB
OFR IO-F-IR2 Optical Isolator		IN to OUT: 2.5 dB Isolation = -33 dB @ 1540 nm
JDS VOA 7000		IN to 90%: 2.7 dB IN to 10 %: 13.4 dB

Table 6.1 : Summary of Other Optical Devices Used

6.3 Experimental Configurations

A variety of experimental configurations are used in characterizing the performance of an EDFA. Some require extensive set-up times, while others are simple variations on existing set-ups. All optical interconnections are made easy by the use of FC/APC connectors, which have low back-reflections (better than -60 dB) and 0.1 - 0.2 dB insertion losses.

6.3.1 Measurement of DC Amplifier Gain

This measurement is perhaps the most informative and yields optical gain versus signal input power to the amplifier, and is typically done for a variety of 980 nm pump laser drive currents. Refer to Figure 6.3 for the set-up required to determine the DC gain of the amplifier. In this configuration, the average optical output power from a 1550 nm DFB is adjusted to -3.0 dBm by using the trim pot on the package; a second trim pot is also adjusted to temperature-tune the wavelength to a desired value, typically between 1550 and 1552 nm. It is important that the power level and wavelength then stay constant for the remainder of the experiment; any changes here will cause the wavelength of operation to change, affecting the insertion loss of the monochromator and causing variations in the results. The isolator was inserted following the DFB to prevent feedback to the laser from reflections or backward-travelling ASE. Following the isolator, the JDS VOA is inserted to allow computer control over the signal level presented to the EDFA. The 10% arm is fed to an optical power meter whose reading is calibrated to display the actual optical power entering the amplifier via the 90% arm. Readings from the optical power meter can be collected via the GPIB and are used to calculate Gain of the amplifier.

The JDS WDM#2 is used to combine the pump and signal for delivery to the amplifier, and the EDFA then follows in the set-up, with the output coupled to the monochromator via an FC/APC-to-cleaved-bare-fiber jumper, which is positioned at the entrance slits. In this configuration, the monochromator is used to reject as much ASE as possible before detection. The Newport 835 optical power meter fitted with a 1 mm diameter Ge head was used at the exit slit to detect the filtered light. The detector

was not reverse biased and had an optical-power-equivalent noise floor of about -65 dBm when used at the O/P of the monochromator.

The entire experiment was controlled with a LabVIEW™ program which first set a particular signal I/P power level to the EDFA by controlling attenuation of the VOA, then waited for a period of time for the gain to stabilize.[2] To obtain smooth Gain vs. I/P Signal Power curves, delays of 10 s or longer were required before the reading on the Newport power meter had stabilized. Note that time constants associated with the detector are much shorter than 10 s, and therefore are not affecting the measurement. The requirement for long delays must therefore be due to the EDFA, although it is unclear how. After the requisite delay, the reading is then taken, the data plotted to the computer screen for real-time monitoring of the experiment, and accumulated in a computer file for subsequent processing.[3] It is important to note that when measuring DC signal O/P from the monochromator, in-band ASE is present and forms a substantial percentage of the overall detected power when the DFB I/P signal is small. To correct this problem, a measure of the ASE when no signal is present is made and this number is subtracted from all O/P power readings before the gain is evaluated. This assumes that the ASE contribution is fairly constant in the small signal regime and this correction technique results in good results (See Figure 6.4 and Figure 6.5). As a final note, it is important to ensure that the Anritsu power meter, used to measure the I/P power to the amplifier, and the Newport power meter, used to measure

2. At very low I/P signal powers to the EDFA (typically < -35 dBm), the In-band ASE comprises a large percentage of the light detected at the monochromator O/P. If readings are averaged over long periods of time, the signal component be better estimated (Note also that the ASE power level is known *a priori* by separate measurement and is subtracted from the total measured). Also note that at times the pump power varies due to changes in coupling when the temperature changes; this will also affect gain measurements.
3. See Appendix E for a copy of this program.

the O/P after the monochromator insertion loss, are calibrated against each other so that differences in readings do not impact the gain measurements.

As a final comment, an AC measurement of the gain can be made by modifying the configuration of Figure 6.3 to include a signal generator and lock-in amplifier and by replacing the Newport optical power meter with a large-area PIN/transimpedance amplifier configuration. The signal generator would be used to modulate the DFB in the 5 - 10 kHz range and the Lock-in detection should provide better rejection of the unmodulated ASE. This set-up was found to be difficult to implement due to apparent GPIB incompatibilities between the lock-in amplifier and the VOA, and was not further explored.

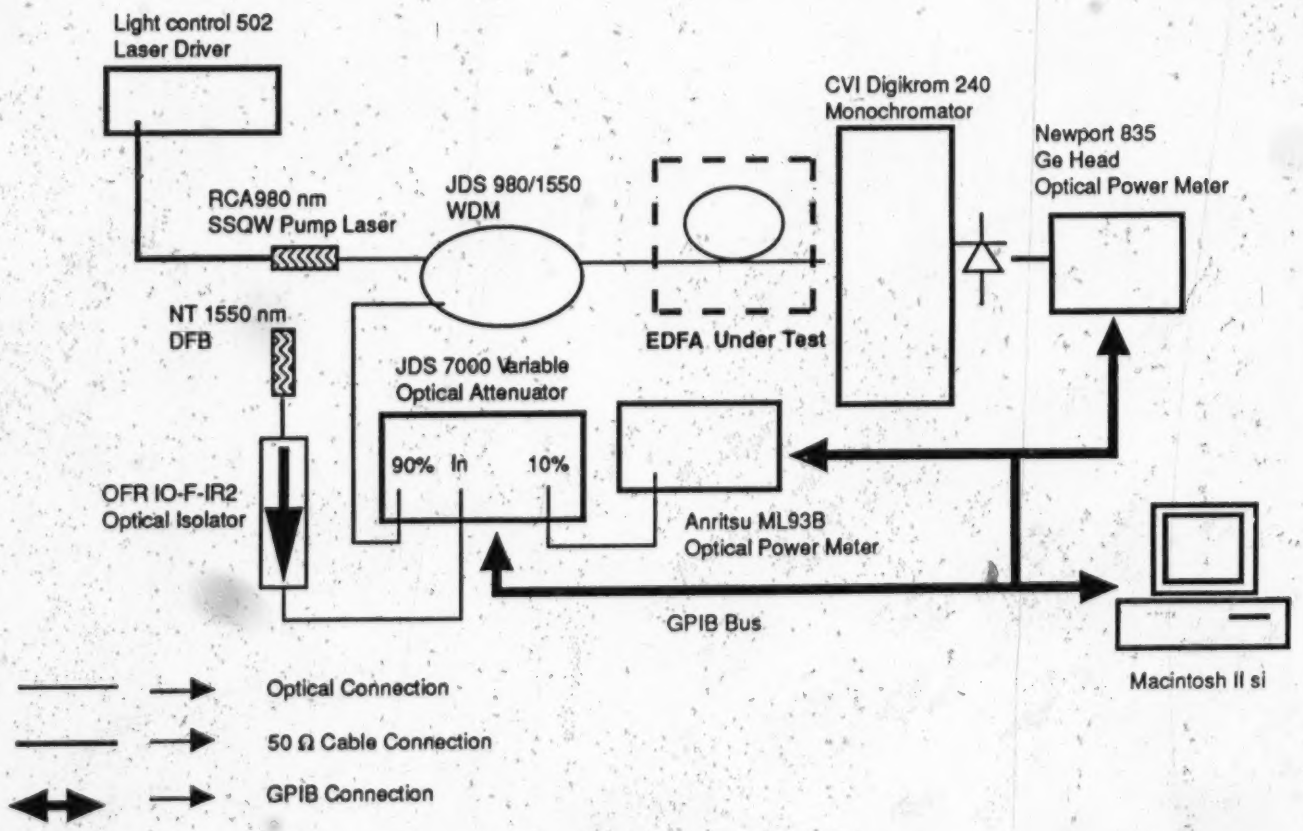

Figure 6.3 : Experimental Configuration for DC Gain Measurements

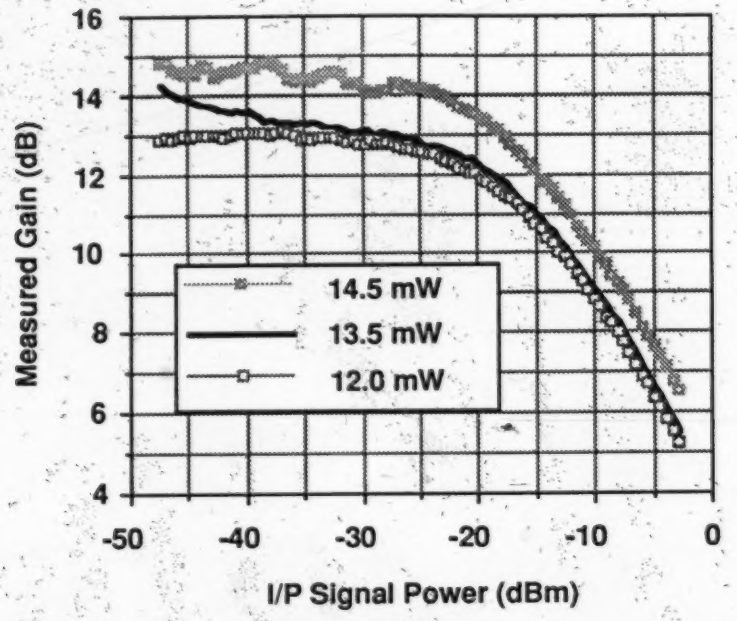

Figure 6.4 : DC Gain vs. Signal I/P Power for Various Pump Powers. EDFA = NOI3a, Laser = OZ#2

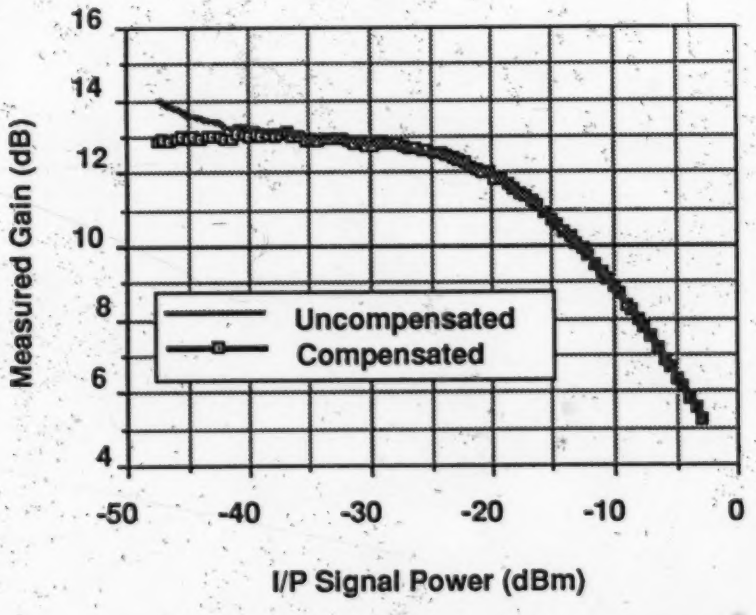

Figure 6.5 : Effectiveness of ASE Compensation Technique for DC Gain Measurements

6.3.2 Measure of ASE Power Levels and Spectra

In order to measure the amount of ASE in both the forward and backward travelling directions, the set-up in Figure 6.6 was used:

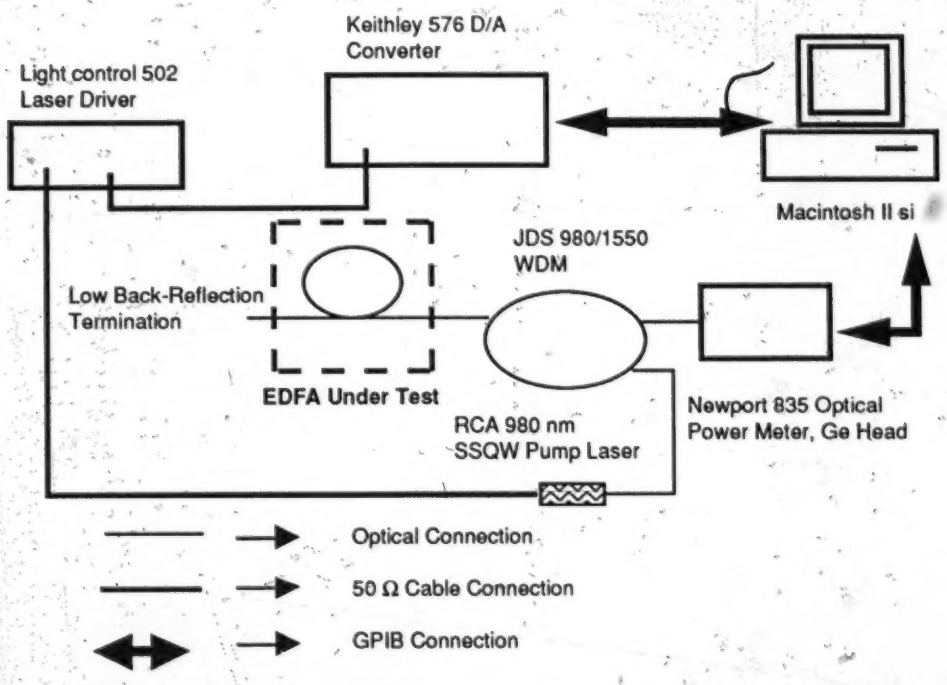

Figure 6.6 : Experimental Configuration to Measure Backward-travelling ASE

To measure forward-travelling ASE, the terminated end above was connected to a cleaved fiber and delivered to the monochromator, with the 1550 nm I/P port of the WDM terminated for low back-reflection. One of the analog voltage O/P ports on the Keithley 576 D/A convertor was used with the modulation I/P port of the Light Controls 502 Laser Drive, to set the pump drive current, where the transconductance of this port was about 40 mA/V. A test would then consist of setting a pump drive current, waiting for 2 - 3 s, and taking a reading with the Newport optical power meter. As configured above, only that ASE in the optical bandwidth presented at the

monochromator exit slits would be observed; by removing the monochromator, total ASE power could be measured. For forward-travelling ASE, a piece of Si had to be inserted before the Ge detector to suppress residual pump; the insertion loss of this filter was 1 dB at 1550 nm. Care had to be taken to determine the actual forward- and backward-travelling ASE power levels exiting directly from the EDFA as these two quantities are impacted by different insertion losses in the measurements. For example, the backward-travelling ASE suffers a 0.7 dB insertion loss due to transmission through the WDM before entering the monochromator, whereas forward-travelling does not. The results in Figure 6.7 below are corrected for all insertion loss noted.

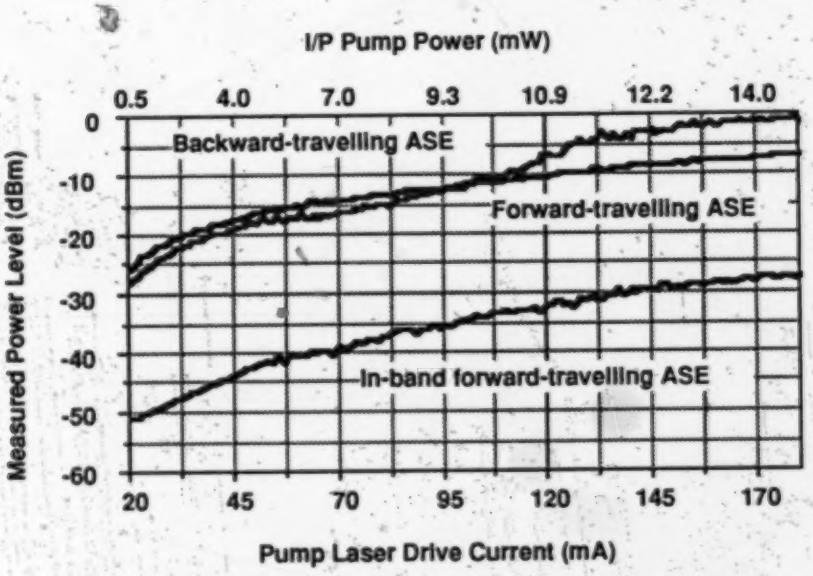

Figure 6.7 : Total Forward- and Backward-travelling ASE and In-band Forward-travelling ASE (BW = 0.8 nm centered at 1550 nm) vs. Pump Drive Current. EDFA = NOI3a, Pump Laser = OZ#1

The above results confirm that higher levels of backward-travelling ASE are generated, due to the dynamics of signal evolution as discussed in Chapter 4. As well, with the noted optical bandwidth, the in-band ASE is observed to constitute less than 1% of the

total forward-travelling ASE. These levels of ASE power are qualitatively consistent with predictions made in Chapter 4, where the bandwidth was 1 nm, and thus slightly higher values were noted.[4]

To measure the forward-travelling ASE spectrum, the set-up in Figure 6.8 is used.

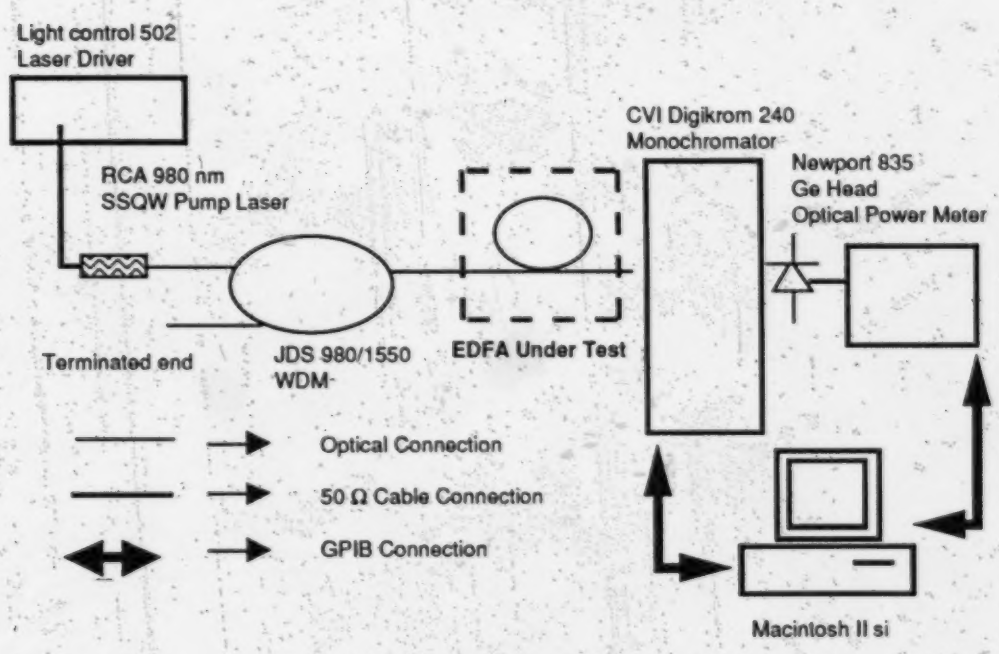

Figure 6.8 : Experimental Configuration to Measure Forward-travelling ASE Spectrum

Here, a test consists of first selecting a wavelength by controlling the grating position of the monochromator, then waiting 2 to 3 s and measuring the power from the optical power meter. The 1550 nm I/P leg of the WDM is terminated with a return loss of better than -60 dB due to the inclusion of an unmated FC/APC connector. Although residual pump should theoretically not reach the detector, since we have tuned the,

4. Note that the results of Chapter 4 are for a *different* fiber, and therefore can only be compared with the results here in qualitative terms.

grating to the wavelength of the signal, it is possible that some scattered residual pump may pass through the slits and influence the results. If pump rejection is a concern then the second JDS WDM could be inserted after the EDFA under test. This is not a concern for the backward-travelling ASE spectral sweep, where the WDM is inserted between the EDFA and the monochromator and thus launches the light away from the detector. Sweeps of the ASE spectra appear in Figure 6.9 below.

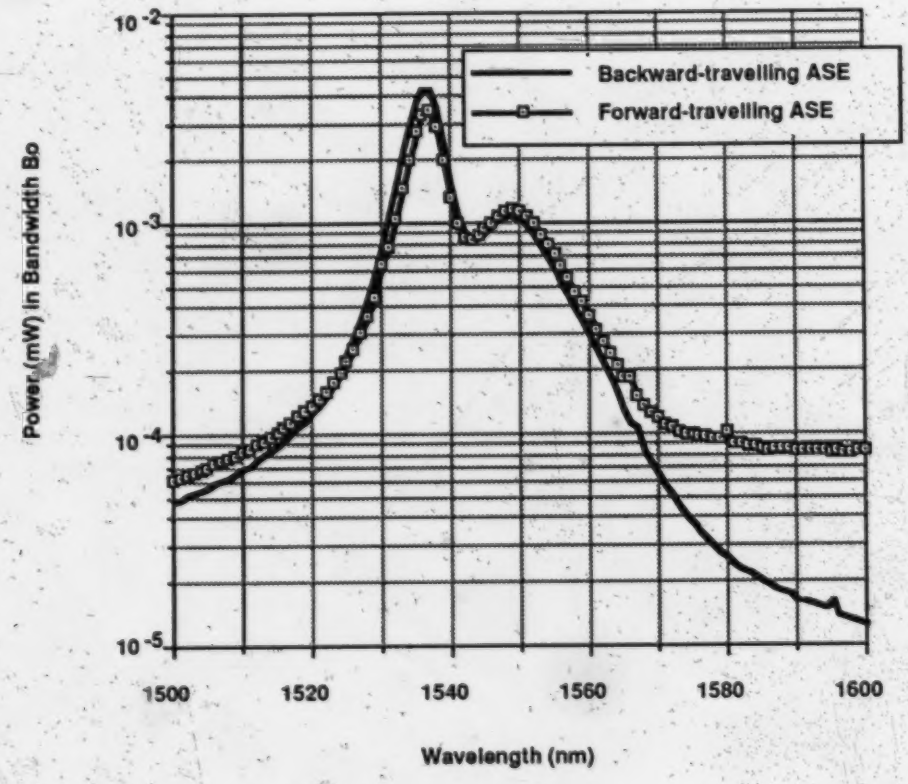

Figure 6.9 : Forward and Backward-travelling ASE Spectra vs. Wavelength for EDFA NOI3a. Measurement Bandwidth = 0.9 nm

For the results shown above, a pump laser current of 139.6 mA was used, and the total backward-travelling ASE was -12.94 dBm, compared to -13.25 dBm for the forward-travelling ASE. It is interesting to note that most of the power in the backward-

travelling ASE appears around the peak at 1537 nm, and the spectral density at 1550 nm is slightly lower for the backward-travelling ASE, a result that is somewhat surprising but has been confirmed by separate measurement of in-band ASE levels. As a final note, the signal DFB can be included in the set-up and a combined ASE/signal spectrum obtained.

6.3.3 Measurement of EDFA Gain-modulation Frequency Response

It is possible to modulate signals injected into or ASE generated within an EDFA by modulating the gain due to modulation of the pump laser drive current (and thus optical output power). It has been known for some time that the frequency response of this modulation is low-pass, due to the relatively long stimulated transition time from the upper lasing level in the Erbium. The possibility of modulating signals or ASE has some interesting applications in the status monitoring field and could be especially useful in long-haul communication systems. These possibilities are the focus of other research currently being conducted at TR Labs.

As shown in Figure 6.12, the majority of the set-up is similar to that discussed in Section 6.3.1 for DC gain measurement. Here, the HP 8116A GPIB-controllable Function Generator is added to allow modulation of the pump laser drive current. As well, the SR 530 lock-in amplifier with reference supplied from the HP 8116A is added to AC-detect the received signal. The Epitaxx InGaAs 2.0 mm detector and Ithaco 564 transimpedance amplifier form the receiver and it is important to note that under measurement conditions, where a gain of 10^4 V/A was suitable for good signal levels, the bandwidth of the receiver was in the 200 kHz range; thus, any bandwidth limitations observed are expected to be due to the EDFA. The Lock-in then displays the amplitude of the lowpass signal which results from mixing the detected AC signal and

the Reference. This is read over the GPIB after a delay 8.0 s after the setting of the frequency on the function generator.[5] This allowed sufficient time for lock-in and settling of the detected signal amplitude, since the O/P lowpass filter time constant was 1.0 s. Sweeps were done from 10 Hz to 10.5 kHz in two separate runs; run 1 consisted of a sweep from 10 Hz to 150 Hz in steps of 5 Hz, and run 2 consisted of a run from 100 Hz to 10.5 kHz in steps of 100 Hz. Here, a delay of 8.0 s was required as it typically took the Lock-in 4.0 to 5.0 s to capture the Reference at these low frequencies. In addition, the Line (60 Hz) and Linex2 (120 Hz) filters were used and caused notches in the response characteristic which can be removed by interpolation. For run 2, a delay of 5.0 s was sufficient as lock-in occurred more rapidly. Dividing the entire sweep into two separate runs allowed for easy change of sensitivity without transient effects in the detected readings as well. Since very strong signals were present at the Lock-in (an oscilloscope may be used to monitor the AC-detected signals from the Lock-in), the average drive current on Pump laser OZ#1 was reduced to 150 mA and the modulation was 16 mA peak, with a square wave used as the modulating signal. Finally, a number of sweeps can be performed with a variety of I/P signal levels to the EDFA by controlling manually the attenuation of the JDS VOA.

---

5. See Appendix E for a copy of this program

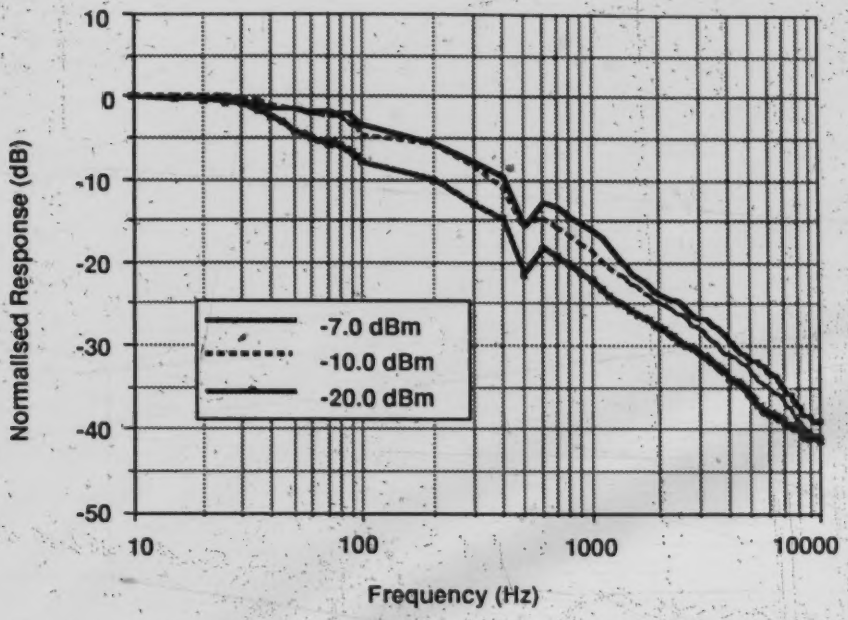

Figure 6.10 : Normalized Frequency Response of EDFA NOI3a for Given Signal I/P Powers

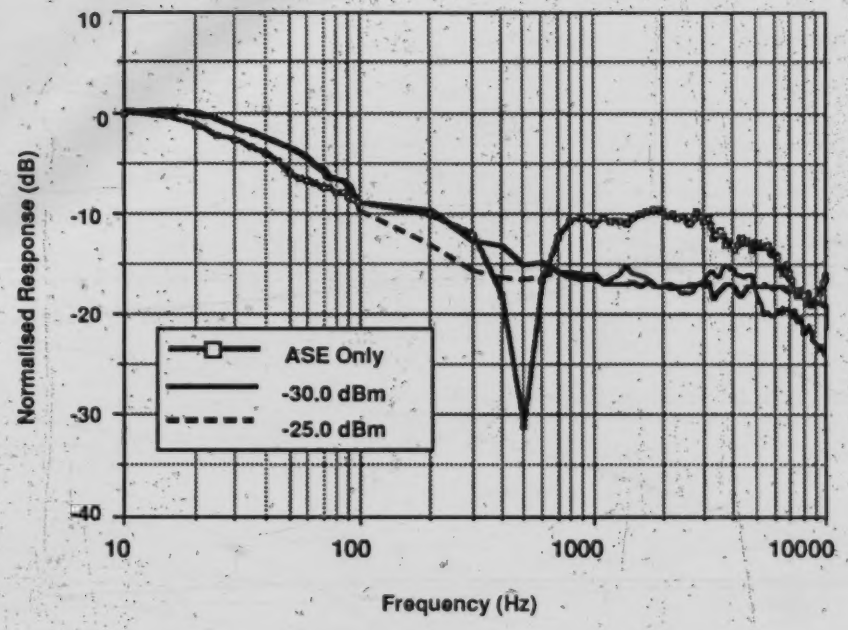

Figure 6.11 : Normalized Frequency Response (dB) for Various Small Signal I/P Powers

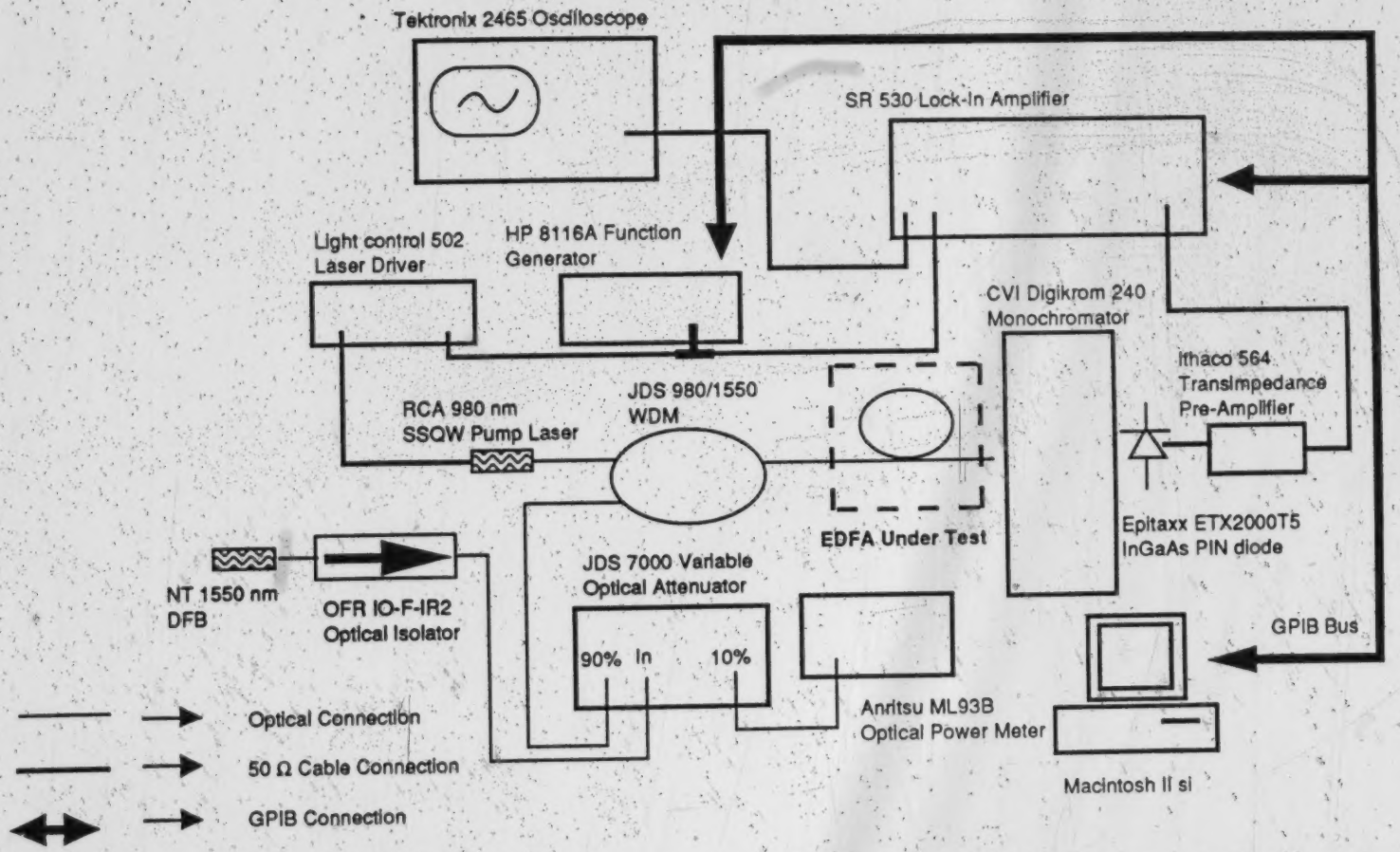

Figure 6.12 : Experimental Configuration for Measurement of EDFA Frequency Response

The 3-dB corner frequencies are as follows:

I/P Signal Power (dBm)	3-dB Corner Frequency (Hz)
-7.0	95
-10.0	85
-20.0	46
-25.0	45
-30.0	45
ASE Only	32

Table 6.2 : 3-dB Frequencies of Gain Modulation Response

It can be seen that the 3-dB frequency of the gain modulation response increases for larger signal input powers. This is due to an effective decrease in the stimulated transition lifetime of the upper lasing level due to the depletion of the upper lasing level due to stimulated emission. This trend in 3-dB corner frequencies has also been reported by Laming *et al* [47]. It is further important to note that the above curves have all been plotted normalized to their own passband values, and not to the same value. When comparing the ASE only run to the -7 dBm run, for instance, the ASE-only run has a passband which is significantly lower, and thus the sensitivity on the Lock-in has to be improved to achieve a similar degree of accuracy. As a final comment, the results in Figure 6.11 are somewhat suspect past about 100 Hz due to the presence of a measurement system noise floor.

6.3.4 Measurement of Residual Pump

Measurement of residual pump is of interest in determining the amount of pump absorption within the amplifier, as well as determining possible impact on downstream components such as optical receiver front-ends. The amount of residual pump present at the end of the amplifier depends on a number of factors such as level of signal present in the amplifier, amplifier characteristics, and the spectral characteristics of the pump source. An experimental set-up to measure residual pump power is shown in Figure 6.13.

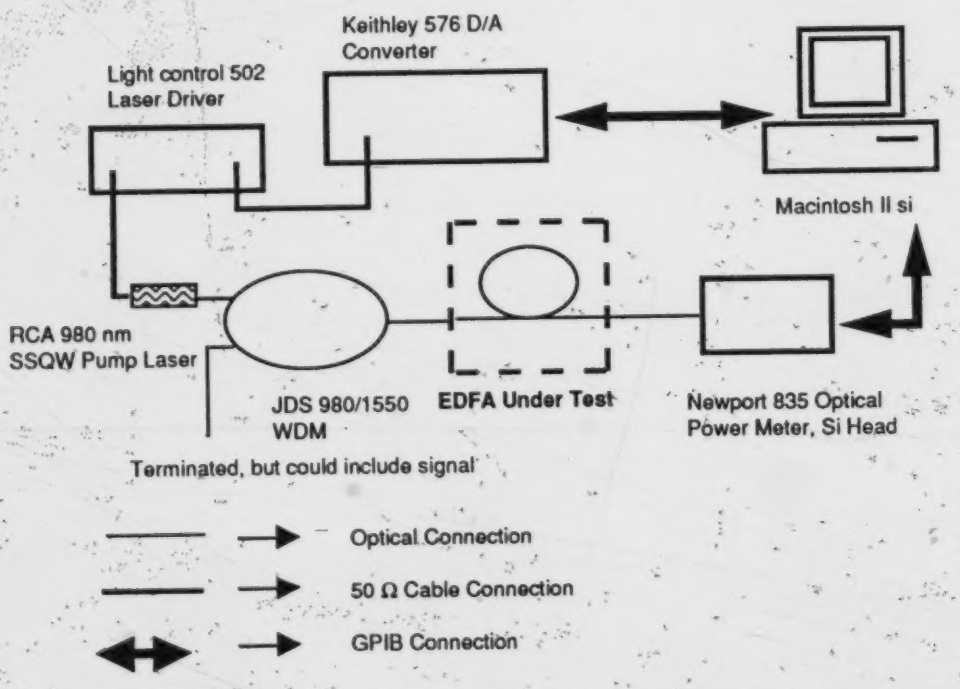

Figure 6.13 : Experimental Configuration to Measure Residual Pump Power

As well, the monochromator can be included before the detector to perform a spectral sweep of the residual pump to examine absorption characteristics of the EDFA.(cf. Figure 6.6). An experimental run, then, consists of first setting the drive current to the laser via the analog output port of the Keithley 576, waiting about 3.0 s, and then

taking a reading from the Newport optical power meter fitted with the Si head; since Si will not absorb wavelengths of light longer than 1100 nm, forward-travelling ASE is automatically rejected. As noted in Figure 6.13, a signal can optionally be added to explore possible changes in pump absorption due to the presence of a signal. Typical residual pump results are shown in Figure 6.14, and Figure 6.15 reveals an estimate to the average pump absorption in dB/m in the amplifier for a given pump drive current. Note that these results are corrected for splice losses, and are source dependent.

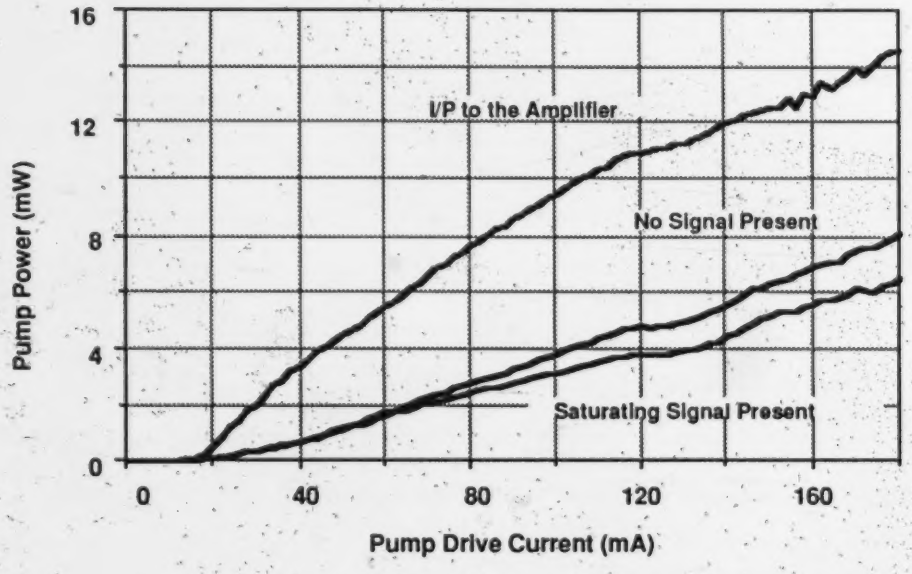

Figure 6.14 : Pump Power at the Input and Output of EDFA NOI3a; Pump Laser = Oz #2

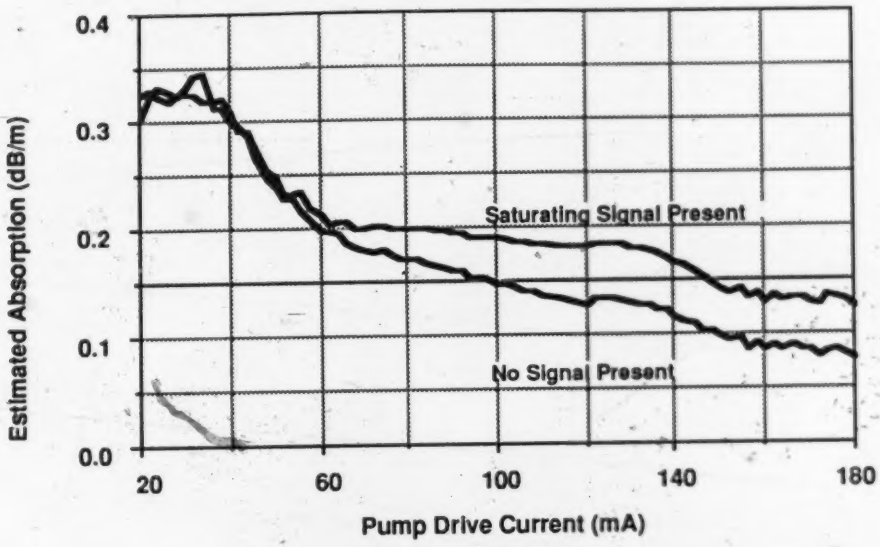

Figure 6.15 : Estimated Average Pump Absorption in dB/m When No Signal and a Saturating Signal is Present; EDFA = NOI3a, Pump Laser = Oz#2

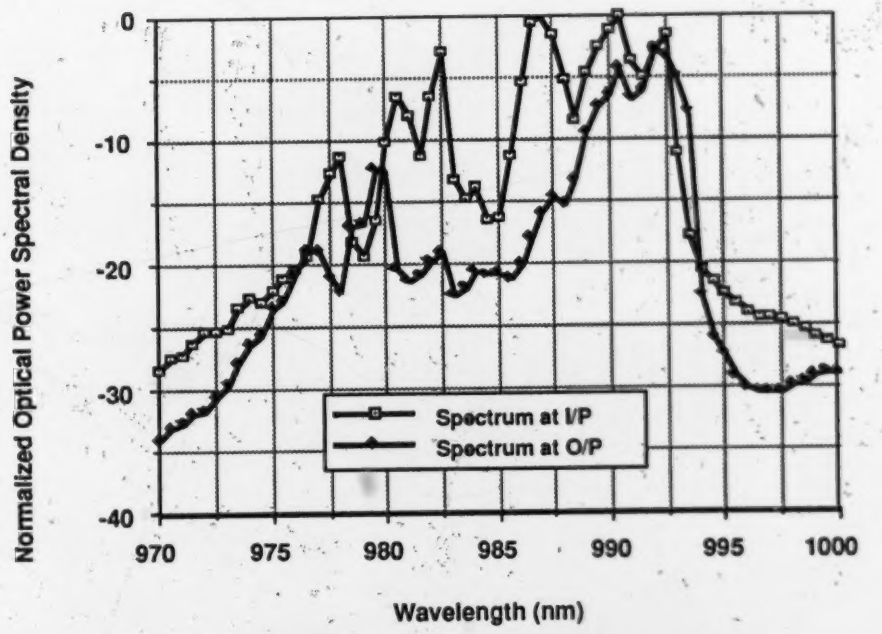

Figure 6.16 : Pump Laser Oz#2 Spectrum at the I/P to and O/P from EDFA NOI3a. Current = 160 mA, DFB Signal of -4.75 dBm Present

Figure 6.16 illustrates the reason why the overall pump power absorption is low; the multi-modedness of the source and the substantial presence of pump at the longer 990 to 993 nm wavelengths, where the pump absorption cross-section is low, explain why a large residual pump is always present, even for longer lengths of Erbium-doped fibers. Locations are noted where the normalized optical power spectral density for the I/P to the EDFA exceeds the O/P values; this is attributable to limits in reproducibility of the results and possible thermal variations between runs. For example, for a 750 μm cavity length and an assumed index of refraction of 3.5, the longitudinal modal spacing at 980 nm is expected to be 0.18 nm, which is less than the resolution of the monochromator when the scan was done.[6] Thus, rather than seeing fine modal structure, an envelope or time-averaged spectrum is observed.

6.3.5 Noise Figure

Of great interest when considering the performance of any amplifier is its noise figure, which measures the difference between the SNR at the input to the amplifier and the SNR at the output. The noise figure for an EDFA can be approximated by eqn 4.1, as discussed earlier, and repeated below for convenience:

$$NF \approx 10\log\left[\frac{P_{ASE}}{(G - 1)B_o h\nu}\right] \tag{6.2}$$

Thus, if the ASE in a known optical bandwidth B_o is measured, and the gain is known, the noise figure can be directly calculated. It is important to consider carefully the various splice losses and insertion losses in the system, and to include their possible impact on the noise figure. Shown in Figure 6.17 are noise figure calculations based

6. The exit slit was 100 μm wide, resulting in a calculated resolution of 0.275 nm at 980 nm (See Eqn. 6.1)

on measurements made for EDFA NOI3a contra-directionally pumped with laser Oz#2 operating at 139.6 mA. The noise figure is reported for a 1550 nm signal of varying power levels while a contra-directional signal at 1553.6 nm is present. The co-directionally pumped results were 3 to 3.5 dB worse.

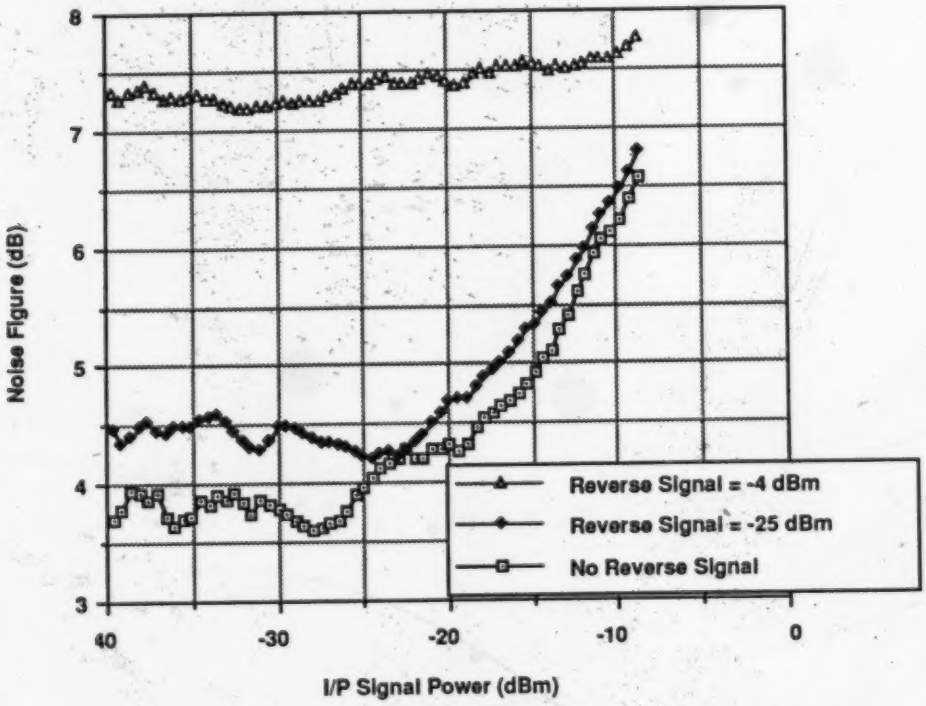

Figure 6.17 : Calculated Noise Figure for a Bi-directional Amplifier with Varying Reverse Signal Power Levels

Some comments must be made about how the gain and ASE were measured. First, the gain was measured while the forward signal power was varied between -40 and -10 dBm, and this was repeated for the reverse signal power levels shown above. Next, the ASE had to be measured without the forward signal present, but with the suppression of ASE that would otherwise occur if the signal was present. To simulate the absent forward signal, the reverse signal was varied and the forward ASE

measured. Since the reverse signal is only 3.6 nm away from the absent forward signal, it is felt that the effect that the signals would individually have on ASE power levels is similar. An alternative to this technique might be to exploit the polarized nature of the signal to filter it out, leaving half the in-band ASE for subsequent measurement.

As can been seen from Figure 6.17, the noise figure is worst for an EDFA which is heavily saturated by the combined power levels of the forward- and backward-travelling signals. This is because the gain reduction is greater than the suppression in ASE levels experienced in this region. In addition, it must be remembered that eqn. 6.2, while approximate at best, does not really apply at all in the saturated regime. Having said this, it is noted note that the contra-directional pumped amplifier has a noise figure that approaches the quantum limit of 3.0 dB to within the value of the input splice loss to the amplifier for no reverse signal present. As well, the trends shown here are similar to those seen in Table 4.17, when full-duplex transmission performance was simulated.

6.3.6 Other Measurements

The scope of measurements that can be made on EDFAs is immense. For example, given a stronger, more versatile pump source, it would be of interest to explore gain and noise figure performance of the EDFAs for a variety of different pump power levels and in both co- and contra-directionally pumped schemes. If two such pumps were present, with appropriate isolators for each pump, it would be interesting to explore bi-directionally pumped amplifier performance. The measurement capability is further enhanced by the fact that all experiments can be easily computer controlled with the LabVIEW™ software alluded to earlier in this chapter.

7.0 An Application of EDFAs to FDM Transmission

There are numerous applications of Erbium-doped fiber beyond its primary use as an amplifier. One such possibility is use as a source at 1.55 μm, where higher powers could be achieved than from conventional semiconductor laser sources. Erbium-doped fibers have been used in a variety of laser configurations, or as broadband, superfluorescent sources for fiber gyroscope applications, for example.[1] Here, the use of a superfluorescent Erbium-doped fiber laser (SFL) followed by an optical filter to form a number of optical carrier frequencies simultaneously for subsequent demultiplexing and modulation is discussed, with a focus on the theory of one particular type of filter, a three-cavity, four-mirror coupled Fabry-Perot type interference filter. Two approaches to the theory are illustrated, followed by a discussion of the characteristics of such filters and design considerations.

7.1 Spectral Slicing

Spectral slicing is a technique with application to WDM systems which avoids the strict transmitter requirements imposed by conventional WDM systems, where separate sources are used for each signal channel.[2] For example, traditional WDM systems operate by selecting a number of laser sources of different center wavelengths for each channel in the network. This has a number of disadvantages. For example, each channel must have a unique type of transmitter, with transmitters from 2 different channels not interchangeable. In addition, current manufacturing technologies limit the tuning range of such lasers to specific spectral regions. Spectral slicing can alleviate this by using a broadband source such as a SFL and selecting desired wavelengths

1. A good summary of the different configurations that have appeared is reference [48]:
2. The designation WDM vs. FDM is one of technicality. A wavelength division multiplexed network is one where the spacing of channels is usually on the order of nms or greater, and where the spacing is thus large when compared to the information bandwidth. For a frequency division multiplexed network, the channel spacing is much less, being measured in units of GHz, which is only a few times greater than the information bandwidth. As well, the channel spacing is directly related to channel bandwidths.

through design of a post filter. This is the approach that will be discussed here, and differs from other discussed approaches [49].

The spectral slicing of a proposed FDM transmitter will result from the transmission characteristic of an interference filter to be designed for implementation in fiber. In general, a trade-off exists between the complexity of the device, both in theoretical description and in implementation, and the Finesse of the device. Previous high finesse optical filters have been designed by cascading Fabry-Perot etalons and then controlling unwanted inter-cavity resonances by using isolators, attenuators, or long lengths [50]. As well, recent work has made attractive fiber implementation of Fabry-Perot filters, with finesses of 100 to 130 reported for insertion losses in the 2 to 5 dB range and free spectral ranges (FSRs) in the GHz range.

7.2 Theory for Multi-cavity Filters

A single Fabry-Perot etalon has the following well-known field reflection and transmission characteristics (see reference [57], p. 128):

$$\frac{E_t}{E_o} = \frac{-t_1 t_2 e^{-j\delta/2}}{1 - r_1 r_2 e^{-j\delta}} \tag{7.1}$$

$$\frac{E_r}{E_o} = \left[\frac{r_1 - r_2 e^{-j\delta}}{1 - r_1 r_2 e^{-j\delta}}\right] \tag{7.2}$$

where r_i and jt_i are the field reflectivity and transmissivity, respectively, at the i_{th} mirror, E_r and E_t are the reflected and transmitted electric fields, E_o is the incident field, and δ is given by (See Figure 7.1):

$$\frac{\delta}{2} = kl' = \frac{2\pi}{\lambda}(l\cos(\phi)) \tag{7.3}$$

It has been assumed here that the mirrors are lossless, so that $r^2 + t^2 = 1$.

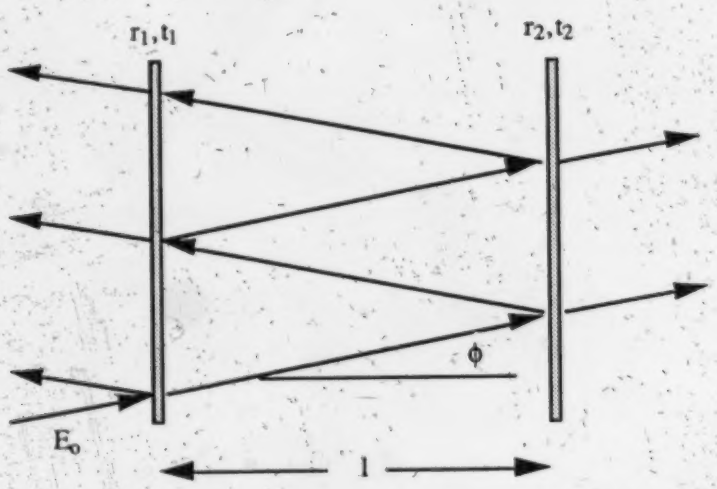

Figure 7.1 : Conceptual View of the Operation of a Fabry-Perot Etalon

The expressions for the reflected and transmitted fields are for a single cavity; it is now of interest to extend the analysis to multiple cavities. Two methods are useful here; the first is called Rouard's Method, and the second involves the use of S and T matrices for mirrors and lengths of dielectrics.

7.2.1 Rouard's Method[3]

The French physicist P. Rouard devised a technique that can be systematically applied to an n-layer dielectric reflection/transmission filter; as mentioned earlier, the mathematics become prohibitively complicated if there are more than four interfaces (i.e. three layers). The formalism used here will also be applicable to the problem of transmission through cascaded mirrors and cavities instead of by stacks of dielectrics as will be presented here.

3. The original theory was developed in 1937. The theory referenced here appeared in reference [51].

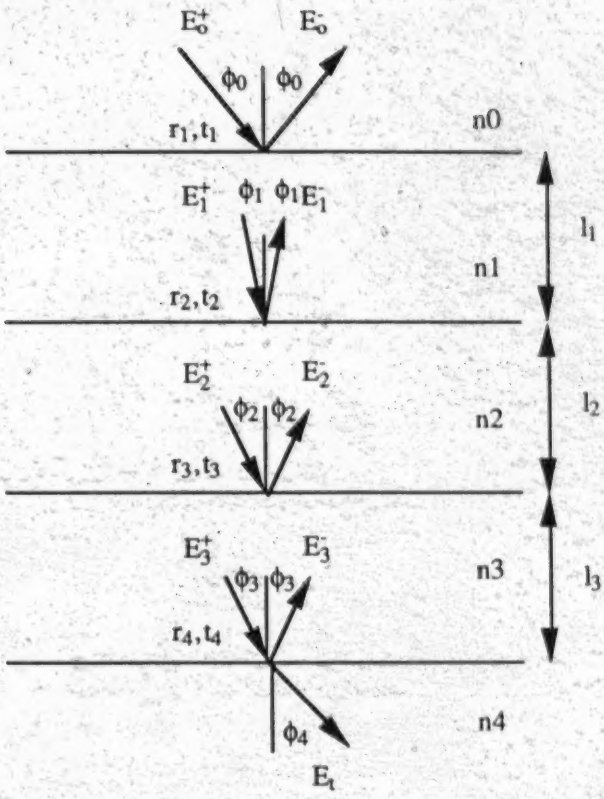

Figure 7.2 : Multi-layer Dielectric Stack with an Incident Field E_o and a Transmitted Field E_t

The analysis starts by writing the expression for a single Fabry-Perot etalon as follows:

$$T = \frac{-t_1 \tau_2 e^{-j\delta_1/2}}{1 - r_1 \rho_2 e^{-j\delta_1}} \qquad (7.4)$$

where r_1 and t_1 are the field reflectivity and transmissivity at the first interface, and δ_1 is the phase change encountered during a round trip of the first layer, and was given by twice the result of eqn. 7.3.[4] ρ_2 is interpreted as the *effective reflectivity* seen at the second interface, and is given by:

4. It is interesting to note that for a dielectric, r_1 is given by :

$$\frac{n_2 - n_1}{n_2 + n_1}$$

and could be positive or negative depending on whether $n_2 > n_1$ or $n_2 < n_1$.

$$\rho_2 = \frac{(r_2 - \rho_3 e^{-j\delta_2})}{1 - r_2\rho_3 e^{-j\delta_2}} \tag{7.5}$$

and

$$\tau_2 = \frac{-t_2\tau_3 e^{-j\delta_2/2}}{1 - r_2\rho_3 e^{-j\delta_2}} \tag{7.6}$$

is interpreted as the *effective transmissivity* of the second interface.

Similar expressions as eqns.7.5 and 7.6 above exist for all subsequent ρ_i and τ_i values.

Substituting eqns. 7.5 and 7.6 into eqn. 7.4, then:

$$T = \frac{-t_1\left[\dfrac{-t_2\tau_3 e^{-j\delta_2/2}}{1 - r_2\rho_3 e^{-j\delta_2}}\right] e^{-j\delta_1/2}}{1 - r_1\left[\dfrac{(r_2 - \rho_3 e^{-j\delta_2})}{1 - r_2\rho_3 e^{-j\delta_2}}\right] e^{-j\delta_1}} \tag{7.7}$$

which leads to a well known expression for a two cavity filter [50]:

$$T = \frac{t_1 t_2 \tau_3 e^{-j\left[\frac{\delta_1 + \delta_2}{2}\right]}}{1 - r_2\rho_3 e^{-j\delta_2} - r_1 r_2 e^{-j\delta_1} + r_1\rho_3 e^{-j(\delta_1 + \delta_2)}} \tag{7.8}$$

if ρ_3 and τ_3 are simply interpreted as the transmissivity and reflectivity of a third mirror. Continuing in this manner and replacing τ_3 and ρ_3 with values similar to eqns. 7.5 and 7.6 to represent the third and final cavity, the following expression is derived:

$$T = \frac{t_1 t_2\left[\dfrac{-t_3 t_4 e^{-j\delta_3/2}}{1 - r_3 r_4 e^{-j\delta_3}}\right] e^{-j\left[\frac{\delta_1 + \delta_2}{2}\right]}}{1 - r_2\left[\dfrac{r_3 - r_4 e^{-j\delta_3}}{1 - r_3 r_4 e^{-j\delta_3}}\right] e^{-j\delta_2} - r_1 r_2 e^{-j\delta_1} + r_1\left[\dfrac{r_3 - r_4 e^{-j\delta_3}}{1 - r_3 r_4 e^{-j\delta_3}}\right] e^{-j(\delta_1 + \delta_2)}}$$

$$= \frac{-t_1t_2t_3t_4e^{-j\left[\frac{\delta_1+\delta_2+\delta_3}{2}\right]}}{1 - r_1r_2e^{-j\delta_1} - r_2r_3e^{-j\delta_2} - r_3r_4e^{-j\delta_3} + r_1r_3e^{-j(\delta_1+\delta_2)} + r_2r_4e^{-j(\delta_2+\delta_3)} + r_1r_2r_3r_4e^{-j(\delta_1+\delta_3)} - r_1r_4e^{-j(\delta_1+\delta_2+\delta_3)}} \quad (7.9)$$

This is the key equation from which all work on the multi-cavity filters is derived. In principle, subsequent mirrors could be added to form additional cavities, but it is easy to see that the expressions would become prohibitively complicated. Since the power spectral density of optical signals at the output of the cavity is of interest, the magnitude squared of the above expression is of interest:

$$T = \frac{T_1T_2T_3T_4}{\left|1 - r_1r_2e^{-j\delta_1} - r_2r_3e^{-j\delta_2} - r_3r_4e^{-j\delta_3} + r_1r_3e^{-j(\delta_1+\delta_2)} + r_2r_4e^{-j(\delta_2+\delta_3)} + r_1r_2r_3r_4e^{-j(\delta_1+\delta_3)} - r_1r_4e^{-j(\delta_1+\delta_2+\delta_3)}\right|^2} \quad (7.10)$$

Further simplification of the above expression is not possible. Notice, however, the grouping of reflectivities and the associated phase terms in the denominator. Reflectivities that appear as coefficients together in any given term always appear with a phase delay due to the distance between the appropriate mirrors. Furthermore, removing any given mirror causes the expression above to simply revert to eqn. 7.8. Eqn. 7.10 therefore possesses all the physical 'features' that might be expected. The above result will now be derived using S and T matrix formalism.

7.2.2 S and T Matrix Method

Consider the multi-stage network as shown below in Figure 7.3.

Figure 7.3: Multi-stage Cascade of Two-port Networks

One useful feature of T matrices is that the T matrix of a cascade of two-port networks is equal to the matrix product of the individual T matrices.[5] Thus, for the above network, the overall T matrix is given by:

$$T = [T_4][T_3][T_2][T_1] \tag{7.11}$$

and so:

$$\begin{bmatrix} b_{out} \\ a_{out} \end{bmatrix} = [T] \begin{bmatrix} b_{in} \\ a_{in} \end{bmatrix} \tag{7.12}$$

For a four-mirror, three-cavity filter, a cascade of seven matrices will be required; $[T_1]$ $[T_3]$, $[T_5]$, and $[T_7]$ will represent the effects of the four mirrors, while $[T_2]$, $[T_4]$, and $[T_6]$ will account for the effects of transits through the cavities. This is schematically represented in Figure 7.4.

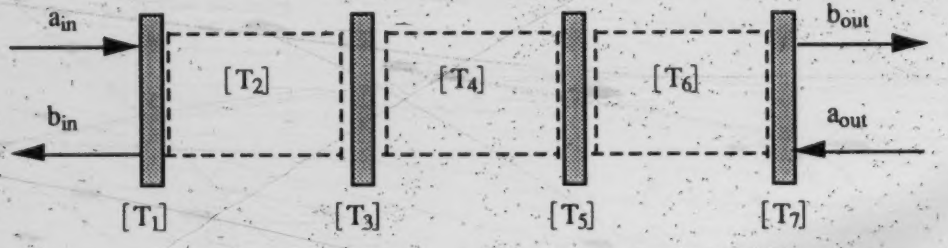

Figure 7.4: T matrix Schematic of a Three-cavity, Four-mirror Fabry-Perot Filter

The S matrix for a mirror can be shown to be:

$$S = \begin{bmatrix} r & jt \\ jt & r \end{bmatrix} \tag{7.13}$$

5. For a summary of other properties of S and T matrices, see Appendix F

Notice that the above matrix complies with eqns. F.7 and F.8 in Appendix F, implying that a lossless, linear mirror is assumed. As an additional note, the matrix for a mirror can vary from that presented above, depending on how the reflection and transmission coefficients are defined. Here, no assumptions are made about the sign of r; it could be positive or negative, as mentioned earlier, but the sign for t is always positive (there is no 'negative transmission'). The T matrix for a mirror is derived to be:

$$T = j/t\begin{bmatrix} 1 & -r \\ r & -1 \end{bmatrix} \tag{7.14}$$

For a length of free space, T can be written by inspection as:

$$T = \begin{bmatrix} e^{-j\phi} & 0 \\ 0 & e^{j\phi} \end{bmatrix} \tag{7.15}$$

where ϕ is the total phase change encountered by transit through a medium of optical length l. Notice that forward- and backward-travelling waves are uncoupled, and since det(T) = 1, a lossless transit is assumed.

The cascade for the overall T matrix may now occur, starting from eqn 7.16 below:

$$T_{overall} = [T_7][T_6][T_5][T_4][T_3][T_2][T_1] \tag{7.16}$$

Starting with $[T_2][T_1]$, it follows that:

$$\begin{bmatrix} e^{-j\delta_3/2} & 0 \\ 0 & e^{j\delta_3/2} \end{bmatrix}\begin{bmatrix} j/t_4 & -jr_4/t_4 \\ jr_4/t_4 & -j/t_4 \end{bmatrix} = j/t_4\begin{bmatrix} e^{-j\delta_3/2} & -r_4e^{-j\delta_3/2} \\ r_4e^{j\delta_3/2} & -e^{j\delta_3/2} \end{bmatrix} \tag{7.17}$$

multiplying by $[T_3]$, a result for a single etalon is derived:

$$T = \frac{1}{-t_3t_4e^{-j\delta_3/2}} \begin{bmatrix} -r_3r_4 + e^{-j\delta_3} & r_3 - r_4e^{-j\delta_3} \\ -r_4 + r_3e^{-j\delta_3} & 1 - r_3r_4e^{-j\delta_3} \end{bmatrix} \tag{7.18}$$

Notice as a check that a familiar result can be derived from this intermediate calculation:

$$1/T_{ab} = S_{12} = \frac{-t_3t_4e^{-j\delta_3/2}}{1-r_3r_4e^{-j\delta_3}} \tag{7.19}$$

Continuing to build the result using the pattern established above will result in the following expression for T:

$$\boxed{T = \frac{T_1T_2T_3T_4}{\left|1 - r_1r_2e^{-j\delta_1} - r_2r_3e^{-j\delta_2} - r_3r_4e^{-j\delta_3} + r_1r_3e^{-j(\delta_1+\delta_2)} + r_2r_4e^{-j(\delta_2+\delta_3)} + r_1r_2r_3r_4e^{-j(\delta_1+\delta_3)} - r_1r_4e^{-j(\delta_1+\delta_2+\delta_3)}\right|^2}} \tag{7.20}$$

Which is the same as reported earlier in eqn. 7.10.

7.3 Analysis of Transmission Result

Given the complex nature of the result derived, it is natural to seek methods of simplifying the formula to give it a more useful form. Unfortunately, this can only be done if some simplifying assumptions are made about some of the variables in the problem. Therefore, for analytic purposes, it will be assumed that all mirror reflectivities (and therefore transmissivities, since lossless mirrors are assumed) are the same, i.e.:

$$r_i = r \tag{7.21a}$$

and also:

$$r_i^2 = r^2 = R \tag{7.21b}$$

$$t_i^2 = t^2 = T \tag{7.21c}$$

Eqn. 7.20 then simplifies to:

$$T = \frac{T^4}{\left|1 - Re^{-j\delta_1} - Re^{-j\delta_2} - Re^{-j\delta_3} + Re^{-j(\delta_1+\delta_2)} + Re^{-j(\delta_2+\delta_3)} + R^2e^{-j(\delta_1+\delta_3)} - Re^{-j(\delta_1+\delta_2+\delta_3)}\right|^2} \tag{7.22}$$

At this time, it is useful to define the following useful relation:

$$FSR_i = \frac{c}{2n_i l_i} \tag{7.23}$$

where

FSR_i = the *Free Spectral Range* of the given cavity *alone* (i.e., uncoupled to any other cavities)

c = speed of light

n_i = the refractive index of the cavity dielectric

l_i = the length of the cavity

δ_i can then be expressed as:

$$\delta_i = \frac{2\pi f}{FSR_i} \tag{7.24}$$

It is now useful to proceed in a number of different directions to derive some interesting results.

7.3.1 Uncoupling of the Cavities

One way to view the multi-cavity filter is to say it is comprised of two cavities of lengths l_1 and l_3 separated by a length l_2. For cascaded two-port networks, recall that this 'coupling cavity' (cavity 2) causes loading effects by cavity 3 on cavity 1 and

vice-versa, exactly analogous to the situation with cascaded electrical networks. If cavities 1 and 3 were uncoupled, then the overall transmission for the system would simply be the product of the transmission expressions for the individual cavities:

$$T_{overall} = T_1 T_3 \tag{7.25}$$

Using the result from eqn. 7.19 (with the simplification for reflectivities), it can be shown that:

$$T_{overall} = \frac{T^4}{\left|\left(1 - Re^{-j\delta_1}\right)\left(1 - Re^{-j\delta_3}\right)\right|^2} \tag{7.26}$$

The denominator can be expanded to give:

$$\left|\left(1 - Re^{-j\delta_1}\right)\left(1 - Re^{-j\delta_3}\right)\right|^2 = \left|1 - Re^{-j\delta_1} - Re^{-j\delta_3} + R^2 e^{-j(\delta_1 + \delta_3)}\right|^2 \tag{7.27}$$

Now, compare this result to the denominator of eqn. 7.10. If cavity 2 is much longer than either cavity 1 or cavity 3, i.e. :

$$l_2 >> l_1, l_3$$

or, equivalently,

$$FSR_2 << FSR_1, FSR_3 \tag{7.28}$$

then

$$\delta_{1,3} + \delta_2 = 2\pi f\left(\frac{1}{FSR_{1,3}} + \frac{1}{FSR_2}\right) \approx \delta_2 \tag{7.29}$$

and so, the denominator from eqn. 7.10 becomes:

$$\text{Denom} \approx \left|1 - Re^{-j\delta_1} - Re^{-j\delta_3} + R^2 e^{-j(\delta_1 + \delta_3)}\right|^2 \tag{7.30}$$

as required. It does not take too much more effort to derive a result for the denominator with no restriction on individual mirror reflectivities. It is:

$$\text{Denom} \approx \left|\left[1 - r_1 r_2 e^{-j\delta_1} - r_3 r_4 e^{-j\delta_3} + r_1 r_2 r_3 r_4 e^{-j(\delta_1 + \delta_3)}\right] + e^{-j\delta_2}(r_1 r_3 + r_2 r_4 - r_2 r_3 - r_1 r_4)\right|^2 \tag{7.31}$$

Here, the first grouping of terms represents the uncoupled-cascade denominator, with the second group of terms the residual. There are, in fact, thousands of different combinations of reflectivities which will zero the residual, other than the solution where all reflectivities are the same. This would be of consideration if design of an uncoupled cavity was sought.

7.3.2 Resonant Behavior of a Three-cavity Filter

The resonant behavior of a three-cavity structure depends on two factors, namely, the relative reflectivities of the mirrors, and the relationships between the lengths (or, FSRs) of the cavities involved. Analysis of equal-length cavities with carefully designed mirror reflectivities has been shown to result in Butterworth filter performance from multistage filters [52]. The focus of the work here is to keep all reflectivities the same but vary the lengths such so very narrow linewidth filters of a desired FSR can be implemented.

At resonance, the transmission T(f) of the filter should equal one. Since the numerator is given by:

$$T^4 = (1-R)^4 \tag{7.32}$$

then this expression is required for the denominator. It turns out that there are two conditions under which this *may be* achieved. The first case is where all three cavities are resonant, i.e.:

$$\delta_1 = 2k\pi,\ k = 0,\pm1,\pm2,\ ... \tag{7.33a}$$

$$\delta_2 = 2m\pi,\ m = 0,\pm1,\pm2,\ ... \tag{7.33b}$$

$$\delta_3 = 2n\pi,\ n = 0,\pm1,\pm2,\ ... \tag{7.33c}$$

or, equivalently,

$$f = kFSR_1 = mFSR_2 = nFSR_3 \tag{7.33d}$$

This situation physically corresponds to the case where a given wavelength of light simultaneously satisfies all round-trip phase conditions in all three cavities to allow resonance. Said differently, all three cavities have lengths equal to some even integer multiple of half the wavelength of the light in question.

The second case which allows resonance is less obvious and gives rise to an undesired "triplet structure" in the vicinity of the main resonance, as shown conceptually in Figure 7.5.

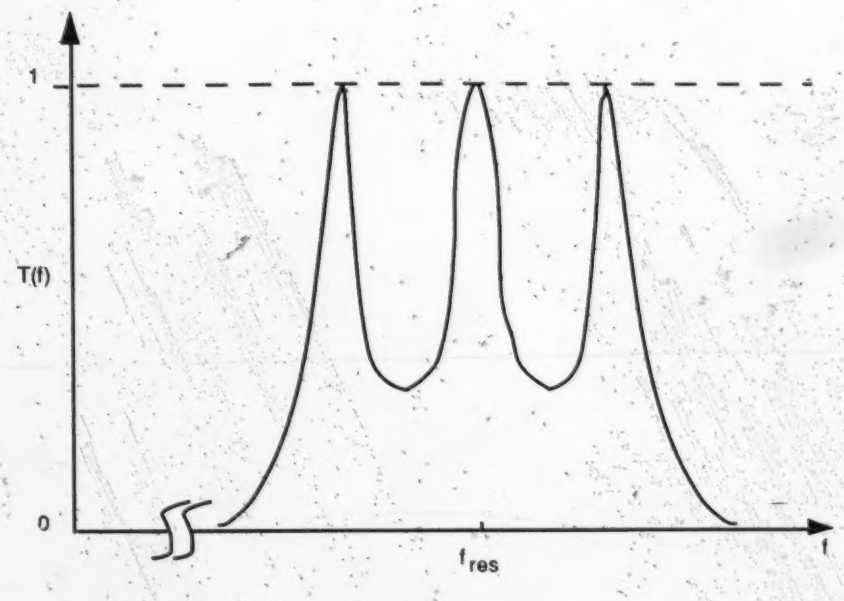

Figure 7.5 : Conceptual View of a"Triplet Structure" in the Vicinity of a Main Resonance

It is very difficult to analytically predict exactly where the "side lobes" to the triplet structure are located for all cases where $r_i \neq r$ and where $\delta_i \neq \delta$. When there is equality, the denominator may be rewritten in the following form (after substantial algebra):

$$\text{Denom} = (1 - R)^4 + 8R(R - \cos(\delta))^2(1 - \cos(\delta)) \qquad (7.34)$$

From this expression, three possible ways of bringing about resonance can be inferred. The first involves setting R = 0. This result might have been anticipated, since it corresponds to removal of the filter altogether and results in T(f) = 1 for all f. The second way to bring about resonance corresponds to $\cos(\delta) = 1$, which amounts to the cases considered previously. The third and final way of zeroing the residual in the denominator above and getting resonant transmission corresponds to setting:

$$\cos(\delta) = R \qquad (7.35)$$

The width of the overall triplet structure gets narrower as R approaches 1, and would have no width for R = 1 (all light is reflected from the filter input). The dip between the main resonance and the side-lobes also becomes shallower as R becomes larger and the two side-lobes merge into the main resonance. This behavior is also noted for the case where $\delta_i \neq \delta$, but no analytic expressions can be derived to accurately predict the location in frequency of the side-lobes. It is also very important to note that in the case where $\delta_i \neq \delta$, the side-lobes do *not* correspond to truly resonant conditions as the peak transmission can no longer equal one.

It is for this reason that narrow-line filters can be obtained from these structures. For certain combinations of lengths of the three cavities, the side-lobe peaks can in fact be made to approach zero, leaving only a very sharply peaked main line at the resonant frequency which will pass signals. Discussion on how to select appropriate combinations of lengths to achieve such filter conditions will appear in the Section 7.4.

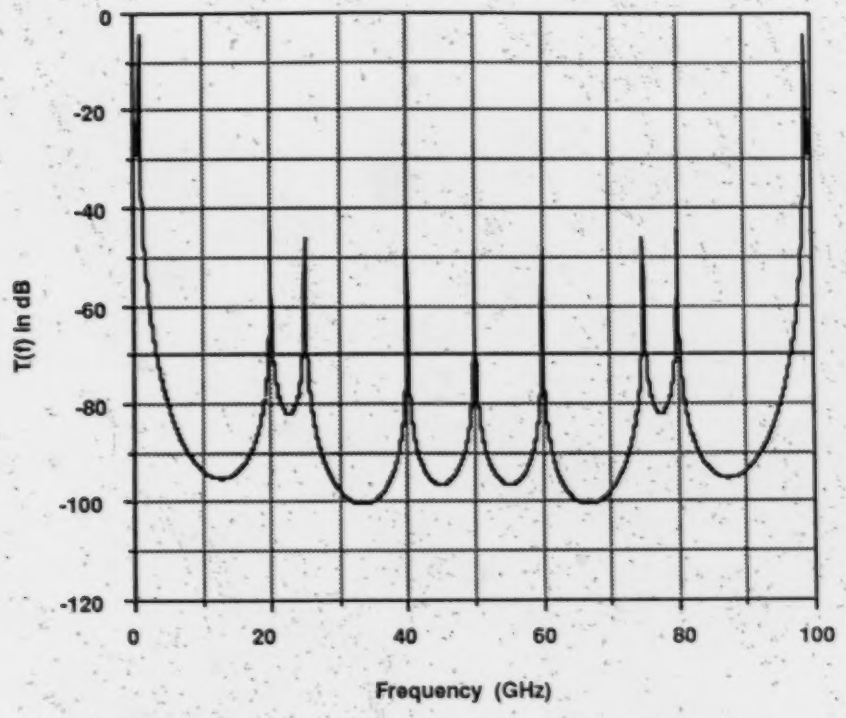

Figure 7.6 : Output Spectrum Corresponding to Cavity FSRs of 20, 100, and 25 GHz Respectively

Some other comments should be made concerning how the individual cavities "express" resonant behavior particular to themselves but not in common with the other two cavities. For example, suppose cavity two is resonant, but the lengths of cavities one and three are such that these cavities are not resonant. A peak will still be observed in the filter output spectrum due to the resonance of cavity two, although T(f) at that point will not equal one. A similar comment holds for the other two cavities when they are individually resonant.

Suppose all three cavities are resonant at some frequency, and this frequency is equal to some integer multiple of the second cavity's FSR, with cavities one and three

having smaller FSRs, as is shown in Figure 7.6.[6] Observe that cavity 2 is fully expressed, with resonances at 100, 200, 300 GHz, etc, with smaller peaks *near* 20 GHz, 40 GHz, 60 GHz, etc., and *near* 25 GHz, 50 GHz, 75 GHz, etc, due to cavities one and three, as summarized in Table 7.1 below.[7]

f (GHz)	T(F) dB	f (GHz)	T(F) dB
0.8924	-0.212	59.994	-48.22
20.015	-39.87	74.986	-43.08
25.014	-43.08	79.85	-39.87
40.004	-48.22	99.1076	-0.212
50.0	-49.09	Linewidth	24.8 MHz

Table 7.1 : Transmission Peaks Due to Cavity One and Three Resonances, and FWHM Linewidth of Main Resonance

The spectrum is noted to be symmetric about $(2n+1)FSR_2/2$, i.e. 50 GHz, 150 GHz, etc. The reason why cavities one and three do not express their resonance at exactly integer multiples of their FSRs is due physically to the effects of coupling or loading to the second cavity. It must be noted, however, that the offsets in frequency are very small.

6. There are, in fact, an infinite number of choices that can be made to satisfy these conditions, but practical design and optimization reduce this number to only a few; this will be discussed further in Section 7.4
7. Figure 7.6 does no accurately represent the peak value of all resonances, due to the relative courseness of the grid and the sharpness of the peaks; Table 7.1 documents the true peak value, as well as the frequency of occurrence.

7.3.3 Linewidth of Main Lobe

The linewidth of the main lobe can be very accurately predicted as follows. First of all, set :

$$\delta_2 = mFSR_2 \tag{7.36}$$

i.e. the second cavity is at resonance. The denominator of eqn 7.10 can now be rewritten as:

$$\text{Denom} = (1 - R)^2(1 - 2R\cos(\delta_1 + \delta_3) + R^2) \tag{7.37}$$

where resonant conditions exist for $\cos(\delta_1+\delta_3) = 1$ as expected. Setting the denominator to a value twice that of the numerator, eqn 7.37 then gives:

$$2(1 - R)^4 = (1 - R)^2(1 - 2R\cos(\delta_1 + \delta_3) + R^2) \tag{7.38}$$

for convenience, use

$$\delta_1 + \delta_3 = 2\pi f\left[\frac{1}{FSR_1} + \frac{1}{FSR_3}\right] = \frac{2\pi f}{FSR_{13}} \tag{7.39}$$

and solve for $f = f_{1/2}$ in eqn 7.38; the result is:

$$f_{1/2} = \frac{FSR_{13}}{2\pi}\cos^{-1}\left[1 - \frac{(1-R)^2}{2R}\right] \tag{7.40}$$

and so the FWHM linewidth of the main resonant peaks is twice this value.

$$\boxed{\Delta f_{1/2} = \frac{FSR_{13}}{\pi}\cos^{-1}\left[1 - \frac{(1-R)^2}{2R}\right]} \tag{7.41}$$

Eqn. 7.41 gives very accurate estimates for the linewidth of the main lobe.[8] Examining this formula, it is noted that as R approaches one, the linewidth vanishes, corresponding to an infinitely sharp "delta-function"-type resonance. Also, it is interesting to note that the linewidth depends on the lengths of the first and third cavities only; clearly, longer cavities resulting in smaller FSRs would be desirable if the narrowest linewidth is to be obtained.

Calculating values for the filter described in Figure 7.6, where R = 0.993, the calculated linewidth is:

$$\Delta f_{1/2} = \frac{11.11\ \text{GHz}}{\pi}\cos^{-1}\left[1 - \frac{(1-0.993)^2}{2\text{x}0.993}\right] = 24.84\ \text{MHz} \tag{7.42}$$

The finesse might be estimated to be:

$$F = \frac{100\ \text{GHz}}{24.8\ \text{MHz}} = 4032 \tag{7.43}$$

where all side-modes have been ignored. Clearly, this is not a good assumption for this filter, which has a strong triplet structure; later, in Figure 7.8, a design with better side-mode suppression will be discussed.

7.3.4 Suppression of Cavity One and Three Resonances

As shown in Figure 7.6, resonant behavior in cavities one and three can lead to unwanted spectral components between main resonant peaks. The degree of suppression of these unwanted components can be predicted as follows. Suppose $FSR_3 = FSR_2$; therefore, only cavity one resonances will contribute to unwanted side-

8. The error is less than 1% at worst

lobes, since $FSR_1 << FSR_2$ for appropriate performance of the filter. Suppose further that $f = kFSR_1$, where k is an integer; then eqn. (7.22) can be written in the following form:

$$T(f) = \frac{(1 - R)^2}{\left[1 - 2R\cos(\delta_3) + R^2\right]} \tag{7.44}$$

where δ_3 would be evaluated at $f = kFSR_1$. Therefore, the argument of the cosine above is:

$$\delta_3(kFSR_1) = 2\pi k \frac{FSR_1}{FSR_{2\text{ or }3}} \tag{7.45}$$

T(f) will be the smallest for $\delta_3(kFSR_1) = 1$, which implies:

$$T(f) = \frac{(1 - R)^2}{(1 + R)^2} \tag{7.46}$$

For R = 0.993, this value is -49.09 dB (c.f. value at 50 GHz in Table 7.1).

It is interesting to note eqn 7.46 is also the expression which describes the *overall* minimum transmission for a single etalon.[9] Since the reciprocity theorem can be applied to the filter of Figure 7.6, i.e. the outputs and inputs can be switched to yield the same response, cavity three can be exchanged for cavity one in this analysis with the same results applying. To conclude, it must be noted that eqn. 7.44, when evaluated at $f = kFSR_1$, only gives an estimate of the overall suppression of unwanted modes; as illustrated in Table 7.1, the actual peak frequencies are shifted slightly from the $f = kFSR_1$ values.

---

9. Note that this is not the overall minimum transmission for the three-cavity filter (See Section 7.3.5); eqn 7.46 does represent the minimum transmission attainable *at a resonance of one of the end cavities.*

7.3.5 Highest Achievable Suppression

The highest suppression attainable occurs at frequencies halfway between main transmission peaks, i.e. for:

$$f = \frac{(2n + 1)}{2} FSR_2 \tag{7.47}$$

These are frequencies about which even symmetry is noted in T(f), i.e:

$$T\left(\frac{FSR_2}{2} - f\right) = T\left(\frac{FSR_2}{2} + f\right) \tag{7.48}$$

Suppose that $FSR_2 = FSR_3$, and further that $FSR_1 = FSR_2/q$, where q is a positive integer. Then, eqn. 7.22 becomes:

$$T(f)_{min} = \frac{(1 - R)^4}{\left((1 + R)^2 + 4R\right)^2}, \text{ for q odd} \tag{7.49a}$$

$$T(f)_{min} = \frac{(1 - R)^4}{(1 + R)^2}, \text{ for q even} \tag{7.49b}$$

For example, if R = 0.993, these expressions can be evaluated to give -104.2 dB for q odd and only -49.09 dB for q even (compare eqn. 7.49b with eqn. 7.46). Clearly, a design where q is odd is preferred.

7.3.6 Non-Ideal Lengths

Suppose a filter is designed under the same assumptions as the previous section This implies that $l_2 = l_3$ and $l_1 = ql_2$. For practical implementation of such a filter, it will be of interest to know what tolerances should exist on the absolute lengths of the various cavities.

7.3.6.1 Changes in L_1 or L_3

Suppose that T(f) = 1, i.e. all three cavities are jointly resonant. Consider what effect a slight change in the length of cavity 3 (or 1, due to reciprocity) might have on the transmission profile. From eqn. 7.22, the following expression for the modified transmission as a function of the relative change in length of the cavity can be written:

$$T(f_{res}) = \frac{(1 - R)^2}{\left[1 - 2R\cos\left[\frac{2\pi k\varepsilon}{L}\right] + R^2\right]} \tag{7.50}$$

where ε/L is the relative length change of the third cavity, and k is the order of the resonance (i.e. $f_{res} = kFSR_2$). It is important to note that changes from eqn 7.50 that loss of transmission for some orders of resonance while others will be unaffected. The effect of variation of the length of one of the end cavities can thus be thought of as a sort of slowly-varying envelope which modulates the output spectrum.

If :

$$\cos\left[\frac{2\pi k\varepsilon}{L}\right] = -1 \tag{7.51}$$

then the transmission response is strongly degraded. This will occur for normally resonant transmission frequencies of:

$$f_{res} = \frac{(2m + 1)}{2}\left(\frac{c}{2n\varepsilon}\right), \text{ where m is an integer} \tag{7.52}$$

For example, if $\varepsilon = \lambda$, where λ might be a wavelength of interest, then the frequencies which lose transmission are:

$$f_{loss} = \frac{1}{4}\frac{c}{n\lambda}, \frac{3}{4}\frac{c}{n\lambda}, \frac{5}{4}\frac{c}{n\lambda}, \ldots \tag{7.53}$$

Transmission at λ would be preserved. However, if the variation were $\varepsilon = \lambda/4n$ then transmission is lost for:

$$f_{loss} = \frac{c}{\lambda}, \frac{3c}{\lambda}, \frac{5c}{\lambda}, \ldots \tag{7.54}$$

which would effectively suppress output at the desired wavelength.

This observation is not good news for the design of these types of filters; if the filter has fiber as a cavity guiding medium, then even changes in fiber length with temperature could result in unacceptable performance. It must also be remembered that changes in one end cavity for a fixed middle cavity have been assumed. In reality, all three cavities would probably vary in length, and this might result in a less severe degradation in performance, due to a degree of auto-tracking.

7.3.6.2 Changes in L_2

Suppose now that the length of cavity two only varies. It turns out that this will have no effect on the peak transmission at any given resonance, but other effects will be noticed:

1) The linewidth of the transmission resonances will increase (eqn. 7.41 no longer applies), and

2) Side-mode suppression will be affected. Since cavity two has been found to express its resonances independent of the two end cavities, alterations in FSR_2 could result in unwanted spectral content away from the desired resonances. This is especially true if the length

variations are not an integer multiple of half-wavelengths, so that the overall round trip length is some integer multiple of wavelengths.

7.4 Conclusions About Design of Multi-cavity Filters

Having discussed various results that may be gleaned from analytic study of the problem of multi-cavity filters, it is now appropriate to summarize the steps that might be taken in the design of a multi-cavity filter.

1. The first step is to select the desired FSR for the overall filter. This will then become FSR_2, as cavity two determines which resonances will be expressed most strongly.

2. The second step involves selecting lengths for cavities one and three. On the surface, it appears that any length which is an integer multiple of cavity two's length will do. However, not all such selections will result in good side-mode or triplet structure suppression. At this point, some criteria must be invoked which will rate different length selections on some basis. One basis that can be chosen is the ratio of power in the transmission peak to the 'noise' in a bandwidth of $\pm FSR_2/2$ around the transmission peak. This could roughly be used as a carrier-to-noise figure of merit for a given selection of cavity one and three lengths. A program has been written which does this, and the number of candidates for successful design drops dramatically.[10] As a final note, it is important to remember that the FSRs of cavity one and cavity three must have FSR_2 as their lowest common multiple i.e. they must share no common resonance less than FSR_2.

---

10. For example, in the design of a filter with a 10 GHz FSR using the criteria that $FSR_2 = FSR_3$, it was found that only 5 candidates produced suitable results, and the $l_1:l_2:l_3$ ratios for these 5 were 9:1:1, 10:1:1, 11:1:1, 12:1:1, and 13:1:1.

3. From this smaller field of candidates, selection of a final design is made based on the following criteria:

   a) If narrow linewidth is desired, eqn. 7.41 would suggest that at least one of the end cavities should have a considerably smaller FSR (i.e. be considerably longer than the other end cavity).

   b) In addition, for better suppression of side-modes, the end cavities should have lengths which are an odd integer multiple of the middle cavity length.

   c) The attainable reflectivities of the mirrors forming the cavities will probably be dictated by technology. The mirrors should have a high degree of flatness over the (apertured) beam diameter, to minimize cavity finesse degradations due to walk-off[11]. If a fiber is used, the effective beam diameter upon incidence of the mirror will be small, and so walk-off effects due to lack of flatness might not degrade performance. However, accurate perpendicularity between the mirror and fiber axis must be maintained.

An optimized design is shown in Figure 7.8 and 7.9 for a filter having a 10 GHz FSR. The various side-mode transmission values are noted in Table 7.2.

---

11. The overall finesse of a two-mirror Fabry-Perot is governed by a number of terms which add as inverse squares; one effect which limits finesse is the flatness of the mirror, which is normally specified as λ/M over a given aperture, where larger M values apply to higher quality mirrors. The finesse due to this effect is given by M/2. It could be expected for the four-mirror filter considered that similar finesse degradations occur.

f (GHz)	T(F) dB	f (GHz)	T(F) dB
0.13865	-14.54	5.45449	-48.92
0.91086	-26.94	6.36341	-47.44
1.81897	-38.38	7.27231	-44.22
2.72769	-44.22	8.18103	-38.38
3.63659	-47.44	9.08914	-26.94
4.54551	-48.92	9.86135	-14.54
5.0	-104.2	Linewidth	1.864 MHz

Table 7.2 : Transmission Peaks and Main-lobe Linewidth for a 10 GHz Filter Design

Note from Table 7.2 that deviations from integer multiples of FSR1, which is 0.90909 GHz for this design, range from 1.77 MHz for k = 1 to 65.4 kHz for k = 5, and that the linewidth calculated from eqn 7.41 is 1.8632 MHz. Also note that the maximum suppression is at 5.0 GHz and has a value of -104.2 dB, in accordance with eqn. 7.49a.

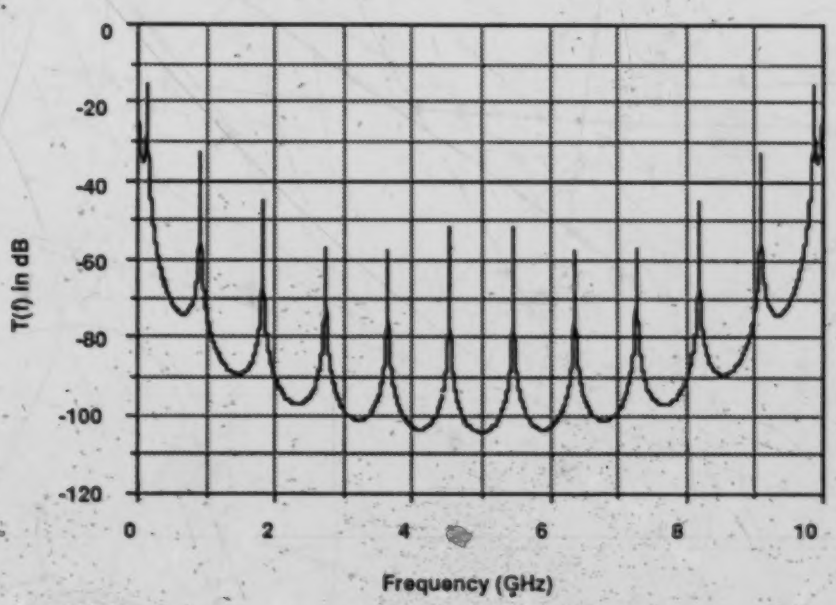

Figure 7.8 : Transmission Characteristic of a Three-cavity Filter Designed for a 10 GHz FSR

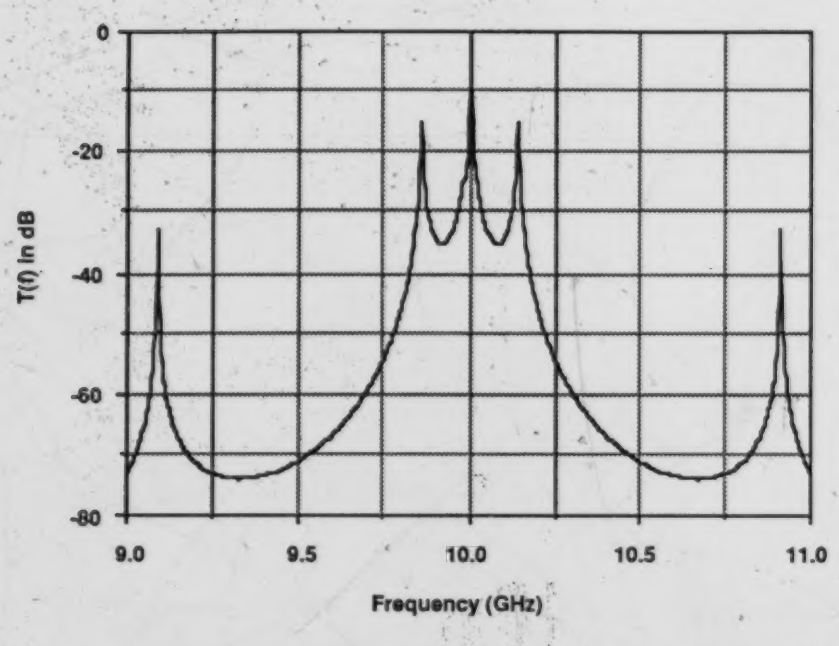

Figure 7.9 : Detail of the Passband Region of the 10 GHz Filter

8.0 Conclusions

This Thesis has reported on the early development of an EDFA design capability at TR Labs. This ability is crucial to an overall thrust of the BNR/ATRC/NSERC Chair to explore high speed fiber optic networks as EDFAs have recently resulted in incredible progress in this field.

First, a model of the behavior of EDFAs was developed that was general enough to allow variation of many amplifier parameters, such as fiber geometry, doping characteristics, and signal and pump input parameters. Some physical interpretation of the theory resulted in some predictions of EDFA performance. This model was then developed into an EDFA simulation package that allowed exploration of signal, ASE, and pump evolution as a function of amplifier length, multiple bi-directional input signals and/or pumps, spectral analysis of output spectra from the amplifier, noise figure, gain, length, and pump transparency power.

The next step was to use the simulation package to understand the behavior of EDFAs. To this end, a modest design was thoroughly studied and formed the basis for comparison to modified designs as selective variations to parameters were studied. Next, all the conclusions of this study were combined with additional observations on EDFA performance characteristics into some guidelines for design of EDFAs in Chapter 5. It was found that trade-offs exist, for example, between high gain devices and low splice-loss capable amplifiers, and that a large number of degrees of freedom exist when designing an EDFA.

Chapter 6 explored the work done in the lab to establish systematic methods for characterizing designed EDFAs, and as well reported on the first amplifier designed by

TR Labs. The performance of this amplifier was poorer than expected for two main reasons:

a) The pump laser used had multiple longitudinal modes, and possessed substantial spectral content towards 990 nm, where absorption by the Erbium is difficult. thus, little pump was actually available for the amplifier, resulting in the low gain performance observed.

b) The fiber delivered by the National Optics Institute was not really close to specification, especially in desired NA and dopant concentration. This, in-turn, degraded performance from that anticipated from the simulation/design reported in Chapter 4.

Chapter 7 discussed one application of an EDFA to a spectrally sliced transmitter for use in an FDM system. Complete theory was discussed for a three-cavity, four-mirror filter, and included thoughts on design of such a filter in a fiber-based environment.

8.1 Future Directions

The work from this thesis can be used as a starting point for future research. There is interest in taking the software design package and integrating it into a block-diagram-oriented fiber systems software package. Since the current theory is device-oriented, supplying specific information about spectra and actual propagation of pump and signals that would not be required in a systems-level design, revision of the theory for subsequent coding with that focus would be required.

In addition, future designs of EDFAs could include Yb, for improved pump absorption at 980 nm. As well, the trade-off between high NA, high gain amplifiers

and devices which couple well to standard telecommunications fiber could be alleviated by design of fibers with mode-field tapering techniques, as alluded to in Chapter 5.

Implementation of the theory discussed in Chapter 7 of the spectrally-sliced EDFA for use in FDM systems is also required. This could form a part of another thrust in the EDFA field towards development of high power, low noise, light sources for 1.55 μm systems, with possible applications in the transmission of AM-VSB television signals over fiber.

Component improvement is also an important consideration for future work. The most important device in an EDFA is the pump laser, and the acquisition at TR Labs of either a Ti:S laser or a single-moded 980 nm semiconductor source will certainly improve performance of future designs of amplifiers, while increasing reliability as well. In addition, the future EDFA work will have to move to higher bit rates, probably 2.4 Gbits/s or greater, in keeping with the focus of the Chair thrust, if TR Labs is to establish a niche in this immense field. This will therefore have to involve acquisition of both higher bandwidth DFB transmitters and receiver front-ends.

In a field expanding as rapidly as the field of optical amplifiers, it is also important to take note of research directions taken by others, and the results achieved there. Of important significance is a recent report of 38.2 dB of gain at 1.31 μm in praseodymium-doped ZBLAN fiber amplifiers [53]. This could spawn new interest in amplifiers at 1.3 μm, which is the wavelength of operation of most fiber optics transmission systems, since this would make integration into existing fiber architectures easier than for EDFAs, which function only at 1.55 μm.

References

[1] Snitzer, E., and Woodcock, R., *Yb-Er Glass Laser*, Applied Physics Letters, Vol. 6, No. 3, February, 1965, pp. 45 - 46

[2] Poole, S., Payne, D., Mears, R., Fermann, M., and Laming, R., *Fabrication and Characterisation of Low-Loss Optical Fibers Containing Rare-Earth Ions*, Journal of Lightwave Technology, Vol. 4, No. 7, July, 1986, pp. 870 - 876

[3] Tachibana, M., Laming, R., Morkel, P., and Payne, D., *Erbium-doped Fiber Amplifier with Flattened Gain Spectrum*, Photonics Technology Letters, Vol. 3, No. 2, February, 1991, pp. 118 - 121

[4] Massicott, J., Wyatt, R., Ainslie, B., and Craig-Ryan, S., *Efficient, High Power, High Gain Erbium-doped Silica Fibre Amplifier*, Electronics Letters, Vol. 26, No. 14, July 5, 1990, pp. 1038 - 1039

[5] Kreidl, J., *Erbium Amplifiers will get Submarine Cable Test*, Lightwave, June, 1991, p. 10

[6] Armitage, J., *Three-level Fiber Laser Amplifier: A Theoretical Model*, Applied Optics, Vol. 27, No. 23, December 1, 1988, pp. 4831 - 4836

[7] Desurvire, E., and Simpson, J., *Amplification of Spontaneous Emission in Erbium-doped Single-mode Fibers*, Journal of Lightwave Technology, Vol. 7, No. 5, May, 1989, pp. 835 - 845

[8] Desurvire, E., Giles, R., and Simpson, J., *Gain Saturation Effects in High-Speed, Multichannel Erbium-doped Fiber Amplifiers at 1.53 μm*, Journal of Lightwave Technology, Vol. 7, No. 12, December, 1989, pp. 2095 - 2104

[9] Desurvire, E., Zyskind, J., and Giles, R., *Design Optimization for Efficient Erbium-doped Fiber Amplifiers*, Journal of Lightwave Technology, Vol. 8, No. 11, November, 1990, pp. 1730 - 1741

[10] Giles, R., and Desurvire, E., *Modeling Erbium-doped Fiber Amplifiers*, Journal of Lightwave Technology, Vol. 9, No. 2, February, 1991, pp. 271 - 283

[11] Pedersen, B., Dybdal, K., Hansen, C., Bjarklev, A., Povlsen, J., Pommer, H., and Larsen, C., *Detailed Theoretical and Experimental Investigation of High-Gain Erbium-doped Fiber Amplifier*, Photonics Technology Letters, Vol. 2, No. 12, December, 1990, pp. 863 - 865

[12] Desurvire, E., Zyskind, J., and Simpson, J., *Spectral Gain Hole-Burning at 1.53 μm in Erbium-doped Fiber Amplifiers*, Photonics Technology Letters, Vol. 2, No. 4, April 1990, pp. 246 - 248

[13] Gloge, D., *Weakly Guiding Fibers*, Applied Optics, Vol. 10, 1971, p. 2252

[14] Giles, R., and Desurvire, E., *Transient Gain and Cross Talk in Erbium-doped Fiber Amplifiers*, Optics Letters, Vol. 14, No. 16, August 15, 1989, pp. 880 - 882

[15] Cheo, P., Fiber Optics: Devices and Systems, 1 ed., Prentice-Hall, 1985, pp. 73

[16] Siegman, A., Lasers, University Science Books, 1986, pp. 286

[17] Yariv, A., Optical Electronics, 3 ed. Holt, Rinehart, & Winston, 1985, pp. 141

[18] Jeunhomme,L., Single-mode Fiber Optics: Principles and Applications, Dekker Series in Optical Engineering, Vol. 4, 1983, pp. 17

[19] Desurvire, E., and Simpson, J., *Evaluation of $_4I_{15/2}$ and Stark-level Energies in Erbium-doped Aluminosilicate Glass Fibers*, Optics Letters, Vol. 15, No. 10, May 15, 1990, pp. 547 - 549

[20] Christodoulides, D., Reith, L., and Saifi, M., *Theory of LED Coupling to Single-mode Fibers*, Journal of Lightwave Technology, Vol. 5, No. 11, November, 1987, pp. 1623 - 1629

[21] Marcuse, D., *Launching Light into Fiber Cores from Sources Located in the Cladding*, Journal of Lightwave Technology, Vol. 6, No. 8, August, 1988, pp. 1273 - 1279

[22] Montecchi, M., Mecozzi, A., Settembre, M., Tamburrini, M., and DiGaspare, L., *Gain and Noise in Rare-Earth-doped Optical Fibers*, Journal of the Optical Society of America B, Vol. 8, no. 1, January 1991, pp. 134 - 141

[23] Miloni, P., and Eberly, J., Lasers, John Wiley & Sons, 1988, pp. 399 - 401

[24] Hall, D., *Optical Amplifiers*, Course 16, Short Course Notes, OFC '90

[25] Ruhl, F., *Prediction of Optimum Fibre Lengths for Erbium Doped Fibre Amplifiers*, Electronics Letters, Vol. 27, no. 9, April 27, 1991, pp. 769 - 770

[26] Miniscalco, W., *Erbium-Doped Glasses for Fiber Amplifiers at 1500 nm*, Journal of Lightwave Technology, Vol. 9, No. 2, February 1991, pp. 234 - 250

[27] Desurvire, E., *Spectral Noise Figure of Er-doped Fiber Amplifiers*, Photonics Technology Letters, Vol. 2, No. 3, March 1990, pp. 208 - 210

[28] Laming, R., and Payne, D., *Noise Characteristics of Erbium-Doped Fiber Amplifier Pumped at 980 nm*, Photonics Technology Letters, Vol. 2, No. 6, June, 1990, pp. 418 - 421

[29] Desurvire, E., *Analysis of Noise Figure Spectral Distribution in Erbium Doped Fiber Amplifiers pumped near 980 and 1480 nm*, Applied Optics, Vol. 29, No. 21, July 20, 1990, pp. 3118 - 3125

[30] Freeman, J., *NOI Erbium-doped Fiber Design*, TR Labs Report TR 91-09(R), April 17, 1991, p. 33

[31] Haugen, J., Freeman, J., and Conradi, J. *Bi-directional Transmission @ OC-12 with Erbium-doped Fiber Amplifiers*, submitted to OFC'92

[32] Miller, S., and Kaminow, I., Optical Fiber Telecommunication II., Academic Press, 1988, p. 270

[33] Shimizu, M., Yamada, M., Horiguchi, M., Takeshita, T., and Okayasu, M., *Erbium-doped Fiber Amplifiers With an Extremely High Gain Coefficient of 11.0 dB/mW*, Electronics Letters, Vol. 26, No. 20, September 27, 1990, pp. 1641 - 1643

[34] Holmes, M, Payne, F., and Spirit, D., *Matching Fibres for Low Loss Coupling into Fibre Amplifiers*, Electronics Letters, Vol. 26, No. 25, Dec. 6, 1990, pp. 2102 - 2104

[35] Ohsashi, M., and Tsubokawa, M., *Optimum Parameter Design of Er-doped Fiber for Optical Amplifiers*, Photonics Technology Letters, Vol. 3, No. 2, February, 1991, pp. 121 - 123

[36] Digonnet, M., and Gaeta, C., *Theoretical Analysis of Optical Fiber Laser Amplifiers and Oscillators*, Applied Optics, Vol. 24, No. 3, February 1, 1985, pp. 333 - 342

[37] Deus, A., and Sunak, H., *Design Considerations for Minimizing Macrobending Loss in Erbium-doped Fiber Amplifiers*, Photonics Technology Letters, Vol. 3, No. 1, January, 1991, pp. 50 - 52

[38] Ainslie, J., Armitage, J., Craig, S., and Wakefield, B., *Fabrication and Optimisation of the Erbium Distribution in Silica Based Fibers*, 12th ECOC Technical Digest, 1988, Part I, pp 62 - 65

[39] Ainslie, J., *Review of the Fabrication and Properties of Erbium-doped Fiber*, Journal of Lightwave Technology, Vol. 9, no. 2, February 1991, pp. 223 - 227

[40] Shimizu, M., Yamada, M., Horiguchi, M., and Sugita, E., *Concentration Effects on Optical Amplification Characteristics of Er-doped Silica single-Mode Fibers*, Photonics Technology Letters, Vol. 2, No. 1, January, 1990, pp. 43 - 45

[41] Kagi, N., Oyobe, A., and Nakamura, K., *Efficient Optical Amplifier Using a Low-Concentration Erbium-doped Fiber*, Photonics Technology Letters, Vol. 2, No. 8, August 1990, pp. 559 - 561

[42] Craig-Ryans, S., Massicott, J., Wilson, M, Ainslie, B, and Wyatt, R., *Optical Study of Low Concentration Er Fibres For Efficient Power Amplifiers*, 14th ECOC Technical Digest, 1990, Part I, pp. 571 - 574

[43] Barnes, W., Poole, S. et al. *Er-Yb and Er Doped Fiber Lasers*, Journal of lightwave Technology, Vo. 7, No. 10, October, 1989, pp. 1461 - 1465

[44] Grubb, S., Cannon, R., Windhorn, T., Vendetta, S., Leilabady, P., Anthon, D., Sweeney, K., Barnes, W., Taylor, E., and Townsend, J., *High-Power Sensitized Erbium Optical Fiber Amplifier*, Post Deadline Paper, OFC' 91, PD-7, pp. 31

[45] Oriel Corporation Product Guide, Vol. 2, p. 198

[46] CVI Digikrom Monochromator User Manual, p. 4

[47] Laming, R., Reekie, L., Morkel, P., and Payne, D., *Multichannel Crosstalk and Pump Noise Characterisation of Er-doped Fibre Amplifier Pumped at 980 nm*, Electronics Letters, Vol. 25, No. 7, March 30, 1989, pp. 455 - 456

[48] Urquhart, P. *Review of Rare Earth Doped Fibre Lasers and Amplifiers*, IEE Proceedings, Vol. 135, Pt. J, No. 6, December, 1988, pp. 385 - 407

[49] Chapuran, T., Wagner, S., Menendez, R., Tohme, H., and Wang, L., *Broadband Multichannel WDM Transmission with Superluminescent Diodes and LEDs*, Bellcore Internal Document, to be published, pp. 1 - 13

[50] Saleh, A., and Stone, J., *Two-Stage Fabry Perot Filters as Demultiplexers in Optical FDMA LANs*, Journal of Lightwave Technology, Vol. 7, No. 2, February, 1989, pp. 323 - 329

[51] Heavens, J. Optical Properties of Thin Solid Films, 1st ed., Dover Ltd, 1965, p. 63

[52] Van de Stadt, H., and Muller, J., *Multi-mirror Fabry-Perot Interferometers*, Journal of the Optical Society of America A, Vol. 2, No. 8, August, 1985, pp. 1363 - 1370

[53] Miyajima, Y., Sugawa, T., and Fukasaku, Y., *38.2 dB Amplification at 1.31 μm and the Possibility of 0.98 μm Pumping in Pr-doped Fluoride Fiber*, OA '91 Conference, July 28, 1991, Post Deadline Paper PdP1, pp. 1 - 4

[54] Barnes, W., Laming, R., Tarbox, E., and Morkel, P., *Absorption and Emission Cross Section of Er-Doped Silica Fibers*, Journal of Quantum Electronics, Vol. 27, No. 4, April, 1991, pp. 1004 - 1010

[55] McMullin, J., *Spontaneous Emission by an Atom Imbedded in an Optical Fiber*, To Be Published, 1990, pp. 1 - 4

[56] Olshansky, R., *Noise Figure for Erbium Doped Fiber Amplifiers*, Electronics Letters, Vol. 24, No. 22, October 27, 1988, pp. 1363 - 1365

[57] Verdeyen, J. Laser Electronics, 2 ed., Prentice-Hall, 1989

Appendix A: Comments on ASE Distributed Source Term

The determination of a distributed sources term for the generation of ASE is discussed in a number of sources ([17], p. 543, [23], p. 399). However, these references assume propagation of a Gaussian beams in free space. To the knowledge of the author, no published sources discuss the same problem in detail for propagation in a fiber, with an emphasis on derivation from fundamental theory.

From a consideration of transitions in an optical medium, the average rate over amplifier length that the intensity of spontaneous emission in a frequency band dν is created can be written as:

$$\text{Source} = h\nu A_{21} g(\nu) d\nu N_2 \Gamma \qquad W/cm^3 \quad (A.1)$$

where

$h\nu$ = the emitted photon energy in J

$A_{21} = 1/\tau$ = the spontaneous emission rate in Hz

$g(\nu)d\nu$ = the relative probability that a photon emitted by a spontaneous transition will appear between ν and $\nu + d\nu$; this will later be related to the stimulated emission cross-section $\sigma_{21}(\nu)$

N_2 = the upper lasing level population in cm^{-3}

Γ = a factor to account for coupling of only a small amount of the total, spontaneously emitted light into a guided fiber mode

It must be remembered from Section 2.2.1 that N_2 is a function of the cross-sectional core area when the theory is applied to a fiber. Following the lead of eqn. 2.21, A.1 is integrated above to yield:

$$\text{Source} = h\nu A_{21} g(\nu) \int_{\text{Area}} N_2 \Gamma d(\text{Area}) \tag{A.2}$$

where eqn A.2 has been divided by dν so that spectral densities are now considered. It is reasonable to assume that Γ will be a function of the transverse coordinates r and θ, since it can be interpreted to describe how well the spontaneously emitted photons are coupled into a guided fiber mode. It would then be intuitively reasonable to assume that Γ is directly proportional to the fiber-mode intensity profile, which delineates the spatial extent of the guided mode. Γ in this context is interpreted as the probability that a spontaneously emitted photon will be coupled into a guided mode. Thus, Γ will be taken to be:

$$\Gamma = \kappa t_{s\,01} \Psi_{01}^2(r, \nu_s) \tag{A.3}$$

where, for Gaussian free-space propagation, $\Gamma = d\Omega/4\pi$ steradians, which is typically evaluated to yield ([17], p. 570):

$$\Gamma = \frac{\lambda^2}{4\pi^2\omega^2} \tag{A.4}$$

where ω is the Gaussian beam radius at the waist of the beam. Eqn. A-2 can now be rewritten as:

$$\text{Source} = h\nu A_{21} g(\nu) \kappa \int_{\text{Area}} N_2 t_{s\,01} \Psi_{01}^2(r, \nu_s) d(\text{Area}) \tag{A.5}$$

Using eqn. 2.37, eqn. A.5 can further be written as:

$$\text{Source} = \frac{A_{21} g(\nu) \kappa}{\sigma_{21}(\nu)} h\nu \gamma_e(\nu) \tag{A.6}$$

Then:

$$\text{Source} = \frac{8\pi\kappa}{\lambda^2} h\nu\gamma_e(\nu) \tag{A.7}$$

where

$$\sigma_{21}(\nu) = \frac{A_{21} g(\nu) \lambda^2}{8\pi} \tag{A.8}$$

has been used [54]. It is thus required that:

$$\kappa = \frac{\lambda^2}{4\pi} \tag{A.9}$$

which is similar to a result previously reported in a much more rigorous treatment [55], [22].[1] The final result for the source term is then:

$$\text{Source} = 2h\nu\gamma_e(\nu) \tag{A.10}$$

which agrees with widely reported results ([7], [11], [22]).

---

1. It is also interesting to note that this result is somewhat reminiscent of the *Effective Aperture* of a short, lossless dipole antenna, which describes the antenna's ability to capture electromagnetic radiation and is much larger than the physical dimensions of the antenna. The Effective Aperture is related to an antenna's *Directivity* by:

   $A = (\lambda^2/4\pi)D$

   One useful reference is:

   Balanis, Antenna Theory: Analysis and Design, Harper & Row, 1982, pp. 59

Appendix B: Splice Loss Calculations

As part of the design process for the EDFAs, a number of splice loss calculations were performed. These calculations used the full splice loss expression, but index matching oil was assumed, so that the gap and core indices were equal. The calculations explored splice loss of Corning SMF-28 fiber with Corning Flexcor 1060 fiber, and the pertinent parameters are summarized in Table B.1.

Parameter \ Fiber type	Flexcor	SMF - 28
n_{core}	1.4637	1.471
2a	5.4 μm	8.3 μm
N.A.	0.136	0.125
ω at 980 nm	6.0 μm	7.7 μm
ω at 1550 nm	9.3 μm	10.5 μm

Table B.1 : Parameters Used in Splice Loss Calculations[3]

It is important to understand the limitations of this model as applied to this problem. First of all, SMF-28 fiber is is not single-moded at 980 nm, and so results at this wavelength will be of limited usefulness. Secondly, since the core indices are different, the average index was used in the formula.

The results are not surprising and show that the worst degradation in splice loss is due to transverse angular misalignment, θ_t, followed by fiber core offset, r_o, and finally end separation, z_o. Degradation due to z_o is seen to be small due to the inclusion of index-matching oil.

3. Some discrepancies exist between measured mode-field diameters form Corning and those calculated from fiber parameters; the numbers above represent measured field diameters.

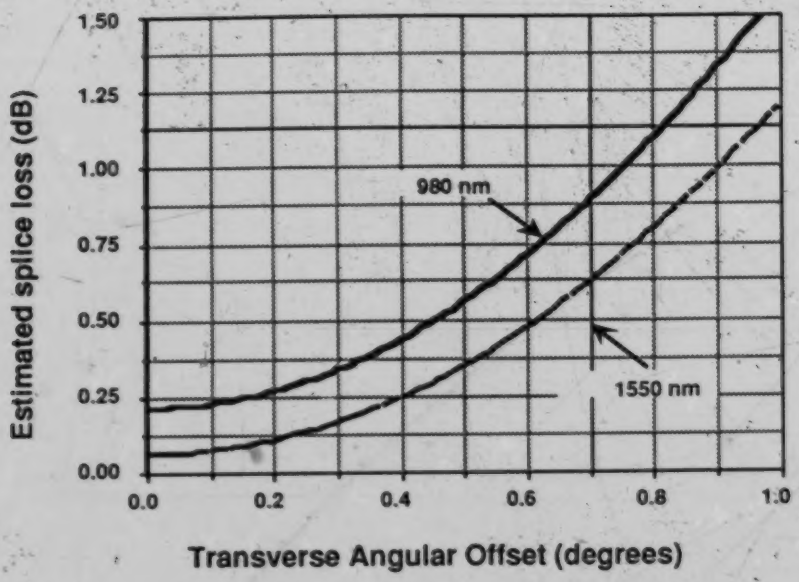

Figure B.1 : Splice Loss Between Flexcor and SMF-28 Fibers vs. Transverse Angular Offset (degrees)

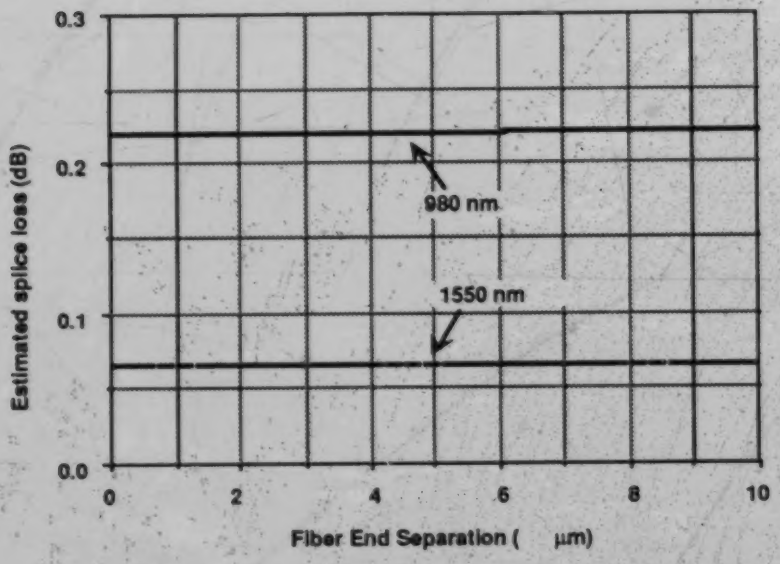

Figure B.2 : Splice Loss Between Flexcor and SMF-28 Fibers vs. Fiber End Separation (µm)

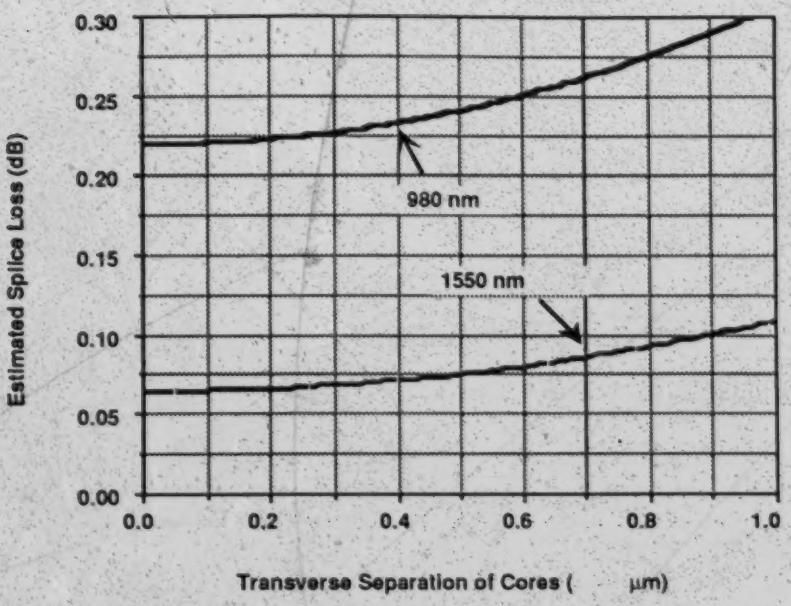

Figure B.3 : Splice Loss Between Flexcor and SMF-28 Fibers vs. Transverse Core Separation (μm)

Appendix C: Erbium Dopant Concentrations

A number of different nomenclatures exist for specifying the concentration of Erbium in the core of a fiber. They include ppm (molar), ppm (wt), mol %, wt%, or ions/cm^3. Of these, the most useful are ppm (molar), and ions/cm^3; these are the designations used both in the simulation and in designs quoted to NOI. the designation ppm (molar) is a comparison of the number of Er ions in the network to the total number of other entities present. Since SiO_2 is by far in the highest concentration, this specification is then made simple by considering only these two terms in the relation, i.e:

$$\text{ppm (molar)} = \frac{\text{total number of Er ions}}{\text{total number of } SiO_2 \text{ molecules}} \qquad \text{(D.1)}$$

The number of SiO_2 molecules in 1 cm^3 is given by:

$$2.2\ \frac{g}{cm^3} \times \frac{1}{60.08}\ \frac{mol}{g} \times 6.02 \times 10^{17} \frac{\text{million } SiO_2}{mol} = 2.2 \times 10^{16}\ \frac{\text{million } SiO_2}{cm^3} \qquad \text{(D.2)}$$

Since, for simulation purposes, the Erbium concentration is specified in terms of ions/cm^3, conversion to ppm (molar) is straightforward. For example, suppose:

$$[Er] = 9.9 \times 10^{18}\ \frac{ions}{cm^3}$$

then, in ppm (molar), the concentration is:

$$[Er] = \frac{9.9 \times 10^{18}}{2.2 \times 10^{16}} = 450 \text{ ppm (molar)} \qquad \text{(D.3)}$$

Appendix D : Comments about Noise Figures

The noise figure is an important figure of merit for an amplifier, and represents the degradation in SNR experienced due to transit through that amplifier; seen another way, it is a measure of the noise added by that amplifier. No ideal amplifier exists, and noise is always added when amplification occurs. In optical amplifiers, this can be justified by the fact that even when stimulated emission dominates the transition down from the upper lasing level, spontaneous emission will also always occur and add incoherent, randomly phased radiation to the signal exiting the amplifier, i.e. noise.

A small body of work exists describing theoretically the noise figure of an optical amplifier [56], [27], [29]. Care must first be taken to distinguish between an *optical noise figure* and an *electrical noise figure*, which assumes conversion from an optical to electrical signal via a photodetector, and thus considers an *optical* SNR at the input and an *electrical* SNR at the output. The optical noise figure will be hereupon referred to and is strictly a ratio of *optical* SNR into the amplifier to *optical* SNR exiting the amplifier.

$$NF_o(z,\nu) = \frac{SNR_{in}}{SNR_{out}} \tag{D.1}$$

At the input to the amplifier (z = 0), there is some average number of signal photons and a variance in this number of photons, given by:

$$\sum(0)^2 = \overline{n(0)^2} - \overline{n(0)}^2 \tag{D.2}$$

where

$$\overline{n(0)^2} = \text{the second moment of n}$$
$$\overline{n(0)}^2 = \text{first moment of n, squared} \tag{D.3}$$

Similar relations exist at the amplifier output, where z = L. Thus, the noise factor[4] is given by:

$$F_o(L) = \frac{\overline{n(0)^2}}{\Sigma(0)^2}\frac{\Sigma(L)^2}{G^2\overline{n(0)^2}} \qquad (D.4)$$

with G^2 being the signal power gain. Defining the term $\Sigma(L)^2$ is the crux of the problem. Intuitively, this term would be expected to depend on the amount of ASE generated within the amplifier, which in-turn depends on the population inversion as outlined in Chapter 2 and Appendix A. However, these terms are a function of z for an end-pumped amplifier such as an EDFA. If the there was no functional dependence on z, i.e. the inversions were constant (which also assumes, therefore, that no saturation is occurring to deplete the inversion), the following result can be derived for the ASE photon spectral density:

$$N = n_{sp}(G - 1) \qquad (D.5)$$

where N can be related to the ASE power exiting the amplifier by a familiar relation:

$$P_{ASE} = 2Nh\nu B_o = 2n_{sp}(G - 1)h\nu B_o \qquad (D.6)$$

4. Recall that the noise factor is related to the noise figure by $NF_o = 10\log(F_o)$

and

$$n_{sp} = \frac{\sigma_{21}N_2}{\sigma_{21}N_2 - \sigma_{12}N_1} \tag{D.7}$$

and is termed the *spontaneous emission factor*.

Eqn. D.7 thus shows that for an amplifier *with uniform inversion over its entire length*, a complete inversion will result in a spontaneous emission factor equal to one. For the case of a real EDFA, where the inversion is not uniform over the entire length of the amplifier, an analogous relation can be written for an integrated or effective spontaneous emission factor, where eqn D.5 still applies but eqns. D.6 and D.7 are no longer valid and are replaced by integrals over length for the gain and ASE noise power, given by:

$$G(z,\nu) = \exp\int_0^z [\sigma_{21}N_2 - \sigma_{12}N_1]\, dz' \tag{D.8}$$

which could be derived easily from eqn 2.2, and

$$N(z,\nu) = G(z,\nu)\int_0^z \left[\frac{\sigma_{21}N_2}{G(z',\nu)}\right] dz' \tag{D.9}$$

Returning now to the problem of the output signal variance, the result for uniform inversions is typically applied with the *integrated values* for G and N in eqns. D.8 and D.9 used. The expression is:

$$\Sigma(L)^2 = G(L,\nu)^2\left\{\Sigma(0)^2 - \overline{n(0)}\right\} + \left\{G(L,\nu)\overline{n(0)} + N(z,\nu)\right\} + \left\{2G(L,\nu)\overline{n(0)}N(z,\nu) + N(z,\nu)^2\right\} \tag{D.10}$$

The first term is interpreted as an "excess noise", the second as a "shot noise", and the third as a "beat noise", but it is important to realize that this result is still describing an

optical signal, because no detection has occurred. Since Poisson statistics are assumed for the input signal, then the variance equals the mean, and so:

$$\Sigma(0)^2 = \overline{n(0)} \tag{D.11}$$

substitution of D.10 into D.4 using D.11 yields:

$$F_o(L,\nu) = \frac{N}{G\overline{n(0)}}\left[\frac{N}{G} + 1\right] + \frac{2N + 1}{G} \tag{D.12}$$

with a large mean photon number, this reduces to:

$$F_o(L,\nu) \approx \frac{2N + 1}{G} \approx \frac{2n_{sp}[G - 1] + 1}{G} \tag{D.13}$$

which in-turn reduces, for large gain G, to:

$$F_o(L,\nu) \approx 2n_{sp} \tag{D.14}$$

where n_{sp} is still defined by eqn. D.5. If the ASE power and gain are known by measurement, then D.5 can be rewritten using D.6 to give:

$$F_o(L,\nu) \approx \frac{P_{ASE}}{h\nu B_o(G - 1)} \tag{D.15}$$

It is important to note that the smallest value n_{sp} can have is one, corresponding to perfect inversion in an ideal three-level laser. Thus, the lowest noise figure, termed the quantum limit, is 3 dB. Examination of eqns. D.10 and D.12 indicate that this limit is due to unavoidable signal-spontaneous "beat noise", and the application of D.15 really assumes that a uniform inversion exists (cf. D.6 and D.7).

Eqn. D.15 is the result used in eqns. 4.1 and 6.2, and is convenient because measurement of the parameters required is relatively straightforward. It is important to recall the assumptions made in this derivation, which include:

1. Small-signal operation (otherwise, eqn. D.10 will not be valid)
2. Poisson input signal statistics
3. Fairly appreciable signal input (but not so large as to cause saturation; values in the -40 to -15 dBm range are typically valid
4. Appreciable Gain
5. Applicability of eqn D.10, which is really derived for the uniform inversion case, to the problem here, where modified expressions for gain G and ASE photon spectral density N are used.

As a final comment the electrical noise factor, subject to the above conditions, is given by:

$$F_e(L,\nu) \approx \frac{2N + (\eta_C \eta_D \eta_F(\nu))}{G} \qquad (D.16)$$

where

η_c = the light-to-detector coupling efficiency

η_D = the detector quantum efficiency

$\eta_F(\nu)$ = the optical transmission of a filter, if used.

If all of these terms are unity, the electrical noise figure is equal to the optical noise figure, but the difference is small for large optical gain anyway.

Appendix E : Sample LabVIEW™ Programs

Two LabVIEW™ programs, one used to measure EDFA gain vs. signal input power, the other used to measure EDFA gain modulation frequency response, are included for reference, and are listed in the output format produced by LabVIEW™. The first entry, entitled "Position in hierarchy", outlines the main program and some of the routines, or *Sub-VIs*, called during execution. The "Connector Pane" entry discusses how parameters would be passed to and from the VI if it were used as a Sub-VI, and comments follow that appear as documentation under the "Get Info" menu entry on the Macintosh. Next comes an illustration of the actual "Front Panel" as seen on the screen during program operation, and this is followed by a number of layers of the "Block Diagram". Comments are included within the Block Diagram to aid in understanding of operation.

GAIN.VI
Friday, August 30, 1991 11:54 AM

Position in hierarchy

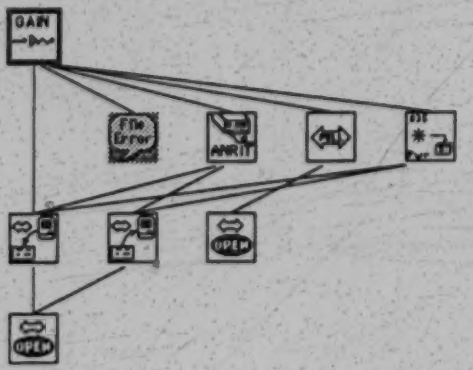

Connector Pane

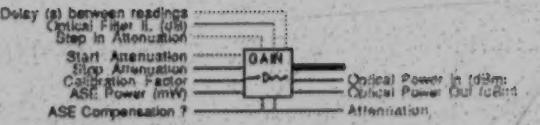

GAIN.VI

Program written by James Freeman, June, 1991. Modified July 24, 1991 to include ASE compensation and real-time Gain vs. I/P Power display.

Sequencing of program events are as follows:

1) Determine the O/P Save File name
2) Enter a loop based on the number of points required to get to stop attenuation from start attenuation for a given increment.

While in the Loop...
1) Write the attenuation to the JDS
2) Read the I/P power to the AMPLIFIER from the Anritsu (Note, use the 10% O/P from the JDS attenuator as the I/P to the Anritsu, and calibrate the reading such that it displays what is actually being delivered via the 90% arm and the WDM to the Amp)
3) Let the reading on the Newport settle
4) Read the O/P power from the Newport Ge head
5) Continue
Other comments
1) If the runs are being conducted w/o the monochromator, the Ge head must have a piece of Si placed in front of it to prevent residual pump from being detected.
2) If runs are conducted with the monochromator, the IL must be characterised prior to the tests. Use slit widths at the O/P which allow roughly full passage of the DFB, eg. 400 um should be good.

Front Panel

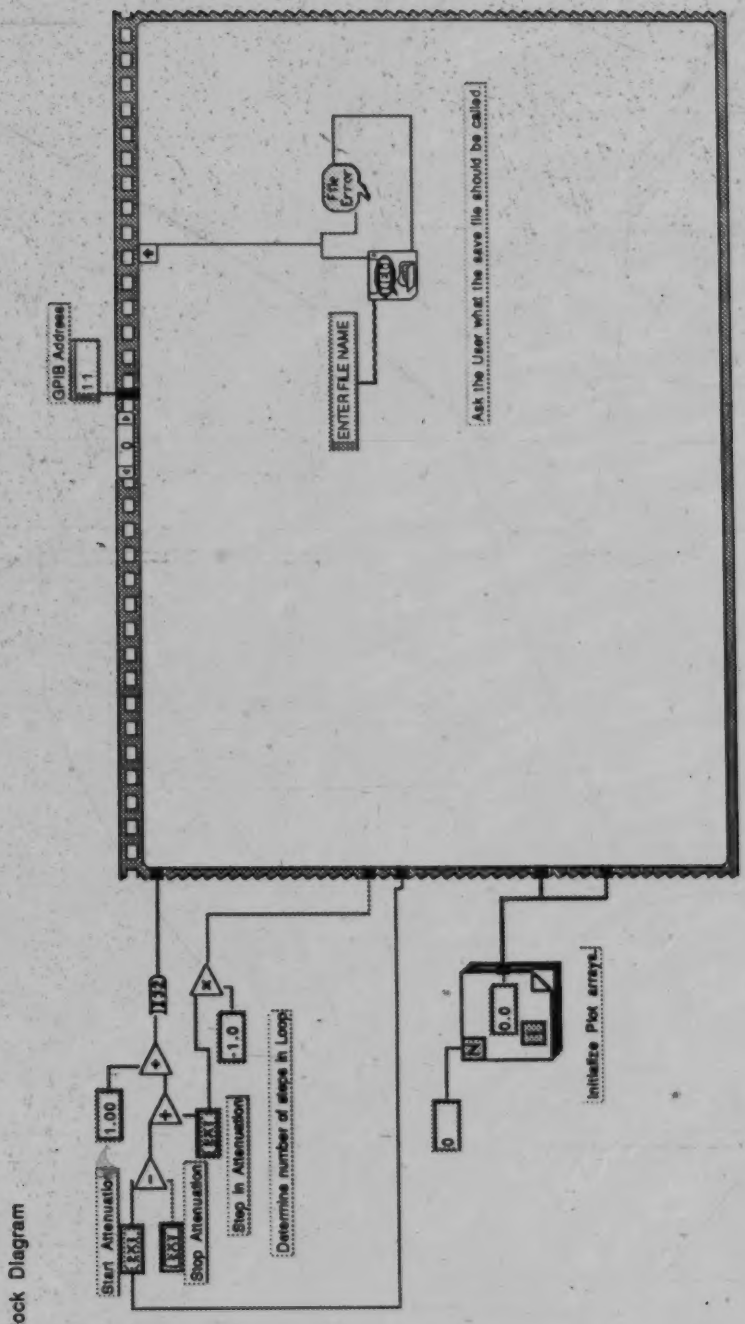

Block Diagram

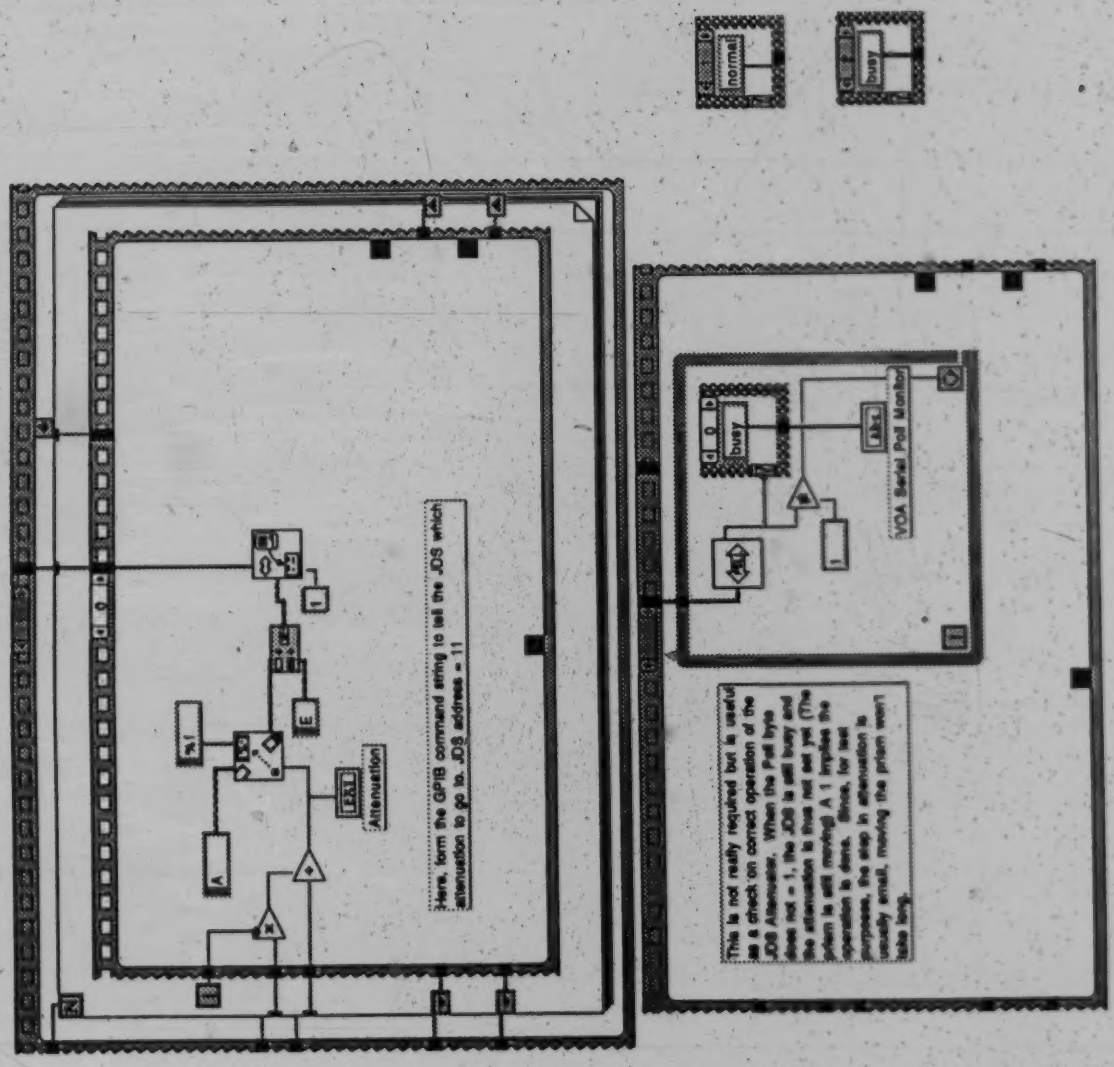
normal
busy
busy
VOA Serial Poll Monitor
This is not really required but is useful as a check on correct operation of the JD3 Attenuator. When the Poll byte does not = 1, the JD3 is still busy and the attenuation is thus not set yet. (The prism is still moving) A 1 implies the operation is done. Since, for test purposes, the step in attenuation is usually small, moving the prism won't take long.
Here, form the GPIB command string to tell the JD3 which attenuation to go to. JD3 address = 11
Attenuation

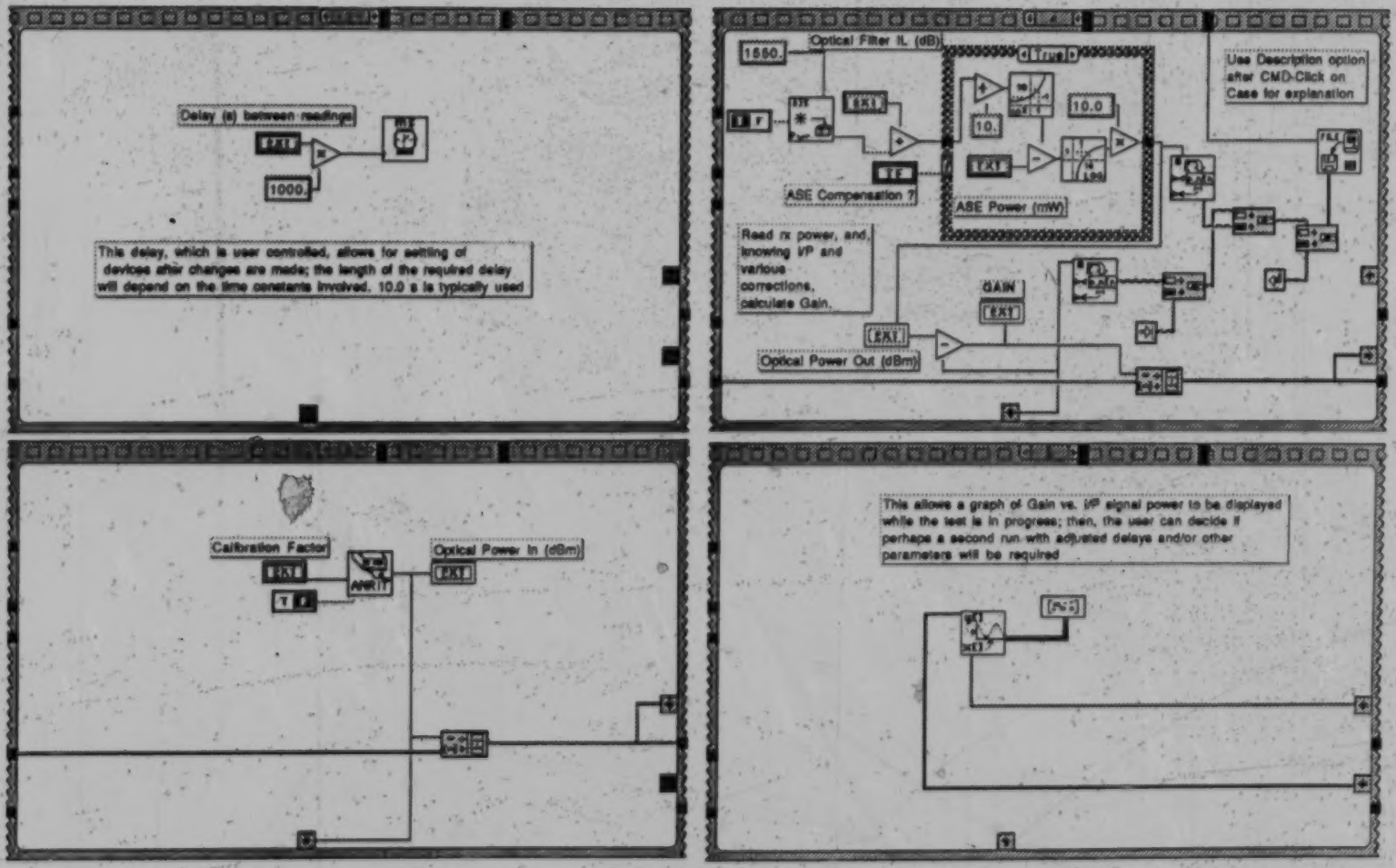
Delay (s) between readings
1000.
This delay, which is user controlled, allows for settling of devices after changes are made; the length of the required delay will depend on the time constants involved. 10.0 s is typically used
1550.
Optical Filter IL (dB)
10.0
10.
ASE Compensation ?
ASE Power (mW)
Use Description option after CMD-Click on Case for explanation
Read rx power, and, knowing I/P and various corrections, calculate Gain.
GAIN
Optical Power Out (dBm)
Calibration Factor
Optical Power In (dBm)
This allows a graph of Gain vs. I/P signal power to be displayed while the test is in progress; then, the user can decide if perhaps a second run with adjusted delays and/or other parameters will be required

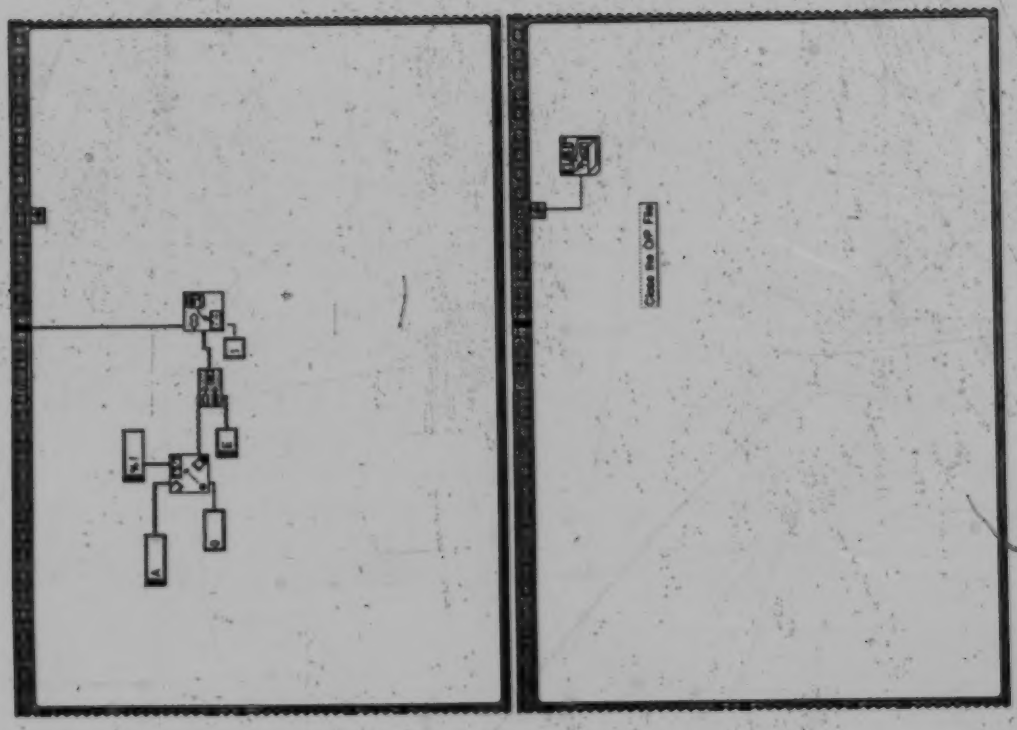
Close the DAT File

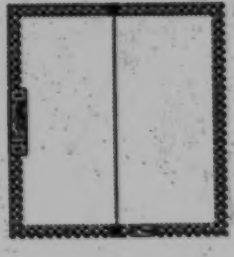

Frequency Response.VI
Friday, August 30, 1991 10:59 AM

Position in hierarchy

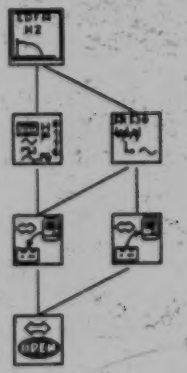

Connector Pane

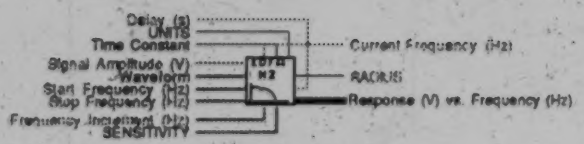

Frequency Response.VI

Frequency Response.VI, written by James Freeman
July, 1991

This VI makes use of the Hp 8116A and the SR 530 lock-in VI to measure the frequency response of the EDFA through modulation of the pump and subsequent detection of the modulated ASE/injected signal. 400 mV is a good choice for modulation depth at 150 mA DC on the pump. 8.0 s delay on the Lock-in when the time constant is 1.0 s is sufficient, and the sensitivity will vary depending on the frequency range being scanned. It might be good to break the range up into two separate runs so that sensitivity may be changed; changing sensitivity while running the program results in transients in the readings, although a longer delay might avert this.

Front Panel

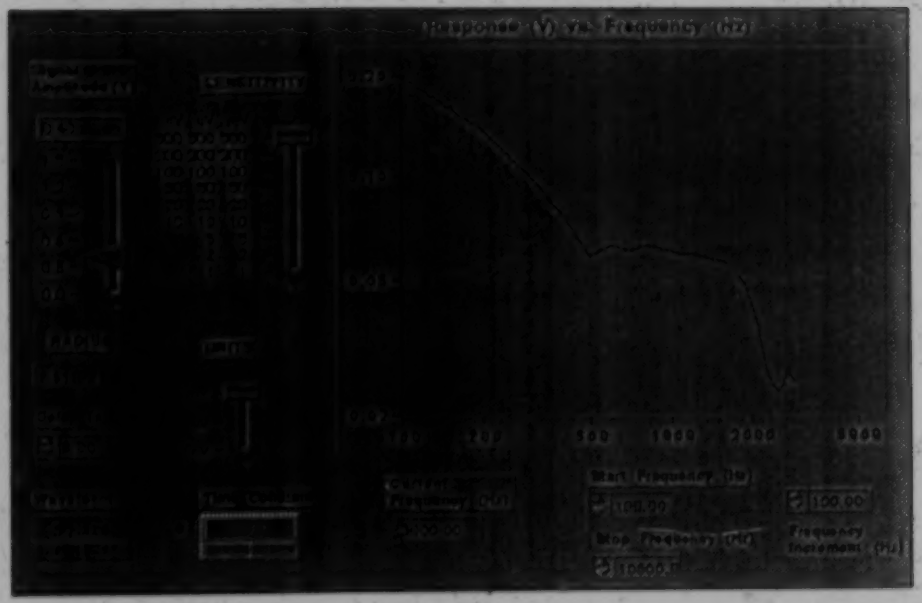
Response (V) vs. Frequency (Hz)
500
1000
2000
5000
Start Frequency (Hz)
100.00
Stop Frequency (Hz)
10000.0
Frequency Increment (Hz)
100.00

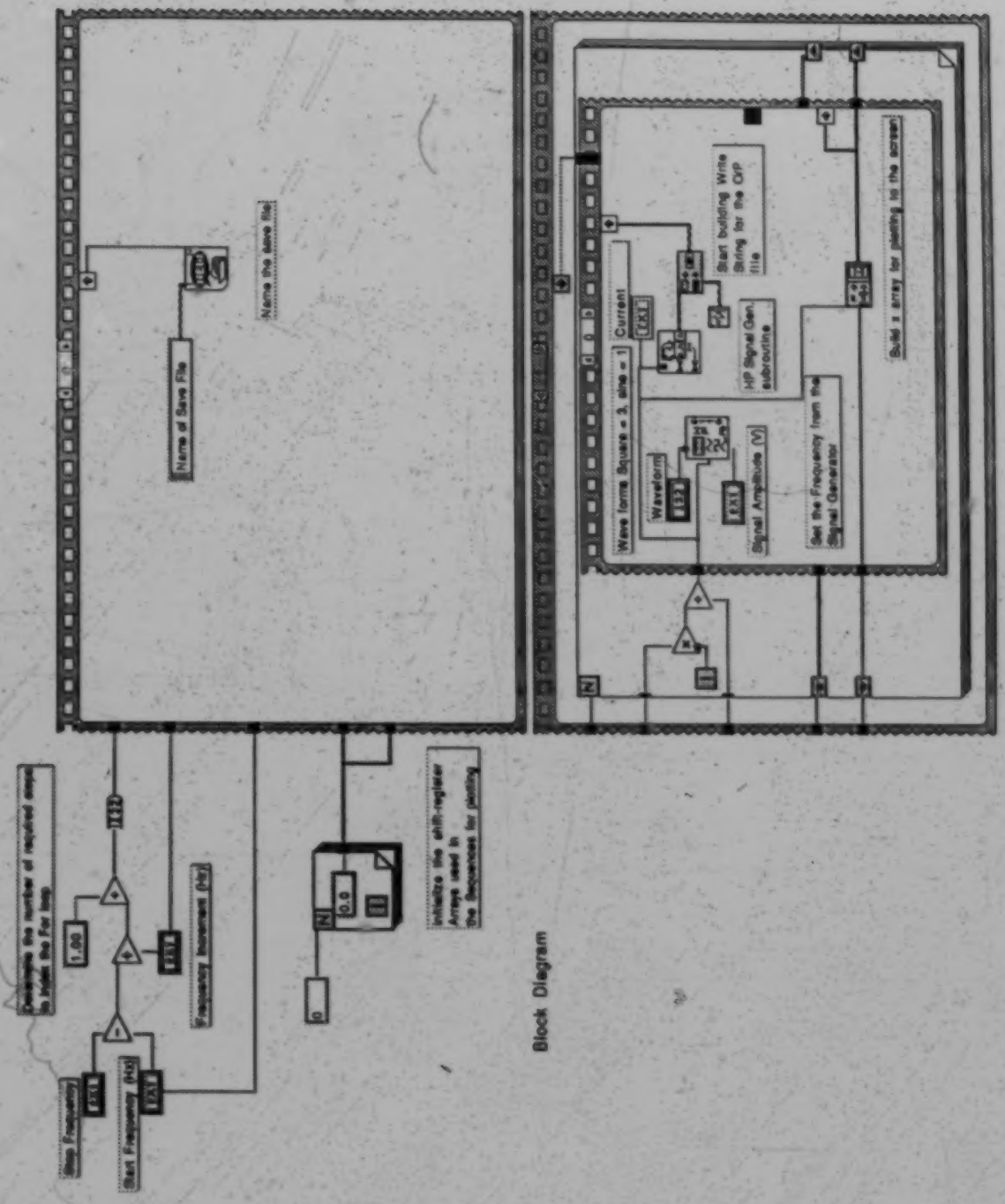
Name the save file
Name of Save File
Determine the number of required steps to build the For loop
Frequency Increment (Hz)
Stop Frequency
Start Frequency (Hz)
Initialize the shift-register Array used in the Sequences for plotting
Wave forms Square = 3, sine = 1
Current
Waveform
Signal Amplitude (V)
Set the Frequency from the Signal Generator
HP Signal Gen. subroutine
Start building Write String for the O/P file
Build a array for plotting to the screen

Block Diagram

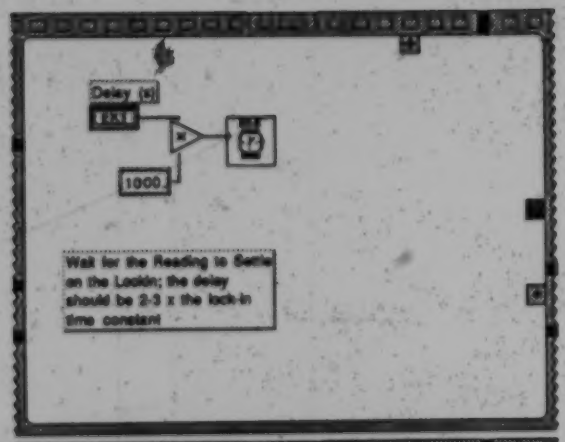
Delay (s)
1000
Wait for the Reading to Settle on the Lockin; the delay should be 2-3 x the lock-in time constant

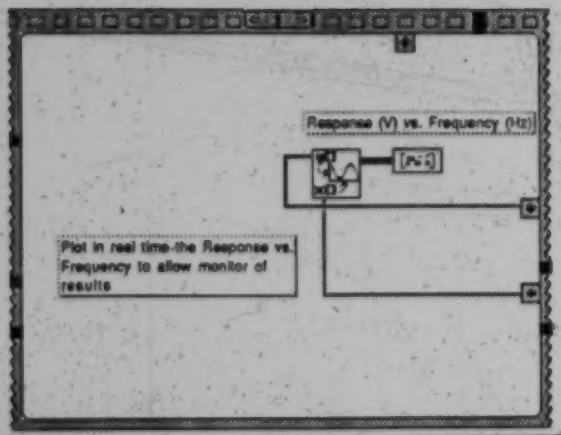
Response (V) vs. Frequency (Hz)
Plot in real time the Response vs. Frequency to allow monitor of results

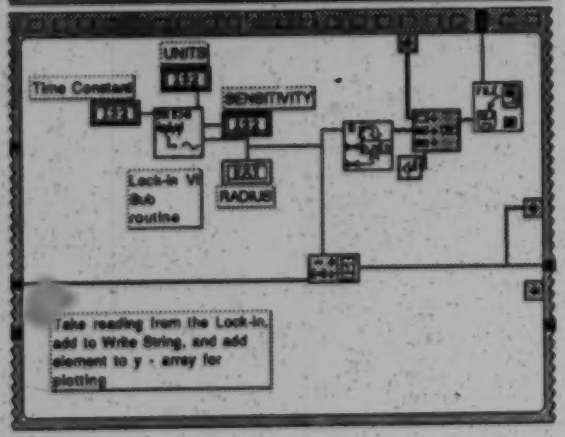
UNITS
Time Constant
SENSITIVITY
Lock-in VI Sub routine
RADIUS
Take reading from the Lock-in, add to Write String, and add element to y - array for plotting

Close the disk file

Appendix F: Comments About S and T Matrices

It is useful to review some of the relations governing the use of S and T matrices.

Figure F.1 : Schematic Representation of a Two -port Network

Given a general two-port network as shown Figure F.1,relations between the outputs and inputs can be written using S or T parameters as follows:

$$b_1 = S_{11}a_1 + S_{12}a_2 \qquad \text{(F.1a)}$$

$$b_2 = S_{21}a_1 + S_{22}a_2 \qquad \text{(F.1b)}$$

$$b_2 = T_{ba}a_1 + T_{bb}b_1 \qquad \text{(F.2a)}$$

$$a_2 = T_{aa}a_1 + T_{ab}b_1 \qquad \text{(F.2b)}$$

The T parameters can be related to the S parameters by:

$$T_{ab} = \frac{1}{S_{12}} \qquad T_{aa} = \frac{-S_{11}}{S_{12}}$$

$$T_{ba} = S_{21} - \frac{S_{22}S_{11}}{S_{12}} \qquad T_{bb} = \frac{S_{22}}{S_{12}} \qquad \text{(F.3)}$$

Now, the forward power transfer function for such a two port network is given by:

$$\frac{|b_2|^2}{|a_1|^2} = |S_{21}|^2 \qquad \text{(F.4)}$$

For any linear, reciprocal network (i.e., the outputs and inputs can be switched with no changes to the observed responses), the following additional relations exist:

$$S_{12} = S_{21} \tag{F.5}$$

and so

$$\frac{|b_2|^2}{|a_1|^2} = |S_{12}|^2 = \frac{1}{|T_{ab}|^2} \tag{F.6}$$

This will turn out to be a very fortunate relationship when a number of components are cascaded to form the multi-cavity filter. Some other relations from S and T parameter theory that will be useful to check the validity of the results are:

1. Reciprocity relation (repeated from above):

$$S_{12} = S_{21}$$

2. Power conservation (for a lossless system):

$$|S_{11}|^2 + |S_{21}|^2 = 1 \tag{F.7a}$$

$$|S_{22}|^2 + |S_{12}|^2 = 1 \tag{F.7b}$$

$$S_{11}^* S_{12} + S_{21}^* S_{22} = 0 \tag{F.7c}$$

3. Determinants (for a reciprocal network):

$$\det(T) = \det(S) = 1 \tag{F.8}$$